AD-A093 493 ATLANTIC RESEARCH CORP ROME NY F/G 17/9
SPACE-BASED RADAR ARRAY SYSTEM SIMULATION AND VALIDATION.(U)
SEP 80 H K SCHUMAN, D R PFLUG, L D THOMPSON F30602-79-C-0116
UNCLASSIFIED RADC-TR-80-294 NL

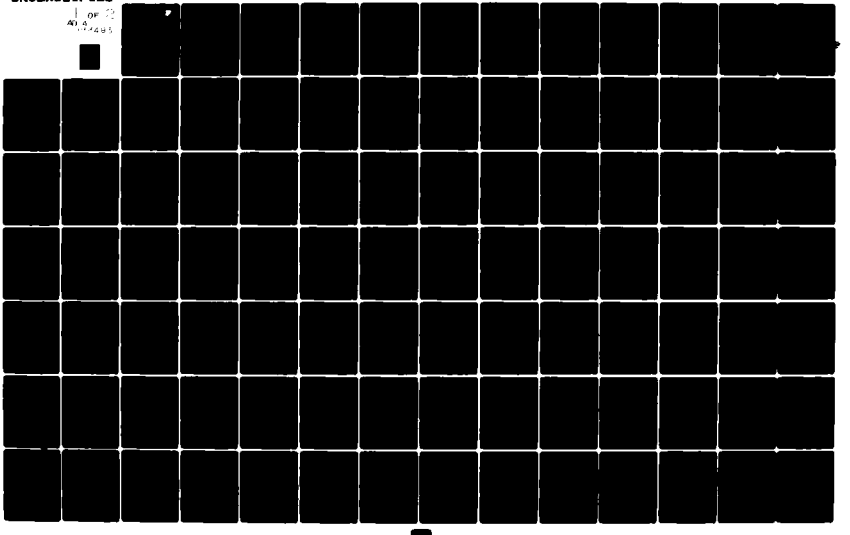

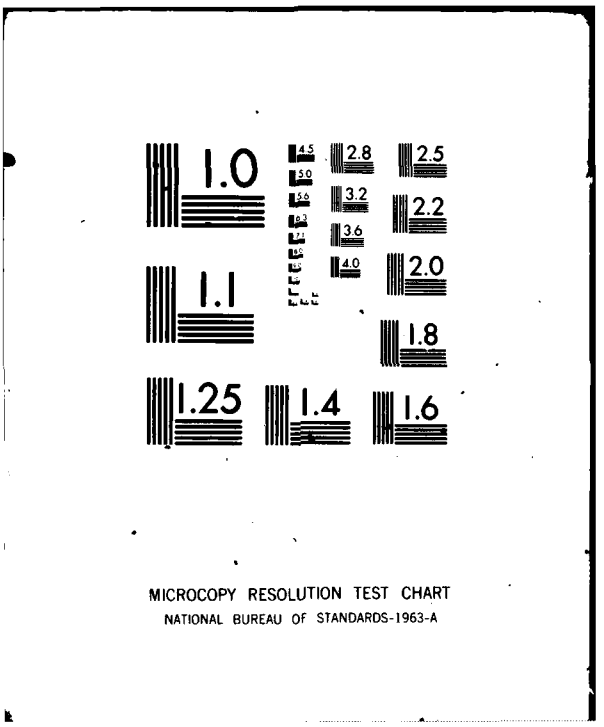

LEVEL II (12) Tu

RADC-TR-80-294
Interim Report
September 1980

SPACE-BASED RADAR ARRAY SYSTEM SIMULATION AND VALIDATION

Atlantic Research Corporation

Harvey K. Schuman
Donald R. Pflug
Larry D. Thompson

ROME AIR DEVELOPMENT CENTER
Air Force Systems Command
Griffiss Air Force Base, New York 13441

This report has been reviewed by the RADC Public Affairs Office (PA) and is releasable to the National Technical Information Service (NTIS). At NTIS it will be releasable to the general public, including foreign nations.

RADC-TR-80-294 has been reviewed and is approved for publication.

APPROVED: Russell C. Steenrod

RUSSELL C. STEENROD, Capt USAF
Project Engineer

APPROVED: Frank J. Rehm

FRANK J. REHM
Technical Director
Surveillance Division

FOR THE COMMANDER: John P. Huss

JOHN P. HUSS
Acting Chief, Plans Office

SUBJECT TO EXPORT CONTROL LAWS

This document contains information for manufacturing or using munitions of war. Export of the information contained herein, or release to foreign nationals within the United States, without first obtaining an export license, is a violation of the International Traffic in Arms Regulations. Such violation is subject to a penalty of up to 2 years imprisonment and a fine of $100,000 under 22 U.S.C 2778.

Include this notice with any reproduced portion of this document.

If your address has changed or if you wish to be removed from the RADC mailing list, or if the addressee is no longer employed by your organization, please notify RADC (OCSA) Griffiss AFB NY 13441. This will assist us in maintaining a current mailing list.

Do not return this copy. Retain or destroy.

UNCLASSIFIED

SECURITY CLASSIFICATION OF THIS PAGE (When Data Entered)

REPORT DOCUMENTATION PAGE

READ INSTRUCTIONS BEFORE COMPLETING FORM

1. REPORT NUMBER: RADC-TR-80-294 (18) (19)	2. GOVT ACCESSION NO.: AD A093493
3. RECIPIENT'S CATALOG NUMBER:	
4. TITLE (and Subtitle): SPACE-BASED RADAR ARRAY SYSTEM SIMULATION AND VALIDATION (6)	5. TYPE OF REPORT & PERIOD COVERED: Interim Report (9) 7 Mar 79 - 7 Mar 80
	6. PERFORMING ORG. REPORT NUMBER: N/A
7. AUTHOR(s): Harvey R. Schuman, Donald R. Pflug, Larry D. Thompson (10)	8. CONTRACT OR GRANT NUMBER(s): F30602-79-C-0116 (15)
9. PERFORMING ORGANIZATION NAME AND ADDRESS: Atlantic Research Corporation, 1721 Black River Blvd, Rome NY 13440	10. PROGRAM ELEMENT, PROJECT, TASK AREA & WORK UNIT NUMBERS: 62702F, 45061437 (16) (17) 14
11. CONTROLLING OFFICE NAME AND ADDRESS: Rome Air Development Center (OCSA), Griffiss AFB NY 13441	12. REPORT DATE: Sep 80 (11)
	13. NUMBER OF PAGES: [redacted] (12) 176
14. MONITORING AGENCY NAME & ADDRESS (if different from Controlling Office): Same	15. SECURITY CLASS. (of this report): UNCLASSIFIED
	15a. DECLASSIFICATION DOWNGRADING SCHEDULE: N/A

16. DISTRIBUTION STATEMENT (of this Report)

Approved for public release; distribution unlimited

17. DISTRIBUTION STATEMENT (of the abstract entered in Block 20, if different from Report)

Same

18. SUPPLEMENTARY NOTES

RADC Project Engineer: Russell C. Steenrod, Capt USAF (OCSA)

19. KEY WORDS (Continue on reverse side if necessary and identify by block number)

Space Fed Lens
Infinite Arrays
Moment Methods
Space-Based Radar
Antenna
RF Lens

20. ABSTRACT (Continue on reverse side if necessary and identify by block number)

The simulation theory and software implementation for a space-based radar RF lens are described. Infinite array theory and moment methods are used to simulate the mutual coupling among the wire radiators on each lens array face, "feedback" coupling from the nonilluminated array to the illuminated array, active progressively phased modules interconnecting the arrays, and arbitrarily shaped thin wire radiating elements. Edge effects are accounted for by iterative techniques. Active impedances,

DD FORM 1 JAN 73 1473 EDITION OF 1 NOV 65 IS OBSOLETE

UNCLASSIFIED

SECURITY CLASSIFICATION OF THIS PAGE (When Data Entered)

412120

element currents, and power gain patterns are computed.

TABLE OF CONTENTS

LIST OF ILLUSTRATIONS

EVALUATION

The objective of this effort is to develop and validate a simulation of the space-based radar (SBR) phased array lens system. This report contains the simulation theory and implementation methods used to set up the simulation. The key accomplishment of this effort has been to establish a new method to perform an analysis, to the accuracy desired, of a large SBR phased array lens system that includes all electrical factors that influence the RF far field pattern. Also, the key parts of the simulation have been validated.

This effort is part of RADC TPO-3A.

Russell C. Steenrod

RUSSELL C. STEENROD, Capt USAF
Project Engineer

SECTION 1

INTRODUCTION

The objective of this contract is to develop and validate a computer program for simulation of space-based radar (SBR) phased array lenses. This simulator will be used to analyze the performance of candidate lenses. The parameters of primary concern are radiation power gain and pattern characteristics.

A typical SBR is shown in Figure 1-1. The transmitter provides the space feed that illuminates the lens during radar transmit. The space feed may be in the form of several independently controlled beams that provide lens radiation pattern shaping, adaptive nulling, and time delayed lens sector illumination. (The time delayed compensation is required because of significantly different transmitter-to-lens path lengths to different points on the lens). Beam steering and, possibly, amplification are performed by the lens.

A lens comprising two arrays of metallic radiators sandwiching a ground screen currently is being modeled in the simulator. A typical lens of this type is shown in Figure 1-2; for simplicity, dipole radiating elements are indicated. The simulator also will be capable of analyzing other element types; e.g., folded dipole, bowtie, turnstile, and parasitic (Figure 1-3). Focusing and scanning of the lens-transmitted main beam is accomplished by electronic modules interconnecting the radiating elements between the illuminated and nonilluminated arrays (Figure 1-4). These modules also may provide power amplification.

An accurate analysis of a large space-based phased array lens, comprising hundreds of thousands of elements, is a formidable problem. Infinite periodic array theory alone is not adequate when, for example, edge effects must be considered. A space-based lens is expected to have stringent constructural and deployment constraints that will result in, at best, a piecewise periodic lattice; e.g., a lens composed of wedge-shaped gores may have nonperiodic spacings in the vicinity of gore interfaces. Another source of nonperiodicity may be inherent in the electronic modules. They may not be identical in the event of selected power failures. (Simple progressive phasing between module settings, however, can be treated with a variation of "standard" infinite array theory as described in this report.)

The large number of elements in the lens arrays and the expected nominal periodicity within sections of each array suggests obtaining a first approximation of element currents from an infinite array analysis of each section since, within a

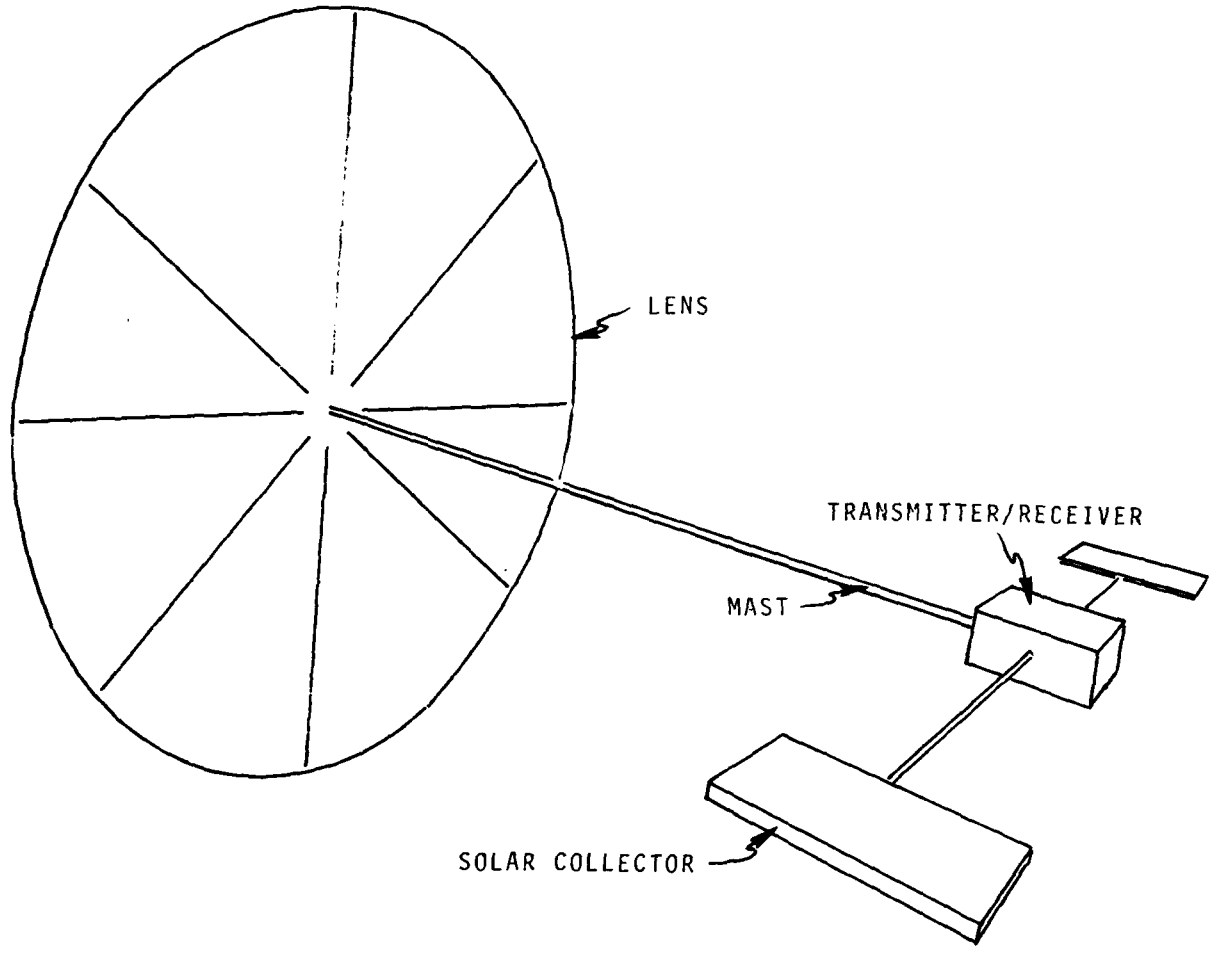

Figure 1-1. Lens Type Space-Based Radar (Side View)

section, periodic elements and nearly uniform module amplitude settings may be assumed. It is expected that, for limited scan angles, the currents on many elements within a section will assume these first-order solutions. The phased array simulator, therefore, makes extensive use of infinite array theory.

A successive approximation method is employed whereby infinite array analysis provides a first approximation of array currents and patterns. Higher approximations then are obtained, with relative ease, by methods that draw upon these first approximation currents. The higher approximations provide corrections to the currents on elements in the vicinity of discontinuities in module amplitude settings or periodicities; e.g., lens edges and section interfaces. Scattering from nearby structures, such as supports and hinges, also may be accounted for in the higher approximations.

The first approximation patterns, although involving large numbers of elements, are computed from closed form expressions. Since the number of elements with currents perturbed from their infinite array values is expected to be relatively small, higher approximation "correction patterns" may be computed by direct summation of the field from each element. The superposition of the first approximation and correction patterns results in the overall pattern. This approach takes maximum advantage of the nominal periodicities and largeness of the arrays. It is as computationally manageable in the radar receive mode as in the radar transmit mode without resorting to reciprocity. This is important since the modules may well be nonreciprocal. This approach also may avoid the need for a fast Fourier transform (FFT) for pattern computation. An FFT is not practical if, for example, fine angular pattern resolution in the vicinity of a null is required.

An infinite array analysis usually assumes plane wave excitation. During radar transmit, the illuminating field is expected to differ smoothly from a plane wave across the face of the lens. This difference is taken into account by expanding the beamformer field in plane waves and analyzing the lens separately for each plane wave component.

The first approximation infinite array method employed here is an extension of a moment method, plane wave expansion technique recently developed by Munk and Burrell.[1] It is applicable to lens arrays composed of arbitrarily-shaped wire radiating elements. The elements may be inclined with respect to the array plane. Feed line scattering, amplitude and phase adjust modules between the arrays, and an imperfect ground screen also are accounted for. In particular, this technique

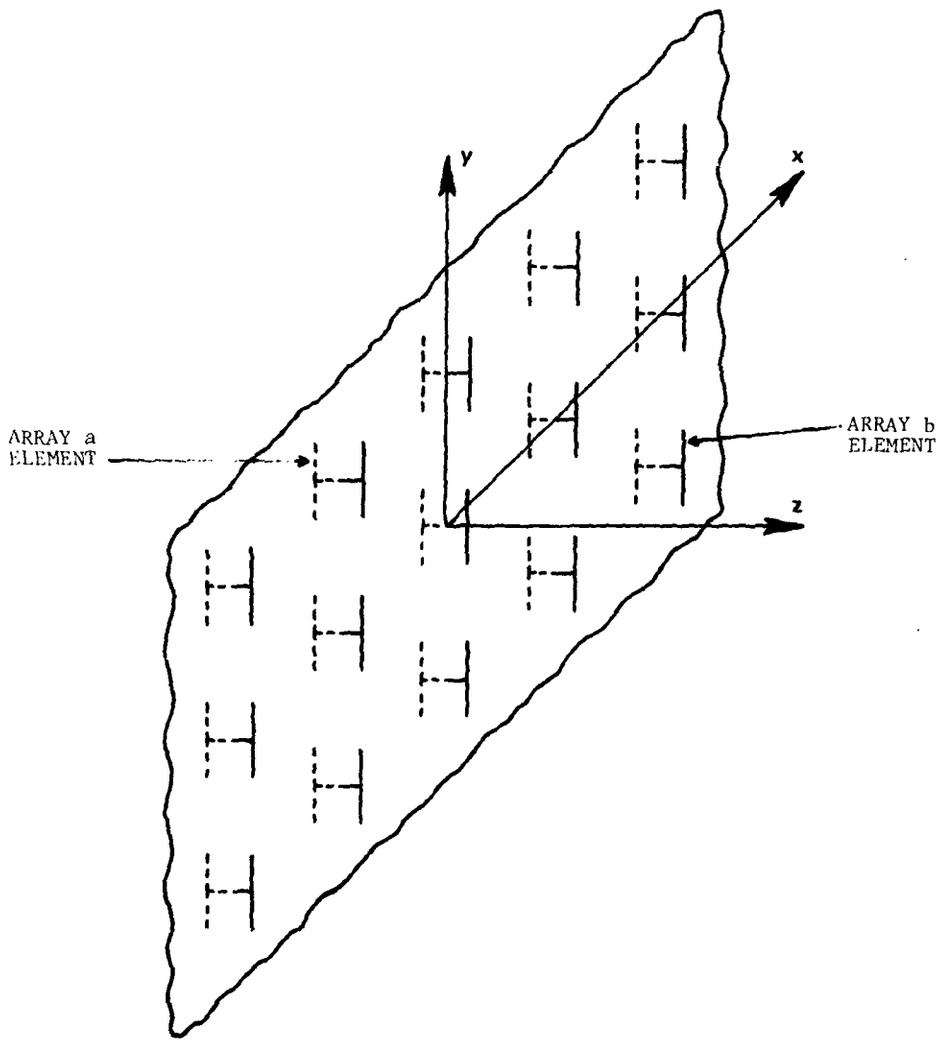

Figure 1-2. Dipole Lens With Ground Screen

permits the modules to be progressively phased, although the module-to-module amplitude adjustment is assumed uniform throughout. The plane wave expansion technique facilitates computing the array-to-array coupling through the imperfect ground screen and suggests straightforward extensions, not discussed here, applicable to dielectric support sheets (e.g., Kevlar and Kapton) on which the radiators may be mounted.

The infinite array lens analysis facilitates computation by providing the first approximation solution to a perturbation problem; it also provides clues to the performance of several important finite (but large) lens characteristics. For example, the array active impedance variation with module phase setting, an important parameter for module designers, can be assessed directly. The effect of imperfect ground screen "feedback" from the target side to the feed side of the lens also can be observed.

A general discussion of the simulator and its current design status is contained in Section 2. A detailed theoretical discussion follows in Section 3. The programming and data flow are discussed in Section 4. Preliminary results and validation are given in Section 5.

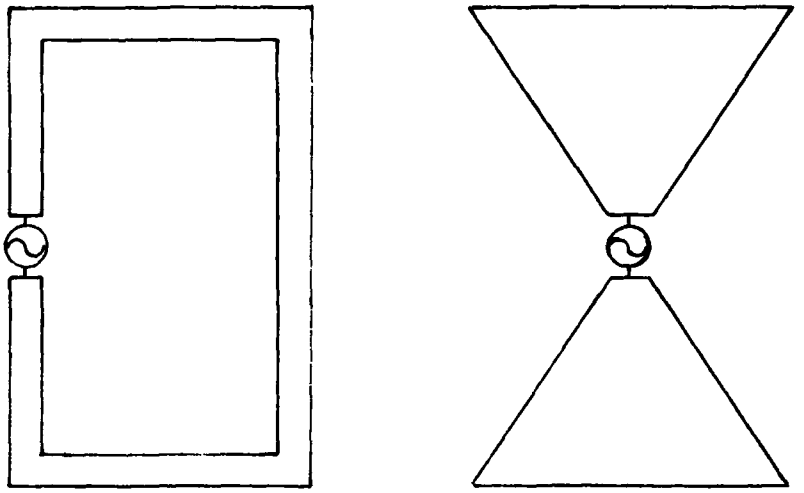

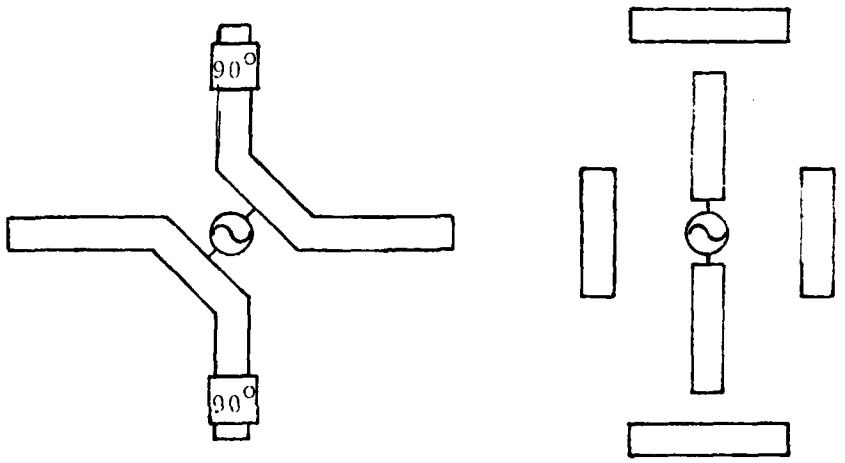

Figure 1-3. Example Array Elements

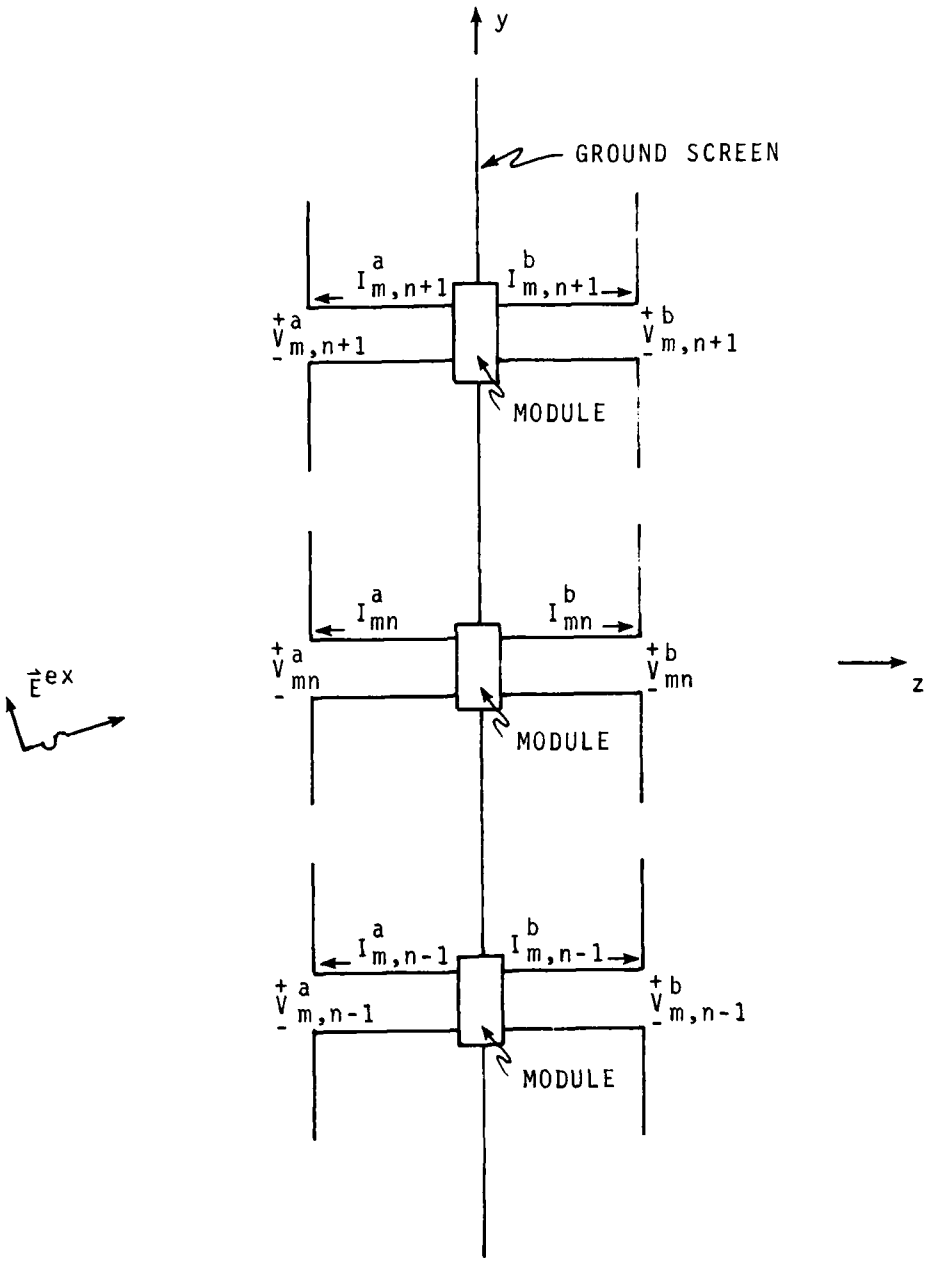

Figure 1-4. Cross Section of Lens

SECTION 2

DISCUSSION

2.1 SIMULATOR CAPABILITIES

The simulator for analyzing candidate SBR phased array lenses must predict the RF impact of the lens on the following SBR gain performance factors:

1. Beam scan coverage,
2. Main beam and sidelobe beam widths, positions, and levels,
3. Null depths and positions,
4. Effective radiated power,
5. Available received power, and
6. Bandwidth

These performance factors must be evaluated as a function of several lens parameters:

1. Structure fabrication and deployment variations
   a. Array lattice tolerance
   b. Element orientations and locations relative to ground screen
2. Space environment effects (heating, etc.); e.g., lens warping
3. Module phase and amplitude variations
   a. Production tolerances
   b. Failures

The sumulator, besides analyzing large periodic planar arrays, thus must account for the effects of lens warping, discontinuous periodicities, and edge elements.

The ground screen for a candidate lens is expected to be of coarse mesh construction to minimize overall weight and temperature gradient effects. For an active lens, where the modules impart gain, the isolation between illuminated and nonilluminated arrays may not sufficiently suppress the "feedback" penetration coupling between these arrays. This interarray radiation coupling must be included in simulations.

The array lattices may be triangular or rectangular; thus, simulations must apply to general rectilinear arrays. The array elements may be turnstiles, dipoles, folded dipoles, etc. They may have parts inclined with respect to the array plane; e.g., V-type dipoles. The effects of scattering from the feed lines and unbalanced mode feed line radiation also must be considered.

A phased array lens simulator, therefore, must consider many effects in accurately modeling SBR lenses. This capability of the simulator leads naturally to its

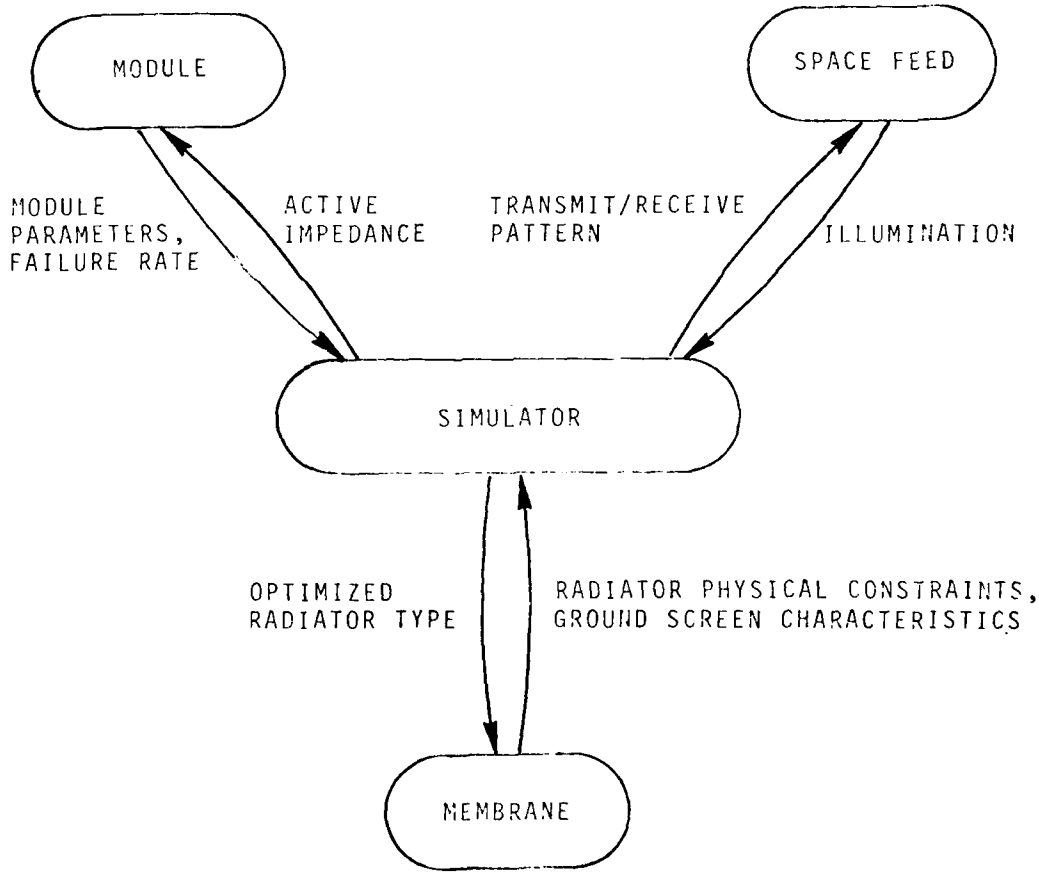

Figure 2-1. Simulator as a Design Tool

use as a lens design tool as well as a means for evaluating designs. The interaction between the simulator and the designing membranes (radiating elements and ground screen), modules, and space feeds is shown in Figure 2-1. The membrane designers can decide on array lattice size and type (rectangular, equilateral triangular, etc), ground screen transmission characteristics, and radiating element physical constraints. The simulator then can be used to "optimize" the choice of a radiating element type, shape, and size within these constraints such that active impedance variation with scan is minimized. The latter is important in module design.

2.2 CURRENT STATUS, FUTURE IMPROVEMENTS, AND EXTENSIONS

The status of key components of the phased array lens simulator is shown in Table 2-1.

The theory category is subdivided into "general" and "detailed." A detailed description includes all equations down to the lowest level. A completed "code" refers to flow charts as well as a computer program. A satisfactory "debug" indicates the code is implemented and providing reasonable results. A successful "validation" connotes agreement with other methods in solving special problems. These other methods could be theoretical, computational, or experimental. Validated results are presented in Section 5. A detailed plan for validating all aspects of the simulator is being prepared and will be published in a separate document.

The only component of the simulator that is not expected to be completed under the current contract is "support structure scattering." A major effrot is required here to implement a geometrical theory of diffraction within the higher approximation moment method code. Another extension to the simulator, not currently envisioned, that fits well within the general framework of a plane wave expansion moment method, is the capability of including the effects of dielectric support sheets such as Kevlar or Kapton. A number of improvements for increasing the computational efficiency and data handling also can be investigated in subsequent efforts; e.g., optimizing the choice of current expansion functions in the infinite array moment method technique. Other methods for improving efficiency will be implemented if time permits (Section 3.2.8).

TABLE 2-1

PHASED ARRAY LENS SIMULATOR DESIGN/IMPLEMENTATION STATUS

	Theory		Code	Debug	Validation	Section
	General	Detail				
Data Management	X	X				4
First Approximation						3.2, 3.4
Impedance Matrix						
Planar Elements	X	X	X	X	X	3.2.2, 3.2.4
Feed Line Scattering	X	X				3.2.3
Feedback Coupling	X	X	X			3.2.1, 3.2.6
Generalized Module	X	X				3.2.6
Space Feed	X					3.2.5
Radiation Pattern	X	X				3.4
Higher Approximations						3.3
Currents	X	X				3.3.1
Radiation Pattern	X	X				3.4
Support Structure Scattering	X					3.3.2

SECTION 3

THEORY

This section describes the theoretical foundation for the phased array lens simulator. Although the theory is directly applicable to active lenses composed of arrays of metallic radiators (dipoles, turnstiles, etc.), it can, with straightforward modification, be extended to apply to other lens types such as those composed of microstrip arrays. The theoretical development is not complete. Most missing details, however, are relatively minor and are expected to be completed and implemented by the end of the current effort.

A theoretical overview is presented in Section 3.1. This is followed (Section 3.2) by a detailed discussion of the application and generalization of infinite array theory and the moment method in arriving at a first approximation to the array element currents. The general theory is described in Sections 3.2.1 and 3.2.2 as it applies to lenses restricted to rectangular array lattices, single-port array elements, planar radiating elements (e.g., no feedline scattering), and a specialized module model. The theoretical extensions that remove these restrictions, modeling of the space feed illuminating the lens, and techniques for increasing computational efficiency are discussed in Sections 3.2.3 through 3.2.8.

The theory for obtaining corrections to the infinite array currents is discussed in Section 3.3. A higher approximation method is developed that employs the infinite array currents as the initial solution in an iterative procedure that accounts for array edges, module failures, support structure scattering, etc.

The theory for efficiently computing the fields radiated by the array element currents is contained in Section 3.4.

3.1 OVERVIEW

The lens array simulator solves a steady state ($e^{j\omega t}$ temporal variation assumed) problem by a successive approximation method. This method is particularly applicable to lenses composed of many radiating elements (perhaps hundreds of thousands) in each of two parallel arrays. The first approximation is based on infinite array theory. This provides approximations to such parameters as radiating element currents, active impedances, coupling between arrays, and radiation patterns (by truncating the infinite array after the currents are found). The resulting radiating element currents are used in obtaining successively better approximations of these

parameters. In this manner, the nominally periodic nature of each of several sections of a lens can be used to advantage in simplifying the overall analysis. The impact of such effects as "feedback" radiation coupling between arrays and active impedance variation with scan can be assessed with infinite array theory alone since most of the elements are expected to appear as if they reside in infinite arrays. The first approximation thus is of use in lens design; e.g., for optimizing radiating element type (dipole, folded dipole, etc.) and ground screen design within such constraints as module load impedance limitations, overall lens weight, and cost.

3.1.1 First Approximation

Infinite array theory is applicable to large numbers of identical elements arranged periodically. A candidate lens is expected to be largely periodic; however, due primarily to manufacturing and deployment constaints, this periodicity is expected to differ between sections of the lens. In the first approximation method, since most sections will be large, infinite array theory is applied separately over each section -- called a "cell." The first approximation current solutions usually are highly accurate within each cell; they may be less accurate near the cell boundaries. Higher approximations for the currents on these elements will provide corresponding corrections to the radiated field (Section 3.1.2). Other anomolies in periodicity within a cell due, for example, to element module failures, also will be resolved by higher approximations. The number of elements requiring analysis beyond the first approximation is expected to be relatively few (perhaps hundreds rather than hundreds of thousands).

Each cell is defined by a periodic lattice, progressive module phasing, uniform module gains, uniform input and output impedances, and identical element orientations. Subdivision into cells is not determined solely by periodicity, but also by relative uniformity of module characteristics and settings, as well as other considerations discussed below.

The illumination across a cell during radar transmit will not be that of a uniform plane wave. Application of infinite array theory, therefore, requires plane wave decomposition of the illuminating incident field. Each plane wave excitation is analyzed and the resulting currents and patterns superimposed. Since a component plane wave excitation may have a phase distribution across the lens that differs from the progressive phase setting of the modules, and since the arrays may significantly couple via RF penetration through the ground screen as well as through the modules, "standard" infinite array theory alone is not adequate. (The reference to

standard infinite array theory here refers to an analysis of a periodic array of identical structures (elements) -- either plane wave or lumped circuit source excited -- where the latter are progressively phased along the array plane. Array elements generally are not identical for the lenses under consideration due to progressively phased modules.) The simulator therefore includes an extension to standard infinite array theory whereby "feedback" modes are identified. Each feedback mode assumes element currents related by (3-1) and (3-2); for simplicity, rectangular lattices are assumed.

$$I^a_{mn(u)} = I^a_{00(u)}\, e^{-jkmd_x(s_x+u\alpha_x)}\, e^{-jknd_y(s_y+u\alpha_y)} \tag{3-1}$$

$$I^b_{mn(u)} = I^b_{00(u)}\, e^{-jkmd_x[s_x+(u+1)\alpha_x]}\, e^{-jknd_y[s_y+(u+1)\alpha_y]} \tag{3-2}$$

Equation (3-1) applies for the illuminated array (array a); (3-2) applies for the nonilluminated array (array b)

where (see Figures 1-2 and 1-4)

m and n are the array element identifying integers (positive and negative where m = n = 0 refers to the "reference" element)

d_x and d_y are the x and y interelement spacings

α_x and α_y are the module x and y directed progressive phase "directional cosine" components

s_x and s_y are the incident plane wave x and y directional cosines

u is the feedback mode integer (u = 0, 1, 2, ...)

k is the propagation constant

The total currents, I^a_{mn} and I^b_{mn}, are obtained by superimposing all feedback mode currents; i.e.,

$$I^a_{mn} = \sum_u I^a_{mn(u)} \tag{3-3}$$

$$I^b_{mn} = \sum_u I^b_{mn(u)} \tag{3-4}$$

The feedback mode reference element currents can be determined iteratively, under certain conditions, by solving first for the zeroth mode currents (u = 0) and so forth (Section 3.2.1). Each higher order mode current is dependent on previous mode computations, but each involves essentially standard infinite array theory.

That (3-1) is a reasonable representation can be argued as follows. The array a current phasing is influenced by the phasing of the incident field. The modules impart an additional phase prior to inducing array b currents. The resulting array b currents radiate through the ground screen and induce an "additional" component of array a currents. The latter, phased by the modules, induces a corresponding component of array b currents and the process continues.

The standard infinite array analysis employed is based on a plane wave expansion formulation for the field from an infinite array of current dipoles developed by Munk and Burrell.[1] This formulation is incorporated into a "pulse expansion function, pulse weighting function" moment method solution for the element currents. Radiating elements that can be well represented as identical arbitrary collections of bent wires of differing radii thus can be analyzed by the simulator. The major portion of the computation time is used in determining a corresponding generalized impedance matrix [Z]. This matrix relates pulse expansion functions in typical moment method fashion with the understanding that each expansion function now is a progressively phased infinite array of current "pulses." It is necessary to solve for the reference element current only since the uniform amplitude, progressive phasing of the element excitation implies the same relationship for the element currents. The matrix equation that must be solved is

$$[Z]\ \bar{I} = \bar{V} \tag{3-5}$$

where the column vectors $\bar{I}$ and $\bar{V}$ correspond to the reference element current distribution and excitation, respectively. The number of simultaneous equations expressed by (3-5) is limited to the number of pulses on a single element; thus, "matrix solution" consumes little computational time. By far the most computational time is used in computing the matrix elements of [Z]. Each matrix element computation involves a truncated doubly-infinite series which is slowly convergent; also, [Z] is not completely independent of excitation. The matrix must be recomputed, for example, for a change in scan angle.

First approximation radiation patterns are computed by superimposing the radiation from each feedback mode current to obtain "total" cell patterns and then superimposing these cell patterns. Since each cellular feedback mode current is a uniform amplitude, progressively phased distribution -- as indicated by (3-2) -- each corresponding radiation pattern is computed easily by pattern multiplication. The simulator employs a closed-form expression for the array factor which applies to a general rectilinear lattice and corresponding cell boundary.

Lens warping is modeled in the simulator by tilting cells to best fit the curvature. Since each cell must be planar, the accuracy with which a warp is to be modeled will impact on the choice of cell size. Greater accuracy usually will result from larger numbers of smaller cells.

3.1.2 Higher Approximations

First approximation currents on array elements near cell boundaries and discontinuous periodicities (e.g., module failure) within a cell are likely to be in error. Corrections are provided by higher approximations; thus, the higher approximation method is applied only in the neighborhood of cell boundaries and other discontinuous periodicities. The higher approximation method can include the effects of scattering from support booms and struts, ground screen edges and creases, etc., in a straightforward manner.

The higher approximation method makes use of first approximation feedback fields penetrating the ground screen and the fields radiated by first approximation currents on neighboring elements. These fields, in addition to the illuminating incident field, form a known excitation from which the second approximation current on an array a element, $I^{(2)a}$, and the current on its array b counterpart, $I^{(2)b}$, are computed. This computation employs a "free space" thin wire moment method in a straightforward manner. Since the radiation coupling through the ground screen is approximated by the first approximation array b to array a feedback fields, the only coupling between the arrays that must be solved "simultaneously" is the module feed line coupling. The latter is incorporated easily in the moment method. The number of neighboring elements, L, that must be considered in this computation is determined by observing the convergence of $I^{(2)a}$ and $I^{(2)b}$ as L is increased. This number is not expected to be large ($L \leq 40$) for reasonable interelement spacings ($\geq \lambda/2$) and most scan angles. The order of the moment method matrix equation that must be solved -- one for each array (a and b) -- is limited to the number of expansion functions on a single radiating element.

The third and higher approximations are obtained in a similar manner. Each approximation uses the previous approximations's currents to obtain the contribution to the exciting fields from neighboring elements. The feedback field remains the same as that computed in the first approximation except for a scalar multiplicative adjustment. The latter is determined as the ratio of most recent port current approximation to first port current approximation for the array b element under consideration.

The corresponding higher approximation radiated field corrections are obtained by summing the fields radiated by the relatively few array elements that undergo higher approximation current corrections.

3.2 FIRST APPROXIMATION CURRENTS

A combined infinite array/moment method technique is applied in obtaining a first approximation of the array element currents in a cell. (A cell is defined in Section 3.1.1 as a section of a lens.) This method is an extension of that developed by Munk and Burrell.[1] It is applicable to a large lens section (cell) composed of identical arbitrarily bent wire radiating elements in each of two parallel arrays; each array may have different elements. It also accounts for amplitude and phase adjust modules interconnecting the arrays and an imperfect ground screen between the arrays. In particular, the technique permits the modules to be progressively phased although the module amplitude adjustments must be uniform throughout the cell.

3.2.1 Port Representation and Solution

A lens formed by two infinite dipole arrays, a and b, in periodic lattices on either side of a finitely conducting infinite ground screen is shown in Figure 1-2. The two arrays and ground screen are parallel. A coordinate system with x and y axes located on the screen also is shown. An exciting plane wave, $\vec{E}^{ex}$, is assumed arriving from the negative z side (behind the screen) and directly incident on array a (Figure 1-4); amplitude and phase adjust modules connect array a to array b. Array a faces the radar transmitter during radar transmit; array a faces the target during receive. Array a thus is always on the illuminated side and array b is always on the nonilluminated side.

The following analysis of this lens is not restricted to dipole array elements. Each element can be a collection of thin bent wires; e.g., folded dipole or dipole with parasitic scatterers. For simplicity, all wires comprising an element are assumed to lie in their respective array plane. This restriction is removed in Section 3.2.3, where elements inclined with respect to the array plane and feed line scattering are considered.

Array a elements may differ from array b elements; however, each element within an array is assumed identical and lying in a rectangular lattice. A generalization to arbitrary rectilinear (triangular, etc.) lattices is described in Section 3.2.4.

The analysis is structured around a port representation. Each pair of terminals entering an array element is assumed to be a port; thus, unbalanced mode currents at each terminal pair are neglected. The module-to radiator feed lines are considered part of the modules. Multiports and unbalanced mode currents are considered in Section 3.2.7.

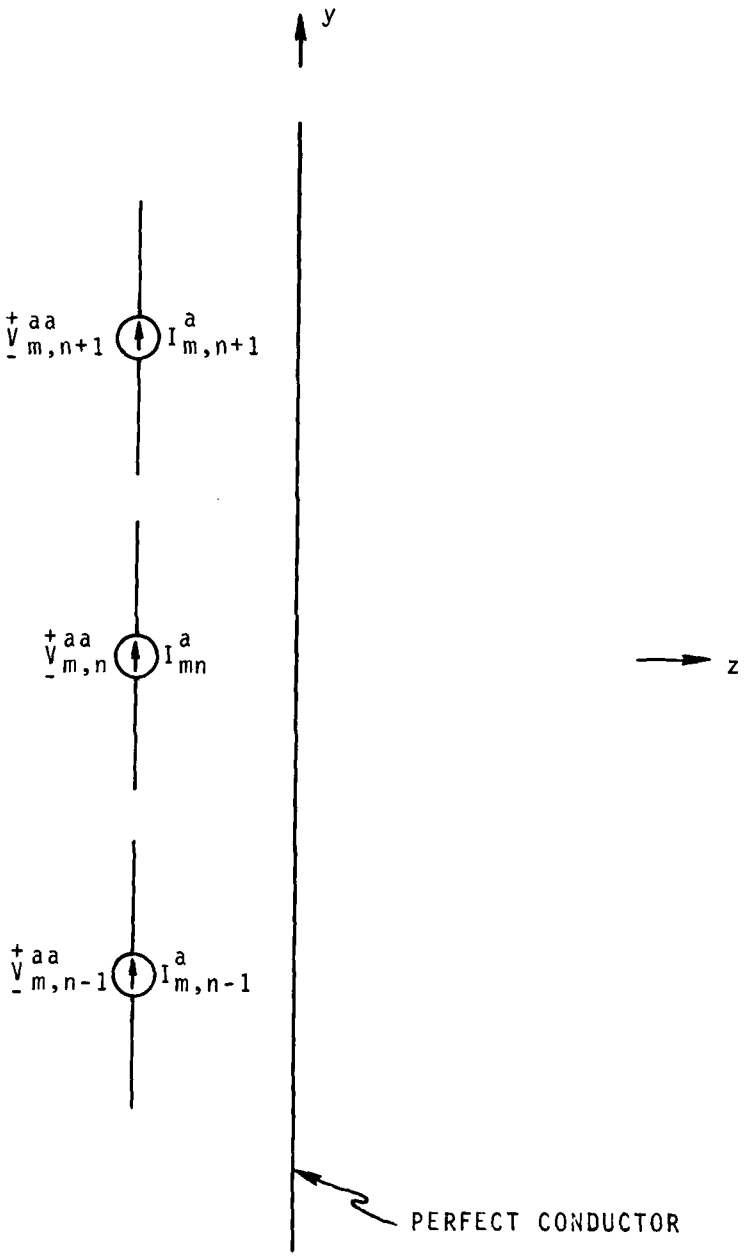

Figure 3-1. Problem Defining V^{aa}_{mn}

The port voltages and currents* are shown in Figure 1-4. The superscript (a or b) indicates the array and the subscript the element location; e.g., mn denotes the m^{th} column from the yz plane and n^{th} row from the xz plane. The m = 0 and n = 0 elements lie on the z axis and are referred to as the reference elements.

Array a and array b port currents are determined by requiring that they satisfy the port boundary conditions

$$V^a_{mn} = V^{aa}_{mn} + V^{ab}_{mn} + V^{ex}_{mn} \tag{3-6}$$

$$V^b_{mn} = V^{bb}_{mn} \tag{3-7}$$

where

V^a_{mn} and V^b_{mn} are related to I^a_{mn} and I^b_{mn} via the mn^{th} module (including feed lines) two-port parameters

V^{aa}_{mn} is the array a mn^{th} element port voltage with $\vec{E}^{ex} = 0$, the ground screen assumed perfectly conducting, and the array a ports excited with the I^a_{mn} as ideal current sources (Figure 3-1)

V^{bb}_{mn} is the array b counterpart to V^{aa}_{mn}

V^{ab}_{mn} is the array a mn^{th} element port voltage with $\vec{E}^{ex} = 0$, all array a ports open-circuited, and the I^b_{mn} as ideal current sources exciting the array b ports (Figure 3-2)

V^{ex}_{mn} is the array a mn^{th} element port voltage with all array a ports open-circuited and the ground plane assumed perfectly conducting (Figure 3-3)

In arriving at (3-6) and (3-7), the finite conductivity of the ground screen is considered significant with regard to feedback from array b to array a. Severe pattern degradation may result if the module amplification is comparable to the ground screen attenuation; therefore, it is important to preserve this effect in the model.

The solution of (3-6) and (3-7) is based on techniques recently developed by Munk and Burrell.[1] Each array element is modeled as piecewise linear and the array is viewed as a collection of infinite arrays, each one corresponding to one linear segment. Since the excitation is assumed to be a plane wave, the relationship of

*Phasors associated with $e^{j\omega t}$ temporal variation are assumed throughout.

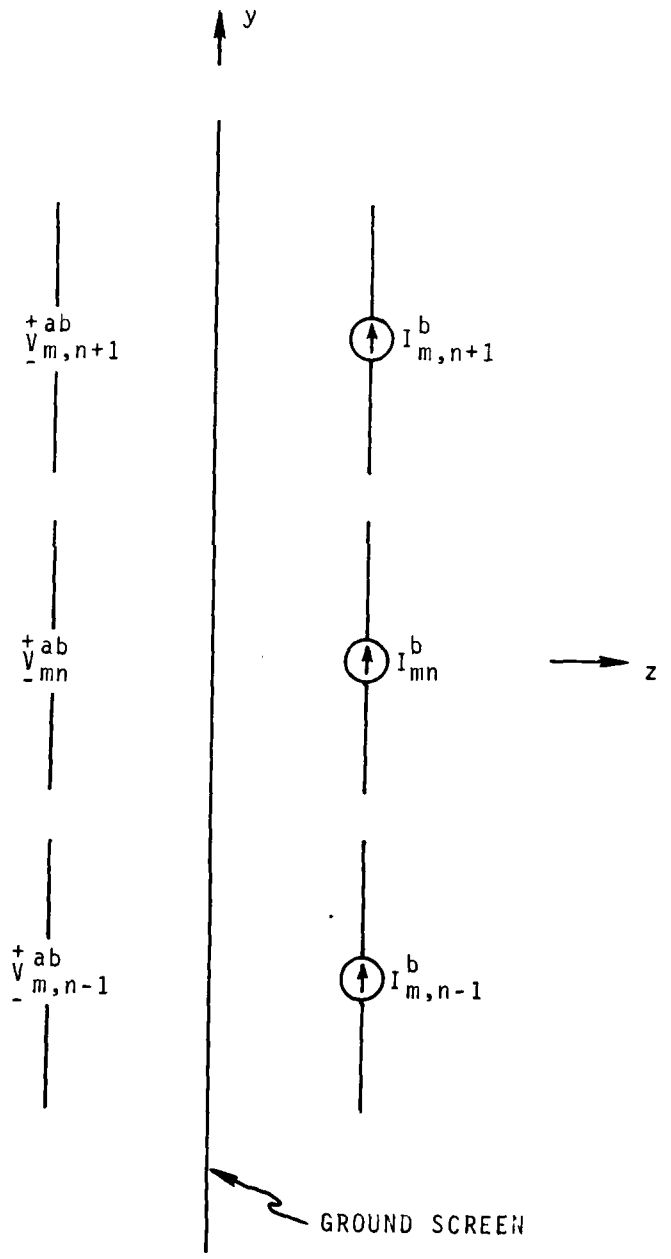

Figure 3-2. Problem Defining V^{ab}_{mn}

the current on the mn^{th} element to the reference (00^{th}) element current is known. It therefore is necessary to solve for the reference element current only. A moment method procedure can be applied where each expansion function is an infinite array of currents corresponding to one linear segment. The field from each "expansion array" is expressed as a doubly infinite sum of plane waves. One advantage of this plane wave expansion is that penetration through imperfect ground screens becomes straightforward.

The method presented here is an extension of Munk and Burrell's work in that interconnecting modules are introduced between arrays and, more importantly, the modules may differ from element to element. In particular, the modules will introduce a linear progressive phase and thus differ in a well-defined manner. The modules are identical for the plane wave excitation

$$\vec{E}^{ex}(\vec{r}) = \vec{E}^{ex}(\vec{0})\, e^{-jks_x x}\, e^{-jks_y y}\, e^{-jks_z z} \tag{3-8}$$

The induced port currents become

$$I^a_{mn} = I^a_{00}\, e^{-jkmd_x s_x}\, e^{-jknd_y s_y} \tag{3-9}$$

$$I^b_{mn} = I^b_{00}\, e^{-jkmd_x s_x}\, e^{-jknd_y s_y} \tag{3-10}$$

where

$r = x\hat{x} + y\hat{y} + z\hat{z}$ is a field point

$\hat{x}, \hat{y}, \hat{z}$ are the rectangular coordinate system unit vectors

k is the propagation constant

s_x, s_y, s_z are the directional cosines of the propagation direction of $\vec{E}^{ex}$

d_x and d_y are the x and y interelement spacings

I^a_{00} and I^b_{00} are the reference element port currents.

The justification for (3-9) and (3-10) can be demonstrated from linearity considerations; a similar form applies to the induced port voltages. Equations (3-9) and (3-10) are not sufficiently general if the modules are progressively phased. If the phase imparted by the mn^{th} module with respect to the reference module is

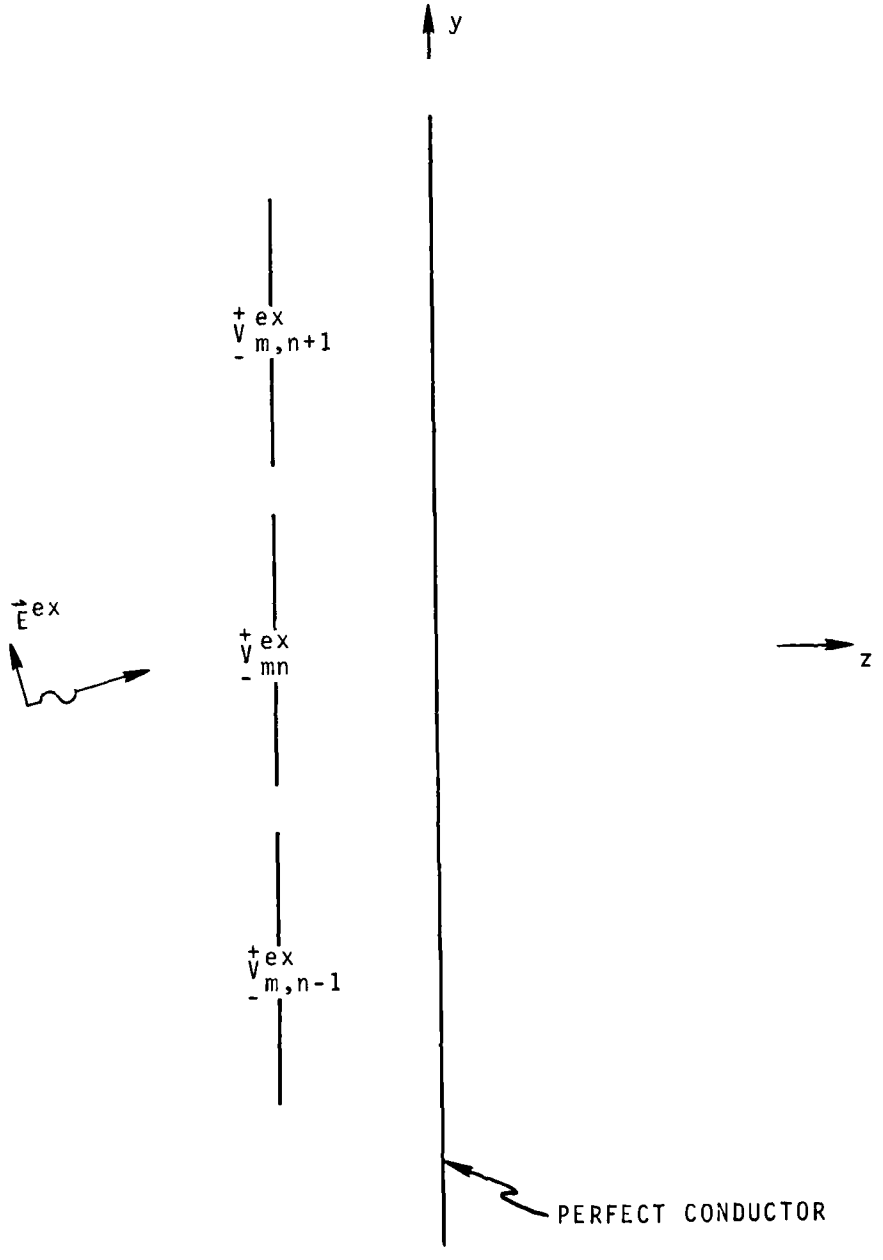

Figure 3-3. Problem Defining V^{ex}_{mn}

$-k\,(md_x\,\alpha_x + nd_y\,\alpha_y)$, the feedback phenomenon due to the imperfect ground screen suggests* port currents of the forms

$$I^a_{mn} = \sum_{u=0}^{\infty} I^a_{00(u)}\, e^{-jkmd_x(s_x+u\alpha_x)}\, e^{-jknd_y(s_y+u\alpha_y)} \tag{3-11}$$

$$I^b_{mn} = \sum_{u=0}^{\infty} I^b_{00(u)}\, e^{-jkmd_x[s_x+(u+1)\alpha_x]}\, e^{-jknd_y[s_y+(u+1)\alpha_y]} \tag{3-12}$$

where u is referred to as a feedback mode number. The $I^a_{00(u)}$ and $I^b_{00(u)}$ are the u^{th} mode coefficients of array a and array b reference element port currents determined, as described below, by satisfying (3-6) and (3-7) with (3-11) and (3-12).

With port currents expressed by (3-11) and (3-12), V^{aa}_{mn}, V^{bb}_{mn}, V^{ab}_{mn} in (3-6) and (3-7) become

$$V^{aa}_{mn} = \sum_{u=0}^{\infty} z^{aa}_{s_x+u\alpha_x,\,s_y+u\alpha_y}\, I^a_{00(u)}\, e^{-jkmd_x(s_x+u\alpha_x)}\, e^{-jknd_y(s_y+u\alpha_y)} \tag{3-13}$$

$$V^{bb}_{mn} = \sum_{u=0}^{\infty} z^{bb}_{s_x+(u+1)\alpha_x,\,s_y+(u+1)\alpha_y}\, I^b_{00(u)}\, e^{-jkmd_x[s_x+(u+1)\alpha_x]}\, e^{-jknd_y[s_y+(u+1)\alpha_y]} \tag{3-14}$$

$$V^{ab}_{mn} = \sum_{u=0}^{\infty} z^{ab}_{s_x+(u+1)\alpha_x,\,s_y+(u+1)\alpha_y}\, I^b_{00(u)}\, e^{-jkmd_x[s_x+(u+1)\alpha_x]}\, e^{-jknd_y[s_y+(u+1)\alpha_y]} \tag{3-15}$$

where

$z^{aa}_{s_x,s_y}$ is the array a active impedance when driven by port currents (3-9) and the ground screen perfectly conducting

$z^{bb}_{s_x,s_y}$ is the array b active impedance when driven by port currents (3-10) and the ground screen perfectly conducting

---

* The modules impart a phase on the array a currents. The resulting array b currents radiate through the ground screen and induce an "additional" component of array a currents. The latter, phased by the modules, results in a corresponding component of array b currents and the process continues.

$z^{ab}_{s_x,s_y}$ is the active mutual impedance from array b ports to array a ports with array b excited by port currents (3-10) and array a open-circuited (feed lines removed)

Specifically,

$$z^{aa}_{s_x,s_y} = \left.\frac{V^{aa}_{00}}{I^{a}_{00}}\right| \text{ perfect ground screen} \tag{3-16}$$

$$z^{bb}_{s_x,s_y} = \left.\frac{V^{bb}_{00}}{I^{b}_{00}}\right| \text{ perfect ground screen} \tag{3-17}$$

$$z^{ab}_{s_x,s_y} = \left.\frac{V^{ab}_{00}}{I^{b}_{00}}\right| \text{ imperfect ground screen, array a ports open-circuited} \tag{3-18}$$

where I^{a}_{00} and I^{b}_{00} are reference element port currents with the arrays excited by port currents related by (3-9) and (3-10). A moment method technique for computing $z^{aa}_{s_x,s_y}$, $z^{bb}_{s_x,s_y}$, and $z^{ab}_{s_x,s_y}$, based on Munk and Burrell's work, is described in Section 3.2.2. An expression for the short-circuit array a port currents

$$I^{ex}_{mn} = I^{ex}_{00}\, e^{-jkmd_x s_x}\, e^{-jknd_y s_y} \tag{3-19}$$

due to $\vec{E}^{ex}$ with the ground screen perfectly conducting, is determined in Section 3.2.2. The V^{ex}_{mn} in (3-6) then are given by

$$V^{ex}_{mn} = -\, z^{aa}_{s_x,s_y}\, I^{ex}_{mn} = -\, z^{aa}_{s_x,s_y}\, I^{ex}_{00}\, e^{-jkmd_x s_x}\, e^{-jknd_y s_y} \tag{3-20}$$

where the reference direction for I^{ex}_{mn} is the same as for I^{a}_{mn} in Figure 3-1. Equation (3-20) can be derived by considering the V^{ex}_{mn} in Figure 3-3 as ideal voltage sources. The current flowing through these sources then is the superposition of currents due to $\vec{E}^{ex}$ with the V^{ex}_{mn} sources shorted and the V^{ex}_{mn} sources with $\vec{E}^{ex}$ removed. Since the open-circuit port currents are zero,

$$I^{ex}_{mn} + V^{ex}_{mn} \,/\, z^{aa}_{s_x,s_y} = 0 \tag{3-21}$$

and (3-20) follows.

The mn^{th} port voltages and currents are assumed related by the mn^{th} module (including feed lines) impedance parameters according to

$$V^a_{mn} = - z^{aa}_{mod} I^a_{mn} - z^{ab}_{mod} I^b_{mn} \tag{3-22}$$

$$V^b_{mn} = - z^{ba}_{mod} e^{-jkmd_x \alpha_x} e^{-jknd_y \alpha_y} I^a_{mn} - z^{bb}_{mod} I^b_{mn} \tag{3-23}$$

For simplicity, the module progressive phase setting appears only in the array a to array b mutual impedance parameter. General module models are considered in Section 3.2.6. In combination with (3-11) and (3-12), (3-22) and (3-23) become

$$V^a_{mn} = - z^{aa}_{mod} \sum_{u=0}^{\infty} I^a_{00(u)} e^{-jkmd_x(s_x+u\alpha_x)} e^{-jknd_y(s_y+u\alpha_y)} - z^{ba}_{mod} \sum_{u=0}^{\infty} I^b_{00(u)} e^{-jkmd_x[s_x+(u+1)\alpha_x]} e^{-jknd_y[s_y+(u+1)\alpha_y]} \tag{3-24}$$

$$V^b_{mn} = - z^{ba}_{mod} \sum_{u=0}^{\infty} I^a_{00(u)} e^{-jkmd_x[s_x+(u+1)\alpha_x]} e^{-jknd_y[s_y+(u+1)\alpha_y]} - z^{bb}_{mod} \sum_{u=0}^{\infty} I^b_{00(u)} e^{-jkmd_x[s_x+(u+1)\alpha_x]} e^{-jknd_y[s_y+(u+1)\alpha_y]} \tag{3-25}$$

Equations (3-6) and (3-7), in combination with (3-13), (3-14), (3-15), (3-20), (3-24), and (3-25) become, after dividing through by $e^{-jkmd_x s_x} e^{-jknd_y s_y}$ and grouping terms,

$$\sum_{u=0}^{\infty} z^{aa}_u e^{-jkmd_x u\alpha_x} e^{-jknd_y u\alpha_y} I^a_{00(u)} + \sum_{u=0}^{\infty} z^{ab}_{u+1} \left[e^{-jkmd_x(u+1)\alpha_x} e^{-jknd_y(u+1)\alpha_y} I^b_{00(u)} \right] = z^{aa}_{s_x, s_y} I^{ex}_{00} \tag{3-26}$$

$$\sum_{u=0}^{\infty} e^{-jkmd_x(u+1)\alpha_x} e^{-jknd_y(u+1)\alpha_y} \left[z^{ba}_{mod} I^a_{00(u)} + z^{bb}_{u+1} I^b_{00(u)} \right] = 0 \tag{3-27}$$

where

$$z^{aa}_u = z^{aa}_{mod} + z^{aa}_{s_x+u\alpha_x,\ s_y+u\alpha_y}$$

$$z^{ab}_{u+1} = z^{ab}_{mod} + z^{ab}_{s_x+(u+1)\alpha_x, s_y+(u+1)\alpha_y}$$

$$z^{bb}_{u+1} = z^{bb}_{mod} + z^{bb}_{s_x+(u+1)\alpha_x, s_y+(u+1)\alpha_y}$$

Since the arrays are assumed infinite, corresponding to any practical module imparted phase shifts, $-kmd_x\alpha_x - knd_y\alpha_y$, the phasing of the modules repeats every rectangular section of M by N elements; i.e., M, M', N, and N' can be found such that

$$\frac{kd_x\alpha_x}{2\pi} = \frac{M'}{M} \tag{3-28}$$

$$\frac{kd_y\alpha_y}{2\pi} = \frac{N'}{N} \tag{3-29}$$

Equations (3-26) and (3-27) then become

$$\sum_{u=0}^{\infty} e^{-j2\pi muM'/M}\, e^{-j2\ nuN'/N}\, z^{aa}_u\, I^a_{00(u)} + \sum_{u=0}^{\infty} e^{-j2\pi m(u+1)M'/M} \left[e^{-j2\pi n(u+1)N'/N}\, z^{ab}_{u+1}\, I^b_{00(u)}\right] = z^{aa}_{s_x,s_y}\, I^{ex}_{00} \tag{3-30}$$

$$\sum_{u=0}^{\infty} e^{-j2\pi m(u+1)M'/M}\, e^{-j2\pi n(u+1)N'/N}\left[z^{ba}_{mod}\, I^a_{00(u)} + z^{bb}_{u+1}\, I^b_{00(u)}\right] = 0 \tag{3-31}$$

These equations must hold for all m and n. Premultiplication of each by $e^{j2\pi mvM'/M}\, e^{j2\pi nvN'/N}$, where v is an integer, summation over one "progressive phase period" $1 \le m \le M$ and $1 \le n \le N$, and interchange of summations results in

$$\sum_{u=0}^{\infty} \sum_{n=1}^{N} \sum_{m=1}^{M} \left[e^{j2\pi m(v-u)M'/M}\, e^{j2\pi n(v-u)N'/N}\right] z^{aa}_u\, I^a_{00(u)} + e^{j2\pi m(v-u-1)M'/M}\, e^{j2\pi n(v-u-1)N'/N}\, z^{ab}_{u+1}\, I^b_{00(u)} = \sum_{n=1}^{N} \sum_{m=1}^{M} e^{j2\pi mvM'/M}\, e^{j2\pi nvN'/N}\, z^{aa}_{s_x,s_y}\, I^{ex}_{00} \tag{3-32}$$

$$\sum_{u=0}^{\infty} \sum_{n=1}^{N} \sum_{m=1}^{M} e^{j2\pi m(v-u-1)M'/M} \, e^{j2\pi n(v-u-1)N'/N}$$

$$\left[z_{mod}^{ba} \, I_{00(u)}^{a} + z_{u+1}^{bb} \, I_{00(u)}^{b} \right] = 0 \tag{3-33}$$

Now

$$\sum_{n=1}^{N} \sum_{m=1}^{M} e^{j2\pi m(v-u)M'/M} \, e^{j2\pi n(v-u)N'/N} = 0 \tag{3-34}$$

unless $(v-u)M'/M$ and $(v-u)N'/N$ are both integers; similarly

$$\sum_{n=1}^{N} \sum_{m=1}^{M} e^{j2\pi m(v-u-1)M'/M} \, e^{j2\pi n(v-u-1)N'/N} = 0 \tag{3-35}$$

unless $(v-u-1)M'/M$ and $(v-u-1)N'/N$ are both integers. Assume that only lower ordered feedback modes are significant, as is expected to be the case if the ground screen attenuation sufficiently exceeds module amplification. Then, if M or N is sufficiently large, it follows that the terms in (3-32) and (3-33) containing the left-hand side of (3-34) can be assumed nonzero only for $u = v$ and the terms containing the left-hand side of (3-35) can be assumed nonzero only for $u = v - 1$.

The solutions to (3-32) and (3-33) then are determined iteratively as follows.

From (3-32), with $v = 0$,

$$z_{0}^{aa} \, I_{00(0)}^{aa} = z_{s_x,s_y}^{aa} \, I_{00}^{ex} \tag{3-36}$$

$$I_{00(0)}^{a} = \frac{z_{s_x,s_y}^{aa}}{z_{0}^{aa}} \, I_{00}^{ex} \tag{3-37}$$

From (3-33), with $v = 1$,

$$z_{mod}^{ba} \, I_{00(0)}^{a} + z_{1}^{bb} \, I_{00(0)}^{bb} = 0 \tag{3-38}$$

$$I_{00(0)}^{b} = - \frac{z_{mod}^{ba}}{z_{1}^{bb}} \, I_{00(0)}^{a} \tag{3-39}$$

or

$$I^{b}_{00(0)} = - \frac{z^{ba}_{mod}\, z^{aa}_{s_x,s_y}}{z^{bb}_{1}\, z^{aa}_{0}} \tag{3-40}$$

From (3-32), with v = 1,

$$z^{aa}_{1}\, I^{aa}_{00(1)} + z^{ab}_{1}\, I^{b}_{00(0)} = 0 \tag{3-41}$$

$$I^{a}_{00(1)} = - \frac{z^{ab}_{1}}{z^{aa}_{1}}\, I^{b}_{00(0)} \tag{3-42}$$

or

$$I^{a}_{00(1)} = \frac{z^{ab}_{1}\, z^{ba}_{mod}\, z_{s_x,s_y}}{z^{aa}_{1}\, z^{bb}_{1}\, z^{aa}_{0}}\, I^{ex}_{00} \tag{3-43}$$

And so forth; in general,

$$I^{a}_{00(u)} = - \frac{z^{ab}_{u}}{z^{aa}_{u}}\, I^{b}_{00(u-1)} \tag{3-44}$$

$$I^{b}_{00(u)} = - \frac{z^{ba}_{mod}}{z^{bb}_{u+1}}\, I^{a}_{00(u)} \tag{3-45}$$

for u = 1, 2, ... In conjunction with (3-11) and (3-12), equations (3-37), (3-44), and (3-45) solve the problem.

3.2.2 Plane-Wave Expansion Moment Method

The array a and b active impedances, $z^{aa}_{s_x,s_y}$, $z^{bb}_{s_x,s_y}$, array b to array a mutual impedance, $z^{ab}_{s_x,s_y}$, and the array a reference element short-circuit port current, I^{ex}_{00}, are considered in this section. The development is based upon the work of Munk and Burrell.[1]

Consider first either array a or array b with the ground screen absent. Let the array elements be composed of thin wires lying in the plane of the array. (The case of wires with components normal to the array plane can be handled by the procedure developed below if some formulas are replaced with those of Section 3.2.3). Let the array lie in the xy plane. A port voltage or current source array excitation that is uniform, except for the progressive phase $-jk\,(md_x\,s_x + nd_y\,s_y)$ imparted at the mn^{th} element with respect to the reference element ($m = n = 0$), results in the current

$$\vec{I}_{mn}(\vec{r}' + \vec{r}'_{mn}) = \vec{I}_{00}(\vec{r}')\; e^{-jkmd_x s_x}\; e^{-jknd_y s_y} \tag{3-46}$$

along the mn^{th} element wire axis, where $\vec{r}'$ is a point along the reference element wire axis (path C') and $\vec{r}'_{mn}$ is the vector from the reference element feed to the mn^{th} element feed. This form for $\vec{I}_{mn}(\vec{r}'+\vec{r}'_{mn})$ also will arise if the array is excited by a plane wave with directional cosines s_x, s_y, and s_z for the propagation direction. Under this excitation, once $\vec{I}_{00}(\vec{r}')$ is determined, the current on any array element is given by (3-46).

The boundary condition from which $\vec{I}_{00}(\vec{r}')$ is determined is

$$-\vec{E}^{s}_{tan} = \vec{E}^{ex}_{tan} - \vec{E}_{tan} \tag{3-47}$$

along the surface of the reference element, where $\vec{E}^{s}$ is the field radiated by all $\vec{I}_{mn}(\vec{r} + \vec{r}'_{mn})$, $\vec{E}^{ex}$ is an exciting plane wave in the absence of the array (impressed field), $\vec{E}$ is the total field, and the subscript "tan" denotes "component tangential to wire surface." Along perfectly conducting wires, $\vec{E}_{tan} = 0$ at all points except at a source port, where $\vec{E}_{tan}$ is the source field of an ideal port voltage source, V_{00}, and it is assumed that each mn^{th} element is excited by port voltage

$$V_{mn} = V_{00}\; e^{-jkmd_x s_x}\; e^{-jknd_y s_y} \tag{3-48}$$

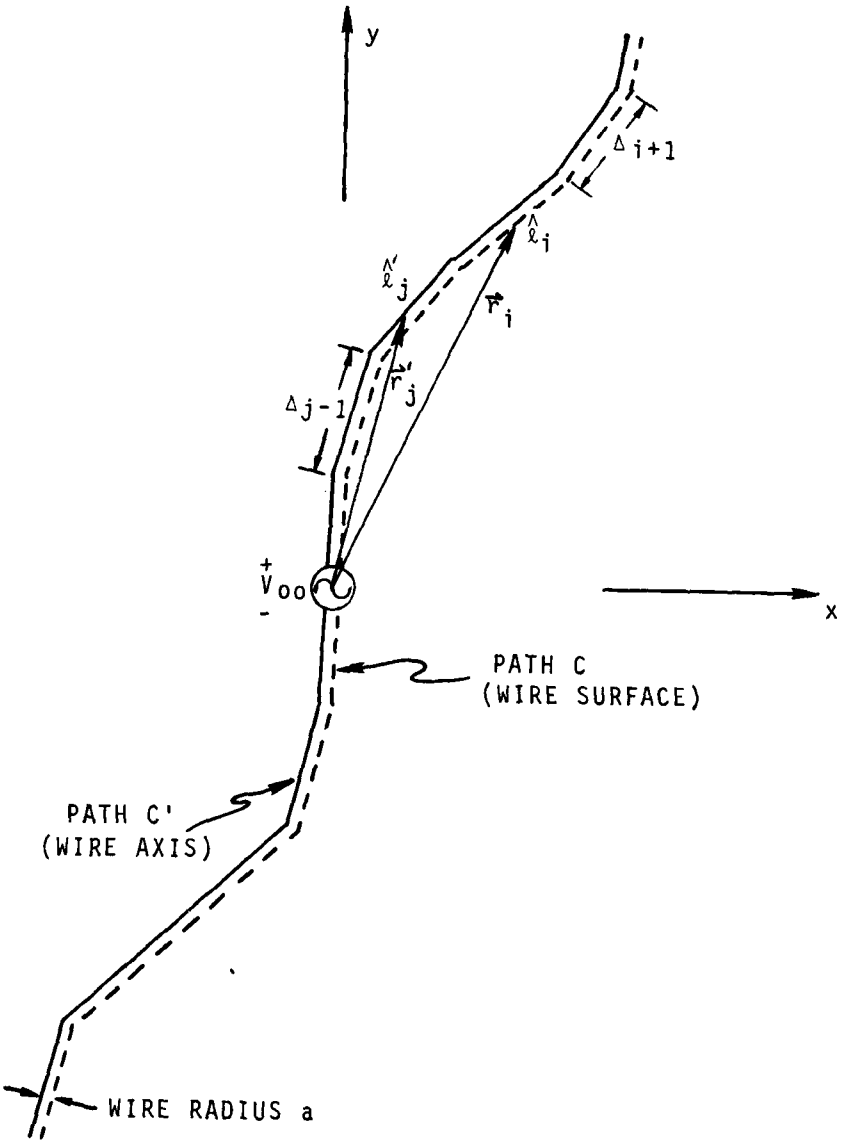

Figure 3-4. Curved Thin Wire Array Reference Element Modeled by Linear Segments

A moment method solution of the thin wire approximation of (3-47) results in an approximation of $\vec{I}_{00}(\vec{r}')$.[2] In this procedure, the wire axis of the reference element is approximated by an N_s straight line segment fit (Figure 3-4). The reference element may be composed of disjoint wires (as with parasitics) and also may have multiple wire junctions (as with top-loaded dipoles). First, $\vec{I}_{00}(\vec{r}')$ is expanded as

$$\vec{I}_{00}(\vec{r}') = \sum_{j=1}^{N_s} I_j \vec{f}_j(\vec{r}') \tag{3-49}$$

where $\vec{f}_j(\vec{r}')$ is an expansion of wire current constrained, for simplicity, to be non-zero only along the j^{th} segment of length Δ_j, and I_j is an unknown coefficient to be determined. The substitution of (3-49) into (3-47) results in

$$-\sum_{j=1}^{N_s} I_j \vec{E}^s_{tan}(r,j) = \vec{E}^{ex}_{tan} - \vec{E}_{tan} \tag{3-50}$$

where $\vec{E}^s(\vec{r},j)$ is the field radiated by the infinite array of j^{th} segment expansion functions, $\vec{f}_j(\vec{r}')\, e^{-jkmd_x s_x}\, e^{-jknd_y s_y}$. With respect to each of N_s weighting functions, $\vec{w}_i(\vec{r})$, the weighted average of (3-50) along a path, C, on the reference element wire surface parallel to C' (Figure 3-4), results in*

$$[Z]\bar{I} = \bar{V}^{ex} + \bar{V} \tag{3-51}$$

where the i^{th} elements of the N_s x 1 column vectors $\bar{I}$, $\bar{V}^{ex}$, and $\bar{V}$ are, respectively,

I_i

$$V_i^{ex} = \int_C \vec{E}^{ex} \cdot \vec{w}_i(\vec{r})\, d\ell \tag{3-52}$$

$$V_i = \int_C \vec{E} \cdot \vec{w}_i(\vec{r})\, d\ell \tag{3-53}$$

and the ij^{th} element of the N_s x N_s generalized impedance matrix [Z] is

$$Z_{ij} = -\int_C w_i(\vec{r}) \cdot \vec{E}^s_{tan}(\vec{r},j)\, d\ell \tag{3-54}$$

---

* For convergence purposes, the path is taken a wire radius in front of the array plane.

where $d\ell$ is an increment of length along C. The reference directions for the paths C and C' are chosen to be the unit vectors $\hat{\ell}_i$ and $\hat{\ell}_j$, respectively, where $\vec{f}_j(\vec{r}') = f_j(\vec{r}')\hat{\ell}_j$ and $\vec{w}_i(\vec{r}) = w_i(\vec{r})\hat{\ell}_i$ (Figure 3-4).

In determing Z_{ij}, the field $\vec{E}^s$ is expanded in a double sum of plane waves as

$$\vec{E}^s(\vec{r},j) = \frac{\eta}{2d_x d_y} \sum_{p=-\infty}^{\infty} \sum_{q=-\infty}^{\infty} e^{-jk(\vec{r}-\vec{r}_j')\cdot\hat{g}_\pm} \vec{h}_{j\pm}\psi'_{j\pm} \tag{3-55}$$

for $(\vec{r}-\vec{r})\cdot\hat{z} \gtrless 0$ where

$$\psi'_{j\pm} = \sum_{-\Delta j/2}^{\Delta j/2} f_j(\vec{r}')\, e^{jk(\hat{\ell}_j'\cdot\hat{g}_\pm)\ell'}\, d\ell' \tag{3-56}$$

r_j' = position vector to the center point of the j^{th} segmert along C'

η = free space wave impedance

$$\vec{h}_{j\pm} = \frac{1}{g_z}(\hat{\ell}_j' \times \hat{g}_\pm) \times \hat{g}_\pm$$

$$\hat{g}_\pm = \hat{x}(s_x + p\frac{\lambda}{d_x}) + \hat{y}(s_y + q\frac{\lambda}{d_y}) \pm \hat{z}\, g_z$$

$$g_z = \left[1 - \left[s_x + p\frac{\lambda}{d_x}\right]^2 - \left[s_y + q\frac{\lambda}{d_y}\right]^2\right]^{1/2}$$

λ = free space wavelength

If the expression under the radical in g_z is negative, g_z is chosen to be negative imaginary; if the expression is positive, g_z is nonnegative real. This assures that all plane wave modal fields travel outward from the array plane and nonpropagating modes attenuate. A plus sign subscript on $\vec{h}_j$, $\hat{g}$, and ψ_j' corresponds to field points $\vec{r}$ in front of the array plane; i.e., $(r - r_j')\cdot\hat{z} > 0$. A minus sign subscript corresponds to field points behind the array plane; i.e., $(r-r_j')\cdot\hat{z} < 0$.

Equation (3-55) is obtained by integrating, with respect to ℓ' over the j^{th} segment, the expression for the field radiated by an infinite array of point current dipoles, $f_j(\vec{r}')\ d\ell'$ (Appendix A).[1] The more general case, where $\vec{f}_j(\vec{r}')$ extends over two or more segments bent with respect to each other, can be treated in a similar,

although more complicated, fashion. Except for notational difference, (3-55) follows the development of Munk and Burrell.[1]

If $\vec{w}_i(\vec{r})$ is restricted to extend over only the i^{th} segment along C of length Δ_i, (3-54), with (3-55), becomes

$$Z_{ij} = -\frac{\eta}{2d_x d_y} \sum_{p=-\infty}^{\infty} \sum_{q=-\infty}^{\infty} e^{-jk(\vec{r}_i - \vec{r}'_j)\hat{g}_+} (\vec{h}_{j+} \cdot \hat{\ell}_i) \psi'_{j+} \psi_{i+} \tag{3-57}$$

where

$$\psi_{i\pm} = \int_{-\Delta_i/2}^{\Delta_i/2} e^{-jk\hat{\ell}_i \cdot \hat{g}_\pm \ell} w_i(\vec{r}) \, d\ell \tag{3-58}$$

and $\vec{r}_i$ = position vector to the center point of the i^{th} segment along C. Only the "+" sign is indicated for $\hat{g}_\pm$ (hence, also for $\psi'_{j\pm}$ and $\vec{h}_{j\pm}$) in (3-57) since the simplying assumption of wires lying only in the xy plane permits choosing $\vec{r}$ as well as $\vec{r}_i$ with no z components. The more general expression for Z_{ij} is derived in Section 3.2.3.

The progressive phasings, s_x and s_y, which, for a particular p and q, cause g_z to be zero, can result in an infinite Z_{ij}. These progressive phasings correspond to "grating lobe singularities" since they correspond to grating lobes just entering the visible range; i.e., nonattenuating plane waves propagating along the array plane. This is one possible source of "blind spots" and rapidly varying active impedances with scan. This is only a "potential" condition for infinite Z_{ij} since, although g_z is in the denominator of $\vec{h}_{j+}$, in some situations a compensating effect occurs. Such is the case, for example, in E-plane scans with periodic infinite arrays of y directed dipoles not widely spaced in the x direction since $\vec{h}_{j\pm} \cdot \hat{\ell}_i = 0$ for p = 0 and q such that $g_z = 0$ (grating lobe singularity). The presence of a perfect ground screen potentially can inhibit a blind spot due to a grating lobe singularity as is shown below.

If the array is a distance d in front of a perfectly conducting infinite ground screen (positive z axis directed from ground screen to array as for array b), the field $\vec{E}^{s,gs}$ (r,j) at any point $\vec{r}$ in front of the ground screen excited by the infinite planar array corresponding to the j^{th} expansion function and its image is given by

$$\vec{E}^{s,gs}(\vec{r},j) = \frac{\eta}{2d_x d_y} \sum_{p=-\infty}^{\infty} \sum_{q=-\infty}^{\infty} e^{-jk(\vec{r}_i-\vec{r}_j)\cdot\hat{g}_\pm} \vec{h}_{j\pm} \psi_{j\pm}$$

$$- \frac{\eta}{2d_x d_y} \sum_{p=-\infty}^{\infty} \sum_{q=-\infty}^{\infty} e^{-jk(\vec{r}-\vec{r}_j+2d\hat{z})\hat{g}_+} \vec{h}_{j+}\psi_{j+} \qquad (3\text{-}59)$$

for $(\vec{r} - \vec{r}_j')\cdot\hat{z} \gtrless 0$. The first term in (3-59) is the ground screen absent contribution given by (3-55). The second term is contributed by the perfect ground screen. It is important to note that $\hat{\ell}_j'$ for the j^{th} expansion function and its image are identical due to the simplifying constraint that all wires lie parallel to the xy plane; i.e., d is independent of j. Thus, $\vec{h}_{j+}$ and ψ_{j+}' for the image term are the same as for the ground screen absent term. The $\vec{h}_{j-}$ and ψ_{j-}' do not occur in the image terms since only field points in front of the ground screen apply.

The ij^{th} element of the generalized impedance matrix for the array in front of a perfect ground screen $[Z^{gs}]$ is given by (3-54) with $\vec{E}^{s,gs}$ replacing $\vec{E}^{s}$; thus

$$Z_{ij}^{gs} = - \frac{\eta}{2d_x d_y} \sum_{p=-\infty}^{\infty} \sum_{q=-\infty}^{\infty} e^{-jk(\vec{r}_i-\vec{r}_j)\cdot\hat{g}_+} \vec{h}_{j+}\cdot\hat{\ell}_i\psi_{j+}\psi_{i+}$$

$$+ \frac{\eta}{2d_x d_y} \sum_{p=-\infty}^{\infty} \sum_{q=-\infty}^{\infty} e^{-jk(\vec{r}_i-\vec{r}_j+2d\hat{z})\cdot\hat{g}_+} \vec{h}_{j+}\cdot\hat{\ell}_i\psi_{j+}'\psi_{i+} \qquad (3\text{-}60)$$

As with (3-57) only the "+" signs for $\hat{g}_\pm$, $\vec{h}_{j\pm}$, and $\psi_{j\pm}'$ appear. A rearrangement of terms in (3-60) results in

$$Z_{ij}^{gs} = - \frac{j\eta}{d_x d_y} \sum_{p=-\infty}^{\infty} \sum_{q=-\infty}^{\infty} e^{-jk[(\vec{r}_i-\vec{r}_j')\cdot\hat{g}_+ + dg_z]} \sin(kdg_z)\, \vec{h}_{j+}\cdot\hat{\ell}_i\psi_{j+}\psi_{i+} \qquad (3\text{-}61)$$

It is apparent from (3-61) that Z_{ij}^{gs} is bounded at a grating lobe singularity since $\frac{\sin kdg_z}{g_z}$ is bounded as $g_z \to 0$ (g_z appears in the denominator of $\vec{h}_{j+}$). This ground screen suppression of a blind spot at a grating lobe singularity assumes the radiating elements lie in the array plane. If, for example, the dipole arms are inclined with respect to the array plane or feed line scattering is present, the ground screen may enhance the blind spot effect at a grating lobe singularity above what it would be if the ground screen is absent; thus, consideration of out-of-plane radiating elements (Section 3.2.3) is important.

With a ground screen present, (3-51) becomes

$$[Z^{gs}]\bar{I} = \bar{V}^{ex,gs} + \bar{V} \tag{3-62}$$

where the element of $\bar{V}^{ex,gs}$ are given by (3-52) with $\vec{E}^{ex}$ expanded to include its reflection from the perfect ground screen; thus, the i^{th} element of $\bar{V}^{ex,gs}$ is given by

$$V_i^{ex,gs} = \left[1 - e^{j2ks_z d}\right] V_i^{ex} \tag{3-63}$$

The shape of the expansion and weighting functions $\vec{f}_j(\vec{r}')$ and $\vec{w}_i(\vec{r})$ affect only $\psi'_{j\pm}$ and $\psi_{i\pm}$ in accordance with (3-56) and (3-58). If $f_j(\vec{r}')$ and $w_i(\vec{r})$ are unit "pulses," then

$$\psi'_{j\pm} = \Delta_j \frac{\sin[k(\hat{\ell}'_j \cdot \hat{g}_\pm)\Delta_j/2]}{k(\hat{\ell}'_j \cdot \hat{g}_\pm)\Delta_i/2} \tag{3-64}$$

and

$$\psi_{i\pm} = \Delta_i \frac{\sin[k(\hat{\ell}_i \cdot \hat{g}_\pm)\Delta_i/2]}{k(\hat{\ell}_i \cdot \hat{g}_\pm)\Delta_i/2} \tag{3-65}$$

The $\frac{\sin x}{x}$ forms in (3-64) and (3-65) exist for all values of x; however, care is required in their computation when x is near zero.

The array b active impedance, $z^{bb}_{s_x,s_y}$ then can be determined by solving (3-62) for the source segment, $i = i_s$, current coefficient, I_{i_s}, with $V_i^{ex,gs} = 0$ for all

i and $V_i = 0$ for all $i \neq i_s$. Then

$$z^{bb}_{s_x,s_y} = \frac{V_{i_s}}{I_{i_s}} \tag{3-66}$$

The array a active impedance, $z^{aa}_{s_x,s_y}$, can be obtained in the same manner.

The array a reference element short-circuit current, I^{ex}_{00}, can be determined by solving (3-62) for I_{i_s}. Now, however, $V_i = 0$ for all i and the elements of $\bar{V}^{ex,gs}$ are given by (3-63) with V^{ex}_i given by (3-52).

The array b to array a mutual coupling, $z^{ab}_{s_x,s_y}$, through the imperfect ground screen can be determined from (3-51) where [Z] is the array a generalized impedance matrix, $V_i = 0$ for all i, and the elements of $\bar{V}^{ex}$ are given by (3-52) with $\vec{E}^{ex}$ replaced by the field $\vec{E}^t$ transmitted through the ground screen with array b excited by current sources given by (3-10). (A means for determining $\vec{E}^t$ is discussed below.)

Thus

$$[Z^a]\bar{I}^a = \bar{V}^t \tag{3-67}$$

where the i^{th} element of V^t is

$$V^t_i = \int_{C^a} \vec{E}^t \cdot \vec{w}^a_i(\vec{r})\, d\ell \tag{3-68}$$

and the "a" superscript stands for "array a." The i_s element, $I^a_{i_s}$, in the solution vector, $\bar{I}^a$ of (3-67), is the short-circuit array a reference element port current. The reference element open-circuit voltage is

$$V^t_{00} = - z^{aa}_{s_x,s_y} I^a_{i_s} \tag{3-69}$$

as is justified by the argument following (3-20); thus,

$$z^{ab}_{s_x,s_y} = - \frac{z^{aa}_{s_x,s_y} I^a_{i_s}}{I^b_{00}} \tag{3-70}$$

The field $\vec{E}^t$ is obtained readily from knowledge of the plane wave transmission coefficients of the ground screen and the plane wave decomposition (3-55). The array b current is determined with array b excited with port current sources (3-10). The array b reference element current is obtained from the solution to (3-47) with $V_i^{ex} = 0$ for all i and

$$V_i = \begin{cases} 0 & i \neq i_s \\ z^{bb}_{s_x,s_y} I^b_{00} & i = i_s \end{cases} \tag{3-71}$$

The solution to (3-51), denoted $\bar{I}^b$, gives rise to the field

$$\vec{E}^i(\vec{r}) = \sum_{j=1}^{N_s} I^b_j \frac{\eta}{2d_x d_y} \sum_{p=-\infty}^{\infty} \sum_{q=-\infty}^{\infty} e^{-jk(\vec{r}-\vec{r}'_j)\hat{g}_-} \vec{h}_{j-\psi_{j-}} \tag{3-72}$$

incident on the ground screen where the subscripted negative signs indicate that (3-72) applies for $(\vec{r}-\vec{r}'_j)\cdot\hat{z} < 0$ (which is appropriate since the ground screen is behind array b). Since $\vec{E}^i$ is a superposition of plane waves, $\vec{E}$ is readily obtained by applying the proper transmission coefficients to each component plane wave. Each plane wave in (3-72) propagates in the $\hat{g}_-$ direction; thus, $\hat{g}_-$ and $\hat{z}$ (the normal to ground screen) form the corresponding "plane of incidence." A unit vector normal to the incidence plane is

$$\hat{n}_\perp = \frac{\hat{g}_- \times \hat{z}}{|\hat{g}_- \times \hat{z}|} \tag{3-73}$$

and a unit vector parallel to the incidence plane and normal to $\hat{g}_-$ is

$$\hat{n}_\parallel = \hat{g}_- \times \hat{n}_\perp \tag{3-74}$$

Any plane wave travelling in the $\hat{g}_-$ direction can be decomposed into two plane waves, one having the $\vec{E}$ field polarized along $\hat{n}_\perp$ and the other having the $\vec{E}$ field polarized along $\hat{n}_\parallel$. If $T_\perp$ and $T_\parallel$ are the corresponding transmission coefficients and $\hat{g}^t_-$ is the transmitted wave direction ($\hat{g}^t_- = -\hat{z}$ for a good conducting screen[3]),

then

$$\vec{E}^t(\vec{r}) = \sum_{j=1}^{N_s} I_j^b \frac{\eta}{2d_x d_y} \sum_{p=-\infty}^{\infty} \sum_{q=-\infty}^{\infty} e^{-jk(\vec{r}-\vec{r}_j')\hat{g}_-^t} [\hat{n}_\perp T_\perp (\hat{n}_\perp \cdot \vec{h}_{j-}) + \hat{n}_{||} T_{||} (\hat{n}_{||} \cdot \vec{h}_{j-})] \psi_{j-}^{t'} \tag{3-75}$$

where $\psi_{j-}^{t'}$ is ψ_{j-}' with $\hat{g}_-^t$ replacing $\hat{g}_-$.

The substitution of (3-75) into (3-68) results in

$$V_i^t = \sum_{j=1}^{N_s} I_j^b \frac{\eta}{2d_x d_y} \sum_{p=-\infty}^{\infty} \sum_{q=-\infty}^{\infty} e^{-jk(\vec{r}-\vec{r}_j')\hat{g}_-^t} \left[(\hat{\ell}_i \cdot \hat{n}_\perp) T_\perp (\hat{n}_\perp \cdot \vec{h}_{j-}) + (\hat{\ell}_i \cdot \hat{n}_{||}) T_{||} (\hat{n}_{||} \cdot \vec{h}_{j-}) \right] \psi_{j-}^{t'} \psi_{i-}^{t} \tag{3-76}$$

and $z^{ab}_{s_x,s_y}$ is determined from (3-67) and (3-70) as previously discussed. In (3-76) ψ_{i-}^t is ψ_{i-} with $\hat{g}_-^t$ replacing $\hat{g}_-$.

3.2.3 Inclined Radiators and Feed Line Scattering

The development in Sections 3.2.1 and 3.2.2 is limited to array radiating elements oriented in the plane of the array. This method can be generalized to handle scattering from element feed lines and radiation and scattering from elements having arms inclined with respect to the array plane (Figure 3-5).

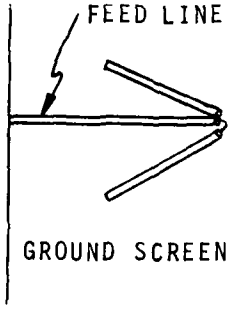

Figure 3-5. Coaxial-Fed Bent-Arm Dipole

Munk and Burrell [1, eq.(3)] obtain the expression for the field from an infinite planar array of point current dipoles. They indicate that this expression is valid for arbitrarily oriented dipoles; the dipoles need not be oriented parallel to the array plane. Munk and Burrell also mention that a moment method can be developed from this expression. This development is carried through for the special case of array elements composed of bent wires confined to the array plane (Section 3.2.2). Expressions based on [1, eq.(3)] that are similar to the mutual impedance expression [1, eq.(19)] given by Munk and Burrell are developed; however, [1, eq.(19)] was derived for the restricted case that mutually coupled antenna segments did not both pass through any plane parallel to the array plane. The generalization of the moment method to handle "out of plane" elements necessitates more complicated expressions. These are derived here.

The field $d\vec{E}$ at $\vec{r}$ due to an infinite planar rectangular array of point current dipoles

$$\vec{f}_{mn}\, d\ell = e^{-jkmd_x s_x}\, e^{-jknd_y s_y}\, f\, d\ell\, \hat{\ell}' \tag{3-77}$$

is given by

$$d\vec{E}(\vec{r},\vec{r}') = \frac{\eta}{2d_x d_y} \sum_{p=-\infty}^{\infty} \sum_{q=-\infty}^{\infty} e^{-jk(\vec{r}-\vec{r}')\cdot\hat{g}_{\pm}}\ \vec{h}_{\pm} f d\ell \tag{3-78}$$

$$(\vec{r}-\vec{r}')\cdot\hat{z} \gtrless 0$$

where the coordinate system is that of Figure 1-2, $\vec{r}'$ is the location of the reference element, m = n = 0, and the remaining variables are as defined in Section 3.2.2 with $\hat{\ell}_j'$ replaced by the unit vector $\hat{\ell}'$. This result is derived in Appendix A for the more general case of rectilinear (skewed grid) lattices. The modifications necessary to extend the results in this section, as well as those in the previous two sections, to general rectilinear lattices is discussed in Section 3.2.4.

Consider now a rectangular array of identical, but arbitrarily bent, thin wire radiator elements. Let the reference element, m = n = 0, be segmented in accordance with the moment method, as in Section 3.2.2, and let $f_j(\ell')$ be the

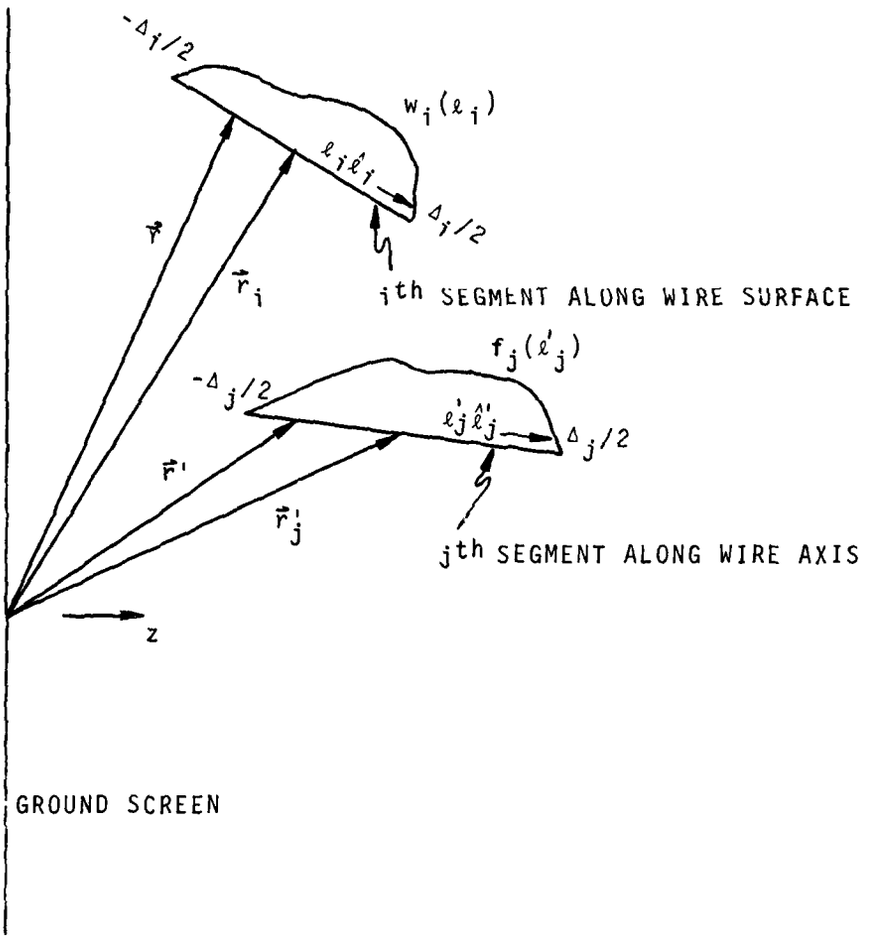

Figure 3-6. Expansion and Weighting Factors for Out-of-Plane Segments

reference element j^{th} segment expansion function. Then, with $\vec{r}' = \vec{r}_j' + \ell_j'\hat{\ell}_j'$ as defined in Figure 3-6,

$$d\vec{E}_j(\vec{r},\vec{r}') = \frac{\eta}{2d_x d_y} \sum_{p=-\infty}^{\infty} \sum_{q=-\infty}^{\infty} e^{-jk(\vec{r}-\vec{r}_j')\cdot\hat{g}_\pm} \vec{h}_{j\pm} e^{jk\ell_j'\hat{\ell}_j'\cdot\hat{g}_\pm} f_j(\ell_j')d\ell_j' \quad (3\text{-}79)$$

$$\text{if } (\vec{r}-\vec{r}_j')\cdot\hat{z} \lessgtr \ell_j'\hat{\ell}_j'\cdot\hat{z}$$

and

$$\vec{E}_j(\vec{r}) = \int_{j^{th}\text{segment}} d\vec{E}(\vec{r},\vec{r}') = \frac{\eta}{2d_x d_y} \sum_{p=-\infty}^{\infty} \sum_{q=-\infty}^{\infty} X_{pq}(\vec{r}) \quad (3\text{-}80)$$

where

$$X_{pq}(\vec{r}) = e^{-jk(\vec{r}-\vec{r}_j')\cdot\hat{g}_\pm} \vec{h}_{j\pm} \int_{-\Delta_j/2}^{\Delta_j/2} e^{jk\ell_j'\hat{\ell}_j'\cdot\hat{g}_\pm} f_j(\ell_j')d\ell_j' \quad \text{if } (\vec{r}-\vec{r}_j')\cdot\hat{z} \gtrless \pm\frac{\Delta_j}{2}|\hat{\ell}_j'\cdot\hat{z}| \quad (3\text{-}81)$$

$$= \pm e^{-jk(\vec{r}-\vec{r}_j')\cdot\hat{g}_+} \vec{h}_{j+} \int_{-\Delta_j/2}^{[(\vec{r}-\vec{r}_j')\cdot\hat{z}/\hat{\ell}_j'\cdot\hat{z}]-\epsilon} e^{jk\ell_j'\hat{\ell}_j'\cdot g_+} f_j(\ell_j')d\ell_j' \quad (3\text{-}82)$$

$$\pm e^{-jk(\vec{r}-\vec{r}_j')\cdot\hat{g}_-} \vec{h}_{j-} \int_{[(\vec{r}-\vec{r}_j')\cdot\hat{z}/\hat{\ell}_j'\cdot\hat{z}]+\epsilon}^{\Delta_j/2} e^{jk\ell_j'\hat{\ell}_j'\cdot g_-} f_j(\ell_j')d\ell_j'$$

$$\text{if } -\frac{\Delta_j}{2}\hat{\ell}_j'\cdot\hat{z} \gtrless (\vec{r}-\vec{r}_j')\cdot\hat{z} \gtrless \frac{\Delta_j}{2}\hat{\ell}_j'\cdot\hat{z}$$

Implied in (3-80) is a j^{th} segment integration with respect to ℓ_j'. This integration divides as indicated in (3-82) when $\vec{r}$ defines a point common to a plane that simultaneously divides the j^{th} segment and is parallel to the array plane. The ℓ_j' coordinate of the point along the j^{th} segment that lies in this plane is defined by equating $\hat{z}$ axis projections of $\vec{r}$ and $\vec{r}_j' + \ell_j' \hat{\ell}_j'$, yielding

$$\ell_j' = \frac{(\vec{r} - \vec{r}_j')\hat{z}}{\hat{\ell}_j' \cdot \hat{z}} \tag{3-83}$$

For $\hat{\ell}_j' \cdot \hat{z} > 0$, i.e., the ℓ_j' direction indicated in Figure 3-6, integration with respect to ℓ_j' from $-\Delta_j/2$ to the value of ℓ_j' defined by (3-83) involves plane waves propagating away from the array plane on the positive z axis side; hence, the + subscript is indicated for $\hat{g}_+$ and $\vec{h}_{j+}$ in the first integral of (3-82). For the integration from the (3-83) value of ℓ_j' to $\Delta_j/2$, the properly chosen plane waves propagate along the negative z axis away from the array plane. Hence, the second integral in (3-82) indicates $\hat{g}_-$ and $\vec{h}_{j-}$ with negative subscripts.

The $-\epsilon$ and $+\epsilon$ appearing in the first and second integrals in (3-82) are included to avoid integrating through the singularity that occurs in the plane of the source array. This singularity is a consequence of the plane wave representation of the field. Although this singularity appears integratable, this adjustment is expected to significantly improve convergence of the doubly infinite sum in (3-80). For nonself-elements, $i \neq j$, ϵ equal to the wire radius is probably adequate. For self-elements, $i = j$, ϵ may have to be smaller.

If $\hat{\ell}_j \cdot \hat{z} < 0$ (i.e., ℓ_j' is directed along the j^{th} segment opposite to that indicated in Figure 3-6), the sign of (3-82) simply changes as indicated by the $\pm$ depending upon

$$-\frac{\Delta_j}{2} \hat{\ell}_j' \cdot \hat{z} \lesseqgtr (\vec{r} - \vec{r}_j') \cdot \hat{z} \lesseqgtr \frac{\Delta_j}{2} \hat{\ell}_j' \cdot \hat{z} \tag{3-84}$$

As discussed in Section 3.2.2, the ij^{th} generalized impedance matrix element, $[Z]_{ij}$, is determined by weighted integration of the j^{th} current segment field along the surface of the i^{th} wire segment. Let $\vec{r}_i$ locate the center point of the i^{th} segment surface path as indicated in Figure 3-6). (For $i \neq j$, the i^{th} segment matching path may be taken along the axis of the i^{th} segment.)

With $\vec{r} = \vec{r}_i + \ell_i \hat{\ell}_i$,

$$[Z]_{ij} = -\int_{-\Delta_i/2}^{\Delta_i/2} w_i(\vec{r}_i+\ell_i\hat{\ell}_i)\hat{\ell}_i\cdot\vec{E}_j(\vec{r}_i+\ell_i\hat{\ell}_i)d\ell_i \tag{3-85}$$

where $\vec{E}_j$ is given by (3-80). For simplicity, assume that the z coordinate projections of all wire segments are either disjoint (nonoverlapping) or identical. Then,

$$[Z]_{ij} = -\frac{\eta}{2d_x d_y}\sum_{p=-\infty}^{\infty}\sum_{q=-\infty}^{\infty} Q_{pq} \tag{3-86}$$

where

$$Q_{pq} = e^{-jk(\vec{r}_i-\vec{r}_j')\cdot\hat{g}_\pm}\,\hat{\ell}_i\cdot\vec{h}_{j\pm}\int_{-\Delta_i/2}^{\Delta_i/2} e^{-jk\ell_i\hat{\ell}_i\cdot\hat{g}_\pm} w_i(\ell_i)d\ell_i \int_{-\Delta_j/2}^{\Delta_j/2} e^{jk\ell_j'\hat{\ell}_j'\cdot\hat{g}_\pm} f_j(\ell_j')d\ell_j' \qquad \text{if } (\vec{r}_i-\vec{r}_j')\cdot z \gtrless 0$$

$$= \pm\left[e^{-jk(\vec{r}_i-\vec{r}_j')\cdot\hat{g}_+}\,\hat{\ell}_i\cdot\vec{h}_{j+}\int_{-\Delta_i/2}^{\Delta_i/2}\left[e^{-jk\ell_i\hat{\ell}_i\cdot\hat{g}_+} w_i(\ell_i)\int_{-\Delta_j/2}^{\ell_i\frac{\hat{\ell}_i\cdot\hat{z}}{\hat{\ell}_j'\cdot\hat{z}}-\varepsilon} e^{jk\ell_j'\hat{\ell}_j'\cdot\hat{g}_+} f_j(\ell_j')d\ell_j'\right]d\ell_i\right] e^{-jk(\vec{r}_i-\vec{r}_j')\cdot\hat{g}_-}\,\hat{\ell}_i\cdot\vec{h}_{j-}$$

$$\int_{-\Delta_i/2}^{\Delta_i/2}\left[e^{-jk\ell_i\hat{\ell}_i\cdot\hat{g}_-} w_i(\ell_i)\int_{\ell_i\frac{\hat{\ell}_i\cdot\hat{z}}{\hat{\ell}_j'\cdot\hat{z}}+\varepsilon}^{\Delta_j/2} e^{jk\ell_j'\hat{\ell}_j'\cdot\hat{g}_-} f_j(\ell_j')d\ell_j'\right]d\ell_i\Bigg]$$

$$\text{if } (\vec{r}_i-\vec{r}_j')\cdot\hat{z} = 0,\ \ell_j'\cdot\hat{z} \gtrless 0$$

If pulse expansion and weighting functions are considered, then Q_{pq} becomes

$$Q_{pq} = e^{-jk(\vec{r}-\vec{r}_j')\cdot\hat{g}_\pm}\ \hat{\ell}_i\cdot\vec{h}_{j\pm}\psi_{i\pm}\psi_{j\pm} \qquad \text{if} \quad (\vec{r}_i-\vec{r}_j')\cdot\hat{z} \gtrless 0$$

$$= \pm\left[e^{-jk(\vec{r}_i-\vec{r}_j')\cdot\hat{g}_+}\ \hat{\ell}_i\cdot\vec{h}_{j+}\ \frac{1}{jk\hat{\ell}_j'\cdot\hat{g}_+}\left[e^{-jk\epsilon\hat{\ell}_j'\cdot\hat{g}_+}\ \Gamma_+ - e^{-jk\hat{\ell}_j'\cdot\hat{g}_+\Delta_j/2}\ \psi_{i+}\right]\right. \tag{3-87}$$

$$\left. -e^{-jk(\vec{r}_i-\vec{r}_j')\cdot\hat{g}_-}\ \hat{\ell}_i\cdot\vec{h}_{j-}\ \frac{1}{jk\hat{\ell}_j'\cdot\hat{g}_-}\left[e^{jk\epsilon\hat{\ell}_j'\cdot\hat{g}_-}\ \Gamma_- - e^{jk\hat{\ell}_j'\cdot\hat{g}_-\Delta_j/2}\ \psi_{i-}\right]\right]$$

$$\text{if} \quad (\vec{r}_i-\vec{r}_j)\cdot\hat{z} = 0;\ \hat{\ell}_j'\cdot\hat{z} \gtrless 0$$

where

$$\psi_{i\pm} = \Delta_{i\pm}\ \frac{\sin\left[k(\hat{\ell}_i\cdot\hat{g}_\pm)\Delta_i/2\right]}{k(\ell_i\cdot\hat{g}_\pm)\Delta_i/2}$$

$$\psi_{j\pm} = \Delta_j\ \frac{\sin\left[k(\hat{\ell}_j'\cdot\hat{g}_\pm)\Delta_j/2\right]}{k(\hat{\ell}_j'\cdot\hat{g}_\pm)\Delta_j/2}$$

$$\Gamma_\pm = \Delta_i\ \frac{\sin A_\pm}{A_\pm}$$

$$A = k(\hat{\ell}_i\cdot\hat{g}_\pm-\hat{\ell}_j'\cdot\hat{g}_\pm\ \hat{\ell}_i\cdot\hat{z}/\hat{\ell}_j'\cdot\hat{z})\Delta_i/2$$

If a ground screen is present a distance, d, behind the array, image fields must be considered in each impedance element computation. Let double primed position vectors and segment path lengths refer to image currents. Then, since the coordinate origin lies on the ground screen,

$$\vec{r}''_j = \hat{x}(\hat{x}\cdot\vec{r}'_j) + \hat{y}(\hat{y}\cdot\vec{r}'_j) - \hat{z}(\hat{z}\cdot\vec{r}'_j) \tag{3-88}$$

$$\hat{\ell}''_j = \hat{x}(\hat{x}\cdot\hat{\ell}'_j) + \hat{y}(\hat{y}\cdot\hat{\ell}'_y) - \hat{z}(\hat{z}\cdot\vec{r}'_j) \tag{3-89}$$

and the ij^{th} element of the generalized impedance matrix for an infinite array over a perfect ground screen becomes

$$\left[Z^{gs}\right]_{ij} = [Z]_{ij} + \frac{\eta}{2d_x d_y} \sum_{p=-\infty}^{\infty} \sum_{q=-\infty}^{\infty} Q^{gs}_{pq} \tag{3-90}$$

where

$$Q^{gs}_{pq} = e^{-jk(\vec{r}_i - \vec{r}''_j)\cdot\hat{g}_+}\, \hat{\ell}_i\cdot\vec{h}''_{j+}\, \psi_{i+}\, \psi^{gs}_{j+}$$

$$\vec{h}''_{j+} = \frac{1}{g_z}(\hat{\ell}''_j \times \hat{g}_+) \times \hat{g}_+$$

$$\psi^{gs}_{j+} = \Delta_j \frac{\sin\left[k(\hat{\ell}''_j\cdot\hat{g}_+)\Delta_j/2\right]}{k(\hat{\ell}''_j\cdot\hat{g}_+)\Delta_j/2}$$

For plane wave incidence excitation, the generalized voltage vector elements given by (3-52) must be appropriately modified to account for reflection.

3.2.4 Skewed Lattices

Many array lattices are skewed rather than rectangular. The infinite array analysis described in this report is applicable, with only minor change, to general

rectilinear (skewed) lattices. Any point in a skewed point lattice can be located by two integers, m and n. The position of the mn^{th} point is given by

$$\vec{r}_{mn} = md_e \hat{e} + nd_y \hat{y} \tag{3-91}$$

where $\hat{e}$ and $\hat{y}$ are the lattice unit vectors with associated interelement spacings d_e and d_y, respectively (Figure 3-7).

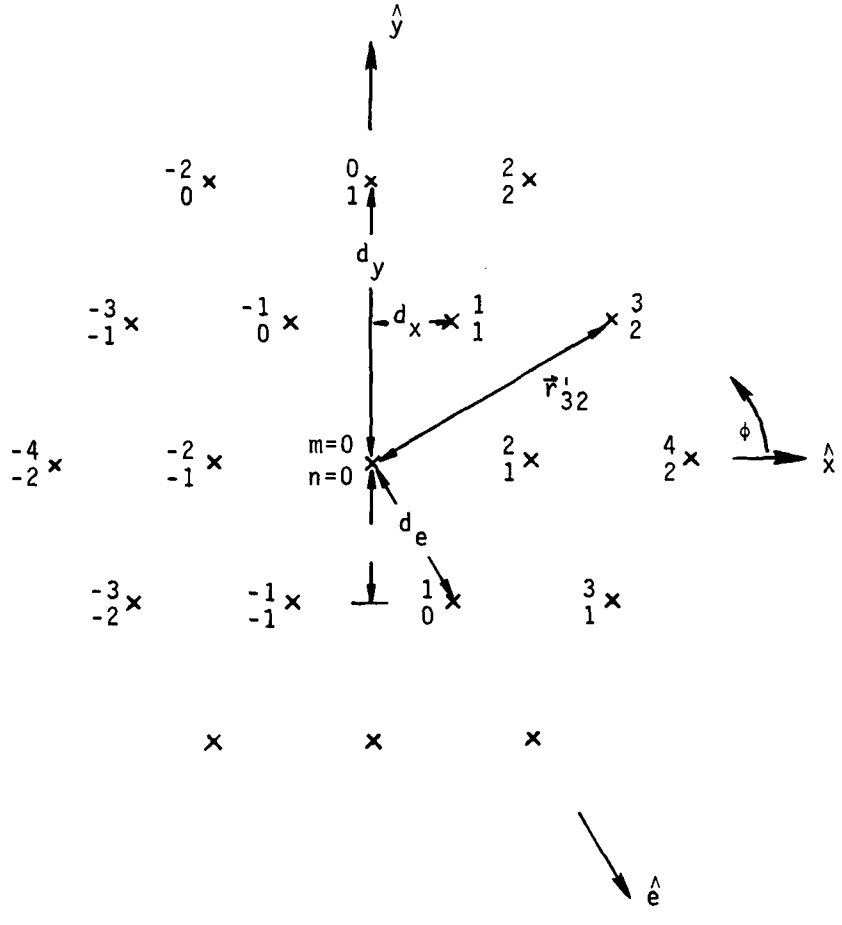

Figure 3-7. General Rectilinear (Skewed) Lattice

The standard x,y,z rectangular and r, θ, ϕ spherical coordinate systems are centered at the m = n = 0 point and oriented as shown in Figure 3-7. If identical radiators are located at the lattice points, the mn^{th} radiator excitation phase that will launch a wave in the $\hat{r}$ direction is expressed by

$$\hat{r}\cdot\vec{r}'_{mn} = md_e s_e + nd_y s_y \tag{3-92}$$

where $s_e = \hat{r}\cdot\hat{e}$, $s_y = \hat{r}\cdot\hat{y}$ and the "^" indicates a unit vector. This phasing also can be expressed in terms of the more standard x axis directional cosine, $s_x = \hat{r}\cdot\hat{x}$, by noting that (see Figure 3-7)

$$d_e\hat{e} = d_x\hat{x} - \Delta y\ \hat{y} \tag{3-93}$$

and, with (3-91),

$$\vec{r}'_{mn} = md_x\hat{x} + (nd_y - m\Delta y)\hat{y} \tag{3-94}$$

Hence,

$$\hat{r}\cdot\vec{r}'_{mn} = md_x s_x + (nd_y - m\Delta y)s_y \tag{3-95}$$

It then can be shown[5] that the skewed lattice infinite array generalized impedance matrices, [Z] and $[Z^{gs}]$, are computed by the formulas developed in Sections 3.2.2 and 3.2.3 if the expressions for $\hat{g}_\pm$ and g_z are replaced by

$$\hat{g}_\pm = \hat{x}\left[s_x + p\frac{\lambda}{d_x} - q\frac{\lambda\Delta y}{d_x d_y}\right] + \hat{y}\left[s_x + q\frac{\lambda}{d_y}\right] \pm \hat{z}g_z \tag{3-96}$$

$$g_z = \sqrt{1 - \left[s_x + p\frac{\lambda}{d_x} - q\frac{\lambda\Delta y}{d_x d_y}\right]^2 - \left[s_y + q\frac{\lambda}{d_y}\right]^2} \tag{3-97}$$

The feedback mode development in Sections 3.2.1 and 3.2.6 also applies to skewed lattices if the phase imparted by the mn^{th} module with respect to the reference module is expressed by $-k(md_e\alpha_e + nd_y\alpha_y)$.

All d_x, s_x, and α_x in these developments are simply replaced by d_e, s_e, and α_e, and the active impedances, $z^{aa}_{s_e,s_y}$, and $z^{bb}_{s_e,s_y}$, and $z^{ab}_{s_e,s_y}$ are understood to be determined with the expressions for $\hat{g}_\pm$ and g_z given above where the relationship between s_e and s_x is found by equating (3-92) and (3-95) resulting in

$$s_e = \frac{d_x s_x - \Delta y s_y}{d_e} \tag{3-98}$$

3.2.5 Space Feed Model

The field illuminating the lens will not be planar during radar transmit; however, a plane wave decomposition of the illumination across the lens face is always possible.[6] Each plane wave component of the illumination can be applied individually and the resulting lens patterns superimposed. The first approximation method is being designed in this manner.

Since, in the first approximation, infinite array theory is applied to each cell individually, a separate plane wave decomposition of the illumination is carried out for each cell. Only a small number of plane wave components must be considered for each case. The maximum cell size may be chosen such that a single plane wave fit to the illumination across a cell is adequate (Appendix B).

The propagation direction of the plane wave is along a line, $\vec{P}$, from the phase center of the feed to the cell center. The field components of the plane wave are the projection of the illuminating field at the center of the cell onto the plane perpendicular to $\vec{P}$. A single plane wave approximation to the illumination across a cell may not be possible if a large number of cells is to be avoided. A 10-percent accuracy in plane wave approximation to the illumination across a cell could result in about 200 cells subdividing the lens (Appendix B). A tighter accuracy will increase this number.

3.2.6 Generalized Module Model

The idealized module model assumed in the Section 3.2.1 development is generalized here. The modules were represented in Section 3.2.1 by two-port, open-circuit impedance parameters. These parameters were assumed uniform from element to element, within a cell, except for the array a to array b "mutual" impedance parameters which differed between elements in progressive phase only. In this section, the module parameters are permitted to be any complex function of the progressive phase setting. The only restriction is that modules with phase settings differing by a multiple of 2π have identical parameter values. Open-circuit impedance parameters do not always exist; e.g., a half-wavelength section of transmission line has no such representation. The following development, therefore, is in terms of two-port scattering parameters. The assumed form of the "feedback" mode expansion (3-12) is modified slightly. This permits a convenient column vector representation. The resulting formulas are shown to reduce significantly for the special case of a passive lens with simple line length phase shifters.

The mn^{th} element array a and array b port currents are assumed to have the forms

$$I^a_{mn} = \sum_{u=-\infty}^{\infty} I^a_{00(u)} \, e^{-jkmd_x(s_x + u\alpha_x)} \, e^{-jknd_y(s_y + u\alpha_y)} \tag{3-99}$$

$$I^b_{mn} = \sum_{u=-\infty}^{\infty} I^b_{00(u)} \, e^{-jkmd_x(s_x + u\alpha_x)} \, e^{-jknd_y(s_y + u\alpha_y)} \tag{3-100}$$

In column vector notation, (3-99) and (3-100) can be represented as

$$\bar{I}_{mn} = \sum_{u=-\infty}^{\infty} e^{-jkmd_x(s_x + u\alpha_x)} \, e^{-jknd_y(s_y + u\alpha_y)} \, \bar{I}_{00(u)} \tag{3-101}$$

where

$$\bar{I}_{00} = \begin{bmatrix} I^a_{00(u)} \\ I^b_{00(u)} \end{bmatrix}$$

$$\bar{I}_{mn} = \begin{bmatrix} I^a_{mn} \\ I^b_{mn} \end{bmatrix}$$

The port conditions that must be satisfied are

$$\bar{V}_{mn} = \begin{bmatrix} V^{aa}_{mn} + V^{ab}_{mn} \\ V^{bb}_{mn} \end{bmatrix} + \begin{bmatrix} V^{ex}_{mn} \\ 0 \end{bmatrix} \tag{3-102}$$

where

$$V_{mn}^{aa} + V_{mn}^{ab} = \sum_{u=-\infty}^{\infty} e^{-jkmd_x(s_x + u\alpha_x)} e^{-jkndy(s_y + u\alpha_y)} \left[z^{aa}_{s_x + u\alpha_x,\ s_y + u\alpha_y} I^{a}_{00(u)} + z^{ab}_{s_x + u\alpha_x,\ s_y + u\alpha_y} I^{b}_{00(u)} \right]$$

$$V_{mn}^{ex} = -z^{aa}_{s_x,\ s_y} I^{ex}_{00} e^{-jkmd_x s_x} e^{-jknd_y s_y}$$

$$V_{mn}^{bb} = \sum_{u=-\infty}^{\infty} e^{-jkmd_x(s_x + u\alpha_x)} e^{-jknd_y(s_y + u\alpha_y)} z^{bb}_{s_x + u\alpha_x,\ s_y + u\alpha_y} I^{b}_{00\ (u)}$$

$$\bar{V}_{mn} = \begin{bmatrix} V^{a}_{mn} \\ V^{b}_{mn} \end{bmatrix}$$

This may be written

$$\bar{V}_{mn} = \sum_{u=-\infty}^{\infty} e^{-jkmd_x(s_x + u\alpha_x)} e^{-jkndy(s_y + u\alpha_y)} \left[z_u \right] I_{00(u)} + e^{-jkmd_x s_x} e^{-jknd_y s_y} \bar{V}^{ex}_{00} \qquad (3\text{-}103)$$

where

$$[z_u] = \begin{bmatrix} z^{aa}_{s_x + u\alpha_x,\ s_y + u\alpha_y} & z^{ab}_{s_x + u\alpha_x,\ s_y + u\alpha_y} \\ 0 & z^{bb}_{s_x + u\alpha_x,\ s_y + u\alpha_y} \end{bmatrix}$$

$$\bar{V}^{ex}_{00} = \begin{bmatrix} -z^{aa}_{s_x, s_y} & I^{ex}_{00} \\ 0 & \end{bmatrix}$$

Let the mn^{th} module (plus feed lines) scattering parameter matrix be denoted $[S_{mn}]$. If the scattering parameter normalizing impedances are R^a and R^b, then

$$\bar{V}_{mn} = [R]^{1/2}([U] + [S_{mn}])\bar{C}_{mn} \tag{3-104}$$

$$\bar{I}_{mn} = [R]^{-1/2}([U] - [S_{mn}])\bar{C}_{mn} \tag{3-105}$$

where

$$[U] = \begin{bmatrix} 1 & 0 \\ 0 & 1 \end{bmatrix}$$

$$[R] = \begin{bmatrix} R^a & 0 \\ 0 & R^b \end{bmatrix}$$

$$\bar{C}_{mn} = \begin{bmatrix} C^a_{mn} \\ C^b_{mn} \end{bmatrix}$$

and C^a_{mn} and C^b_{mn} are the "incident" scattering variables.

Assume that $\bar{C}_{mn}$ may be expanded in "feedback" modes, as is I_{mn}, according to

$$\bar{C}_{mn} \quad \sum_{u=-\infty}^{\infty} e^{-jkmd_x(s_x + u\alpha_x)} e^{-jknd_y(s_y + u\alpha_y)} \bar{C}_{00(u)} \tag{3-106}$$

Then (3-103), (3-104), and (3-106) combine to yield, after division by $e^{-jk(ms_x + ns_y)}$,

$$\sum_{u=-\infty}^{\infty} e^{-jkmd_x u\alpha_x} e^{-jknd_y u\alpha_y} \left[[R]^{1/2}([U] + [S_{mn}])\bar{C}_{00(u)} - [z_u]\bar{I}_{00(u)} \right] = \bar{V}^{ex}_{00} \tag{3-107}$$

Another equation in $\bar{C}_{00(u)}$ and $\bar{I}_{00(u)}$, obtained from (3-101), (3-105) and (3-106), is

$$\sum_{u=-\infty}^{\infty} e^{-jkmd_x u\alpha_x} e^{-jknd_y u\alpha_y} \left[[R]^{1/2}([U] - [S_{mn}])\bar{C}_{00(u)} - \bar{I}_{00(u)} \right] = \bar{0} \quad (3\text{-}108)$$

where $\bar{0}$ is the null column vector.

A set of simultaneous equations is formed from (3-107) and (3-108) in a manner similar to that in forming (3-32) and (3-33). The module phase settings, α_x and α_y, are assumed to satisfy (3-28) and (3-29); thus, $[S_{mn}]$ repeats every M x N elements. Premultiplication of (3-107) and (3-108) by $e^{j2\pi mvM'/M}\, e^{j2\pi nvN'/N}$, where v is an integer, summation over one "progressive phase period," $1 \leq m \leq M$ and $1 \leq n \leq N$, and interchange of summations yields

$$\sum_{u=-\infty}^{\infty} ([F'_{vu}]\bar{C}_{00(u)} - [F_{vu}]\,[z_u]\bar{I}_{00(u)}) = \begin{cases} NM\,\bar{V}_{00}^{ex} & v=0 \\ \bar{0} & v=\pm1,\pm2,\ \ldots \end{cases} \quad (3\text{-}109)$$

$$\sum_{u=-\infty}^{\infty} ([F''_{vu}]\,\bar{C}_{00(u)} - [F_{vu}]\bar{I}_{00(u)}) = \bar{0} \qquad v=0,\pm1,\pm2,\ \ldots \quad (3\text{-}110)$$

where

$$[F'_{vu}] = \sum_{n=1}^{N}\sum_{m=1}^{M} e^{j2\pi m(v-u)M'/M}\, e^{j2\,n(v-u)N'/N}\, [R]^{\frac{1}{2}}([U]-[S_{mn}]) \quad (3\text{-}111)$$

$$[F''_{vu}] = \sum_{n=1}^{N}\sum_{m=1}^{M} e^{j2\pi m(v-u)M'/M}\, e^{j2\pi n(v-u)N'/N}\, [R]^{-\frac{1}{2}}([U]-[S_{mn}]) \quad (3\text{-}112)$$

$$[F_{vu}] = \sum_{n=1}^{N}\sum_{m=1}^{M} e^{j2\pi m(v-u)M'/M}\, e^{j2\pi n(v-u)N'/N}\, [U] = \begin{cases} MN[U] & u=v \\ 0 & \text{otherwise} \end{cases} \quad (3\text{-}113)$$

The simplifications resulting in the right-hand sides of (3-109) and (3-113) assume that $(v-u)M'/M$ and $(v-u)N'/N$ are never integers simultaneously. This condition occurs whenever $(v-u)$ is an integer multiple of M and N simultaneously. This condition is avoided by limiting (3-109) and (3-110) to only the lower valued equations and by limiting the infinite summations to only lower values of $|u|$ This is permissible if only lower-ordered "feedback" modes, u, are significant.

A special case of interest is a passive lens with modules replaced by transmission lines. The relative lengths of line determine the progressive phasing. The scattering parameters for the mn^{th} element become

$$[S_{mn}] = e^{-j2\pi mM'/M}\, e^{-j2\pi nN'/N} \begin{bmatrix} 0 & 1 \\ 1 & 0 \end{bmatrix} \tag{3-114}$$

if $R^a = R^b = R_0$, where R_0 is the characteristic impedance of the transmission lens. Equations (3-111) and (3-112) reduce to

$$[F'_{vu}] = \begin{cases} \sqrt{R_0}\, MN\, [U] & v - u = 0 \\ \sqrt{R_0}\, MN\, [W] & v - u - 1 = 0 \\ 0 & \text{otherwise} \end{cases} \tag{3-115}$$

$$[F''_{vu}] = \begin{cases} MN/\sqrt{R_0}\, [U] & v - u = 0 \\ -MN/\sqrt{R_0}\, [W] & v - u - 1 = 0 \\ 0 & \text{otherwise} \end{cases} \tag{3-116}$$

where

$$[W] = \begin{bmatrix} 0 & 1 \\ 1 & 0 \end{bmatrix}$$

Equations (3-109) and (3-110) then become

$$\sqrt{R_0}\,\bar{C}_{00(v)} + \sqrt{R_0}\,[W]\bar{C}_{00(v-1)} - [z_v]\bar{I}_{00(v)} = \begin{cases} \bar{V}_{00}^{ex} & v = 0 \\ \bar{0} & v = \pm 1, \pm 2, \ldots \end{cases} \tag{3-117}$$

$$\frac{1}{\sqrt{R_0}}\,\bar{C}_{00(v)} - \frac{1}{\sqrt{R_0}}\,[W]\bar{C}_{00(v-1)} - \bar{I}_{00(v)} = \bar{0} \qquad v = 0, \pm 1, \pm 2, \ldots \tag{3-118}$$

Finally, (3-117) and (3-118) can be combined to form

$$\left[\sqrt{R_0}[U] - \frac{1}{\sqrt{R_0}}\,[z_v]\right]\bar{C}_{00(v)} + \left[\sqrt{R_0} + \frac{1}{\sqrt{R_0}}\,[z_v]\right][W]\bar{C}_{00(v-1)} = \begin{cases} \bar{V}_{00}^{ex} & v=0 \\ \bar{0} & v=\pm 1, \pm 2, \ldots \end{cases} \tag{3-119}$$

Equation (3-119) can be solved for $\bar{C}_{00(v)}$ under the previously stated condition that only lower-ordered feedback modes are significant. Then (3-118) can be solved for $I_{00(v)}$.

3.2.7 Multiport Array Elements

The development throughout Section 3.2 has, for simplicity, considered single-port radiating elements. The extension to multiport elements (e.g., crossed dipoles for circular polarization (turnstile antennas) with quadrative phase shifters in the feed lines) is straightforward due to the moment method framework employed [2, Chapter 6]. The present simulator development effort is not expected to implement this extension; however, the important case of turnstile array elements will be modeled by transferring the quadrative phase shifters from the feed line to the appropriate radiating arms. Turnstile antennas for use in an SBR lens array are likely to be designed in just this manner, where the radiating arms are either reactively loaded or shaped to impart the desired quadrature phase relationship.

A loaded wire can be modeled easily within the moment method framework. If lumped impedance loads, $Z_{j'}^{L}$, $j' = 1,2,\ldots,N_s$, are located at segments j'on a wire, the voltage column vector, $\vec{V}$ in (3-51) becomes

$$V = \bar{V}' - [Z^L]\,\bar{I} \tag{3-120}$$

The elements of the column vector, $\bar{V}$, are the values of applied voltage sources at driven segments and $[Z^L]$ is a diagonal matrix with Z^L_j, for its j'^{th} diagonal element. Equation (3-51) then becomes

$$([Z] + [Z^L])\bar{I} = \bar{V}^{ex} + \bar{V}' \qquad (3\text{-}121)$$

Equation (3-121) may be solved for $\bar{I}$ as discussed in Section 3.2.2.

A module to feed line junction (module output) is generally a three-terminal junction with the third terminal necessitated by the ground screen. Nonideal balun arrangements at these module outputs cause unbalanced currents to flow on the feed lines if asymmetries exist. The asymmetries may be electrical (e.g., module phasing for off-broadside beam steering) or structural (e.g., Figure 3-8). The net feed line current, $I_1 + I_2$, is counterbalanced by current I_g on the ground screen; i.e., $I_g = -(I_1 + I_2)$. This net current constitutes the unbalanced mode current. If I_g is significant, a module output generally requires a two-port representation. (This, in turn, leads to a four-port representation for a module with two outputs.) The initial version of the simulator will be capable of modeling a module output only as a single port. The effects of unbalanced mode feed line currents can be accounted for, despite this limitation, if it can be assumed that there is negligible coupling within the module between the balanced and unbalanced mode currents and also between the unbalanced mode currents at the array a and array b module outputs; i.e., only the balanced mode currents are assumed affected by the module circuitry and the feed line unbalanced mode currents arise entirely from scattering. In Figure 3-9, the modules are treated as two ports (one port on each array side) and the corresponding port voltages and currents are transferred to the radiator excitation ports (indicated by the sources) via the feed line transmission line equations. The composite module/feed lines port parameters become those discussed in Sections 3.2.1 and 3.2.6. These port parameters apply strictly to the balanced mode. With radiator excitation ports thus related, each feed line is modeled as a single thin wire. The feed line scattering then is accounted for by the moment method technique discussed in Section 3.2.3. Balanced mode feed line current radiation can be neglected due to the close spacing of the wires in a feed line.

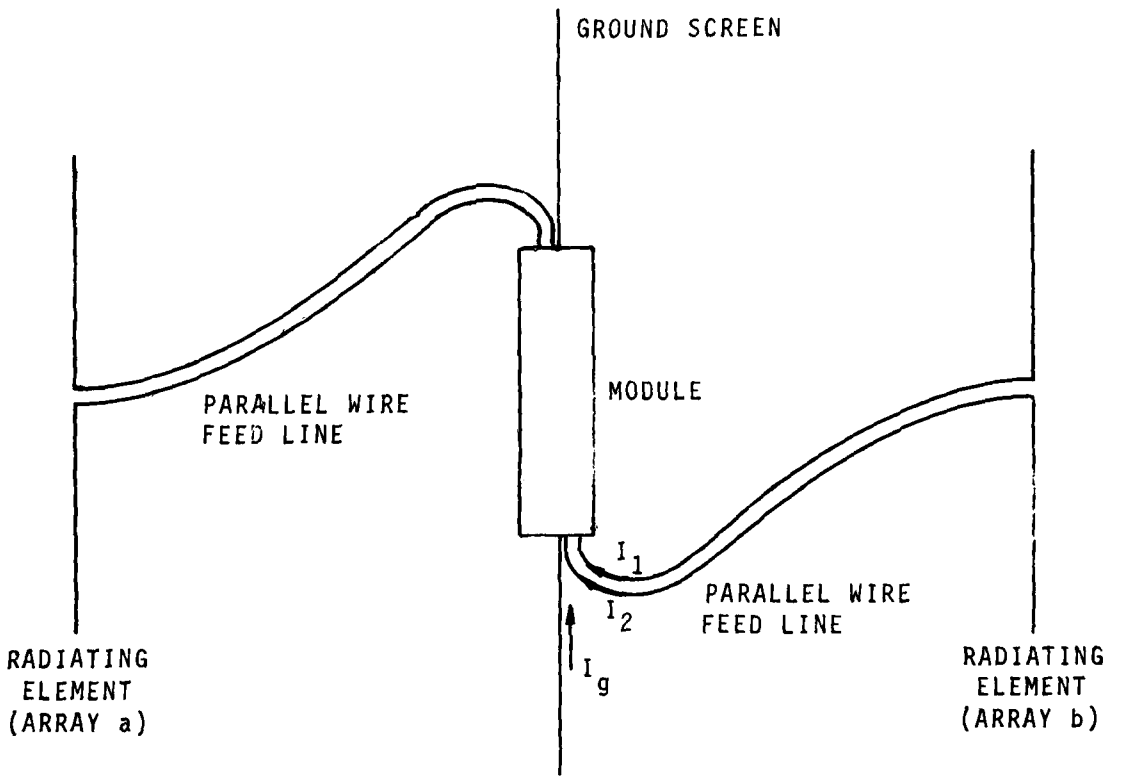

Figure 3-8. Asymmetrical Feed Line Configuration

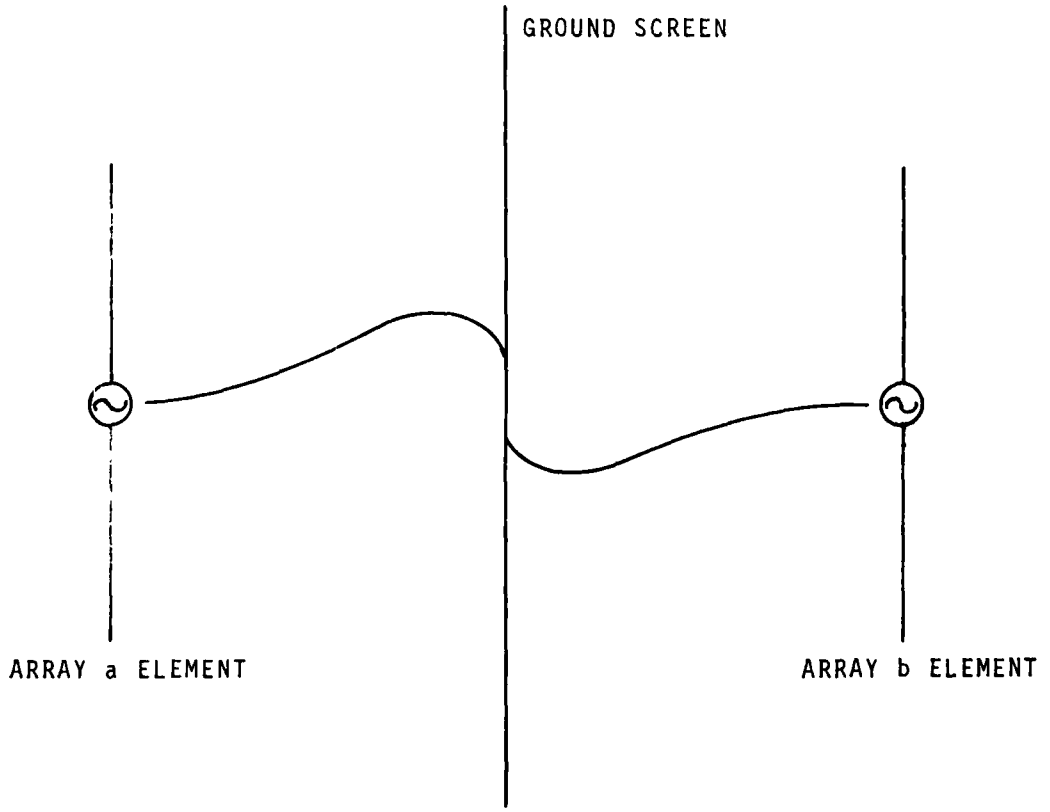

Figure 3-9. Model for Including Feed Line Scattering

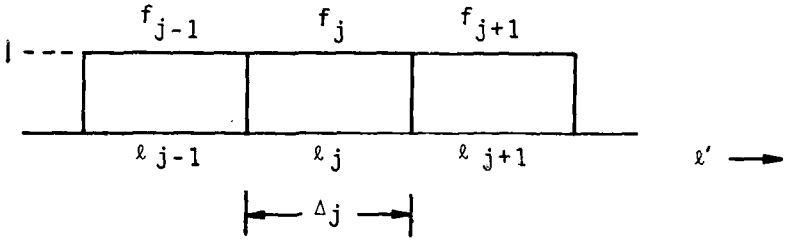

a. Pulse (Piecewise Constant)

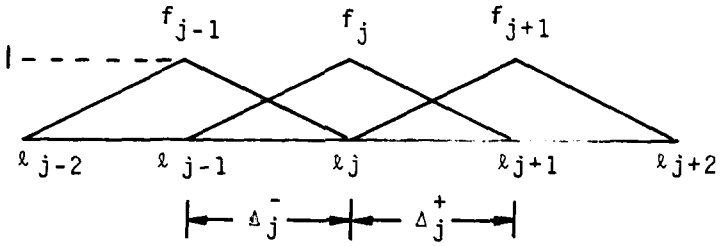

b. Triangular (Piecewise Linear)

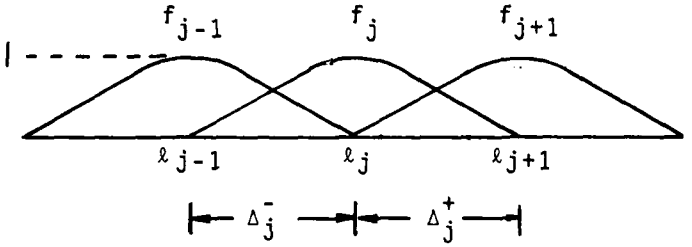

c. Piecewise Sinusoidal

Figure 3-10. Expansion Functions

3.2.8 Increased Computation Efficiency

Evaluation of the generalized impedance matrix [Z] (or $[Z^{gs}]$) of Section 3.2.2 usually requires considerable computer run time. This is especially true for arrays of thin wire radiators oriented parallel to the array plane since the doubly infinite summation in (3-57) then is slowly convergent. Each term in the summation corresponds to a plane wave field averaged over a segment a short wire radius, a, in front of the array plane containing the current filaments. The plane waves corresponding to large $|p|$ or $|q|$ decay exponentially away from the array plane. The arguments of these exponentials are proportional to $\sqrt{\left[p\,\frac{a}{d_x}\right]^2 + \left[q\,\frac{a}{d_y}\right]^2}$, where d_x and d_y are the x and y coordinate interelement spacings; thus, wires that are thin with respect to d_x and d_y result in slow convergence. Examples indicating the number of p and q terms (plane wave modes) typically required are given in Section 5. Several possibilities for reducing the number of times that (3-57) has to be computed are being explored. These techniques, discussed below, also apply to the ground plane case represented by (3-61).

The Toeplitz nature for straight wires is being employed. The [Z] for a straight wire divided into N_s segments has $2N_s - 1$ diagonals. If the segments are of equal length, all elements of [Z] common to a diagonal are equal; i.e., [Z] is Toeplitz. The N_s^2 elements of [Z] are, therefore, determined from only $2N_s - 1$ computations of (3-57) -- one for each diagonal. If an array radiating element is a collection of straight wires, this property applies only to submatrices centered along the main diagonal of [Z]. The order of each submatrix equals the number of segments on the corresponding straight wire.

Except for broadside phasing ($s_x = s_y = 0$), [Z] is not symmetric; however, $[Z]_{ji}$ differs from $[Z]_{ij}$ only by a sign in an exponential. This permits a reduction of almost 50-percent in [Z] computation time.

The development in Section 3.2.2 employed "pulses for expansion, $f_j(\ell')$, and weighting, $w_i(\ell')$, functions; these are indicated in Figure 3-10a. Each pulse occupies one wire segment. The results in Section 5 indicate that many pulses are needed to correctly compute the input reactance of an infinite array of near resonant thin dipoles -- approximately 20 per half wavelength for $a = 0.01\lambda$ and approximately 0.8λ interelement spacing. These results assume equal segment lengths, Δ_j. If tiny Δ_j are required only in the feed region, a large reduction in N_s may be possible by modeling with unequal Δ_j. Results with unequal Δ_j will be available shortly.

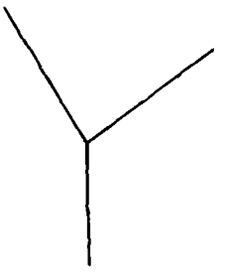

a. Three-Wire Junction

b. One Wire Chosen Terminated at Junction

c. Addition of a Second Wire by Overlapping First Wire

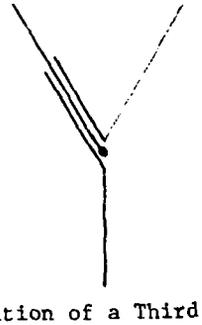

d. Addition of a Third Wire by Overlapping First Wire

Figure 3-11. Modeling a Junction with Overlapping Expansion Functions

Overlapping expansion and weighting functions, such as piecewise linear (Figure 3-10b) or piecewise sinusoidal (Figure 3-10c), can be tried in place of pulses. The overlapping of adjacent functions assures continuity along the wire, possibly resulting in a need for fewer expansion functions to approximate the current than are required with pulses.

Since each overlapping expansion function traverses two segments, each element of the corresponding [Z] is computed by the sum of four terms, each similar to (3-57) but differing in computation of ψ_i and ψ_j. Care is required when treating multiple wire junctions to maintain current continuity at the junctions. This can be accomplished by following a simple rule when modeling wires. To illustrate, consider the three-wire junction shown in Figure 3-11a. The modeling begins by choosing any one of the wires as terminated at the junction (Figure 3-11b). The remaining wires then are added in succession such that each overlaps any previously placed wire (Figures 3-11c and d). This overlapping is accomplished by aligning the junction point with the peak of the end triangle (or sinusoid) function on the wire being added. This method is described in Reference 8 and presented in terms of "independent loop currents" in Reference 9.

The expressions for the pulse, triangle, and sinusoid functions are given in (3-122), (3-123), and (3-124)(Figure 3-10).

For pulses,

$$f_j(\ell') = \begin{cases} 1 & \ell_j - \Delta_j/2 < \ell' < \ell_j + \Delta_j/2 \\ 0 & \text{otherwise} \end{cases} \tag{3-122}$$

For triangles,

$$f_j(\ell') = \begin{cases} (\ell' - \ell_{j-1})/\Delta_j^- & \ell_{j-1} \le \ell' \le \ell_j \\ (\ell_{j+1} - \ell')/\Delta_j^+ & \ell_j \le \ell' \le \ell_{j+1} \\ 0 & \text{otherwise} \end{cases} \tag{3-123}$$

For sinusoids, where $k = \frac{2\pi}{\lambda}$,

$$f_j(\ell') = \begin{cases} \sin k(\ell' - \ell_{j-1})/\sin k\Delta_j^- & \ell_{j-1} \leq \ell' \leq \ell_j \\ \sin k(\ell_{j+1} - \ell')/\sin k\Delta_j^+ & \ell_j \leq \ell' \leq \ell_{j+1} \\ 0 & \text{otherwise} \end{cases} \qquad (3\text{-}124)$$

3.3 HIGHER APPROXIMATION CURRENTS

The first approximation method solves for the array a and array b currents within a cell assuming the cell is infinite in extent, all array a radiating elements are identical, all array b radiating elements are identical, and interconnecting modules between arrays are permitted to differ only in phase settings. The variation in phase settings between modules must be linearly progressive. Each cell, however, will be finite in extent and may exhibit other discontinuities in periodicity due, for example, to module failures or nearby scatterers such as lens, edges, booms, hinges, struts, and other structural supports. The first approximation currents for elements near these discontinuities may be significantly in error. These current predictions can be corrected by the higher approximation method described in the following subsections. Although there are a great many elements (hundreds or more) that may reside near discontinuities, the higher approximation method is expected to prove reasonably efficient. This is because (1) the method makes use of the known first approximation currents and feedback fields penetrating the ground screen and (2) a moment method matrix has to be computed and inverted only once for each type of radiating element (dipole, folded dipole, etc.) in the entire lens. Each approximation uses the results of previous approximations. The required number of approximations depends upon the rapidity of convergence of successive approximations.

3.3.1 Port Representation and Solution

Let the first approximation currents on all lens radiating elements be known. The method for obtaining higher approximation currents on an array a and array b element pair near a discontinuity in periodicity is presented below by considering the second approximaton and extending the results to the n^{th} approximation. A single-port representation of a radiating element is assumed. The method can be expanded to include multiport models. The problem being modeled by the second approximation method is shown in Figure 3-12. The second approximation currents on a lens array a and array b element pair are sought. For discussion purposes, these elements are referred to as the $zero^{th}$ elements and variables corresponding to this element pair are subscripted zero. Nearby element pair currents (subscripted 1, 2,...) that are considered in computing the $zero^{th}$ element pair currents may reside in the same cell or nearby cells. A parenthetical number appearing in a superscript of a variable denotes the level of approximation of the variable; e.g., $V_0^{(2)a}$ is the second approximation port voltage of the $zero^{th}$ array a element, and $I_2^{(1)a}$ is the first approximation oort current on the "second" of the array a "neighboring" elements.

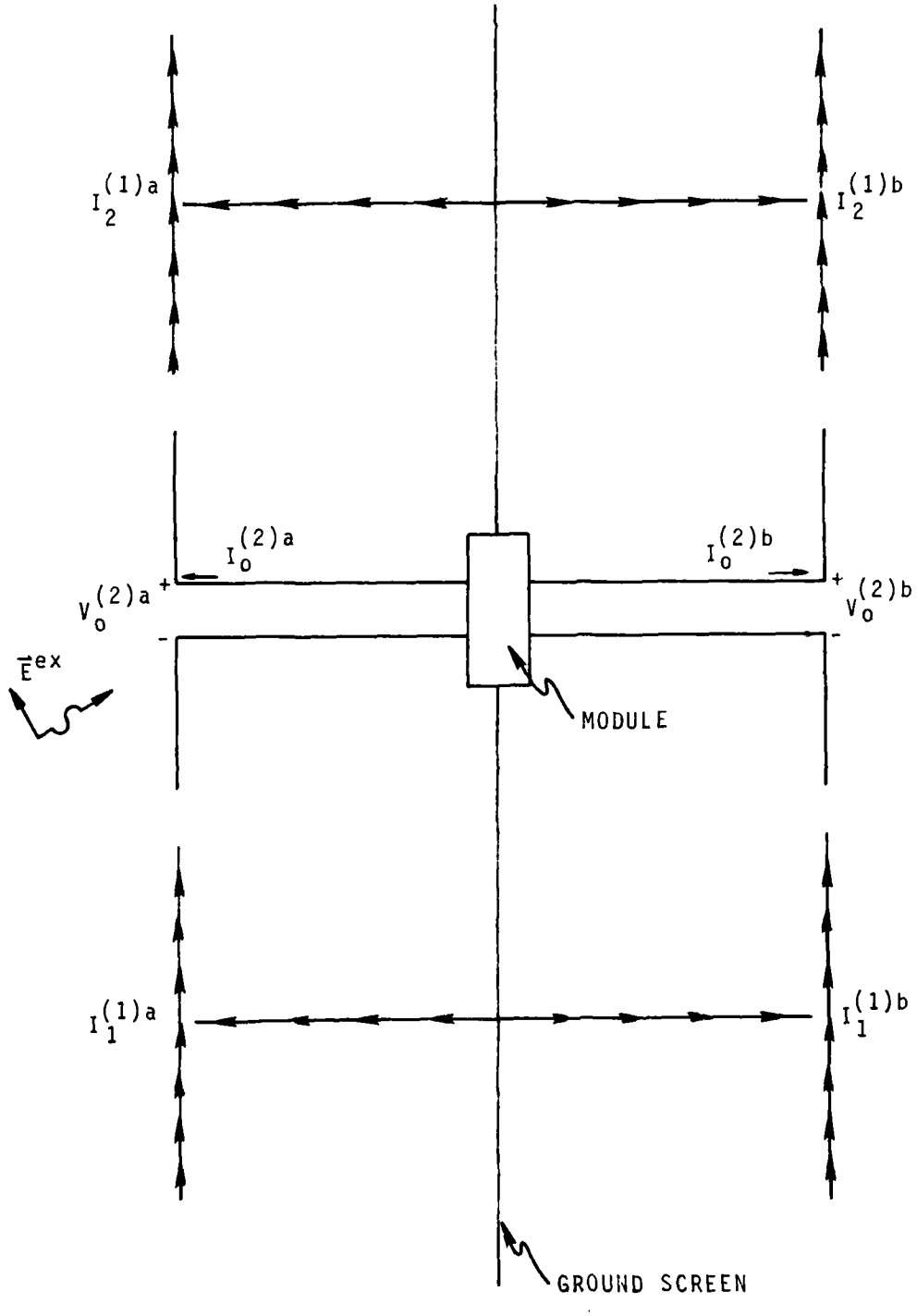

Figure 3-12. Problem for Determining Second Approximation Currents

The incident exciting field (space feed on radar transmit, target return on radar receive) is denoted $\vec{E}^{ex}$. The second approximation port voltages and currents for the element pair under consideration (zeroth element pair) are related by

$$V_0^{(2)a} = z^a I_0^{(2)a} + V_0^{ex} + V_0^{(1)ab} + V_0^{(1)aa'} \tag{3-125}$$

$$V_0^{(2)b} = z^b I_0^{(2)b} + V_0^{(1)bb'} \tag{3-126}$$

where

$z^a (z^b)$ is the impedance of an isolated array a (b) element with the ground screen perfectly conducting

$V_0^{(1)aa'}$ ($V_0^{(1)bb'}$) is the array a (array b) zeroth element open-circuit port voltage due to the nearby array a (array b) first approximation currents with the ground screen perfectly conducting

$V_0^{(1)ab}$ is the array a zeroth element open-circuit port voltage due to the first approximation array b excited field penetrating the ground screen

V_0^{ex} is the array a zeroth element open-circuit port voltage due to $\vec{E}^{ex}$ in the presence of the ground screen

The reference directions for the open-circuited voltages are the same as for $V_0^{(2)a}$ and $V_0^{(2)b}$. The z^a and z^b "isolated element" impedances can be determined with feed line scattering accounted for as suggested by the Figure 3-9 model. The feedback voltage $V_0^{(1)ab}$, is available from the first approximation analysis.

The quantities $V_0^{(2)a}$, $V_0^{(2)b}$, $I_0^{(2)a}$, and $I_0^{(2)b}$ are related by module two-port parameters; e.g., the impedance parameter representation is

$$V_0^{(2)a} = -z_0^{aa} I_0^{(2)a} - z_0^{ab} I_0^{(2)b} \tag{3-127}$$

$$V_0^{(2)b} = -z_0^{ba} I_0^{(2)a} - z_0^{bb} I_0^{(2)b} \tag{3-128}$$

Equations (3-125) through (3-128) can be combined to form

$$(z^a + z_0^{aa}) I_0^{(2)a} + z_0^{ab} I_0^{(2)b} = - V_0^{ex} - V_0^{(1)aa'} - V_0^{(1)ab} \tag{3-129}$$

$$z_0^{ba}\ I_0^{(2)a} + (z^b + z_0^{bb})\ I_0^{(2)b} = -\ V_0^{(1)bb'} \tag{3-130}$$

These equations explicitly relate second approximation port currents and first approximation port voltages.

A thin-wire, pulse expansion-impulse weighting, free-space moment method code can be used to determine z^a, z^b, and V_0^{ex} and, from first approximation currents and fields, $V_0^{(1)aa'}$, $V_0^{(1)bb'}$, and $V_0^{(1)ab}$.[10] Other moment method codes can be used (e.g., see Refs. 8 and 9); however, the pulse expansion code fits well with the pulse expansion infinite array technique employed in the first approximation method of Section 3.2.2.

Moment methods calculate short-circuit currents more efficiently than open-circuit voltages; therefore, V_0^{ex}, $V_0^{(1)aa'}$, $V_0^{(1)bb'}$ and $V_0^{(1)ab}$ are determined from zeroth element array a short-circuit port currents I_0^{ex}, $I_0^{(1)aa'}$, and $I_0^{(1)bb'}$ and zeroth element array b short-circuit port current $I_0^{(1)ab}$ according to

$$V_0^{ex} = -\ z^a\ I_0^{ex} \tag{3-131}$$

$$V_0^{(1)aa'} = -\ z^a\ I_0^{(1)aa'} \tag{3-132}$$

$$V_0^{(1)bb'} = -\ z^b\ I_0^{(1)bb'} \tag{3-133}$$

$$V_0^{(1)ab} = -\ z^a\ I_0^{(1)ab} \tag{3-134}$$

The reference directions for these short-circuit currents are the same as those for $I_0^{(2)a}$ and $I_0^{(2)b}$. The justification for (3-131) through (3-134) follows closely the argument following (3-20).

In the pulse expansion function moment method,[10] an isolated element is modeled as N_s connected segments (Figure 3-4). Let i_s be the number of the segment which contains the element port. A corresponding isolated-element-above-a-ground-screen "generalized admittance matrix" can be determined.[2] Each short-circuit port current in (3-131) through (3-134) can be determined from row i_s of the appropriate generalized admittance matrix and the appropriate "generalized voltage vector"[2] according to

$$I_0^{ex} = \tilde{Y}^a_{i_s} \bar{V}_0^{ex} \tag{3-135}$$

$$I_0^{(1)aa'} = \tilde{Y}^a_{i_s} \bar{V}_0^{(1)aa'} \tag{3-136}$$

$$I_0^{(1)bb'} = \tilde{Y}^b_{i_s} \bar{V}_0^{(1)bb'} \tag{3-137}$$

$$I_0^{(1)ab} = \tilde{Y}^a_{i_s} \bar{V}_0^{(1)ab} \tag{3-138}$$

In (3-135) through (3-138), $\tilde{Y}^a_{i_s}$ ($\tilde{Y}^b_{i_s}$) is the matrix row vector taken from the i_s row of the array a (array b) isolated-element-above-a-ground-plane generalized admittance matrix, $\bar{V}_0^{(1)aa'}$ ($V_0^{(1)bb'}$) is the array a (array b) zeroth-element-above-a-ground-screen generalized voltage vector resulting from the nearby array a (array b) first approximation currents, $\bar{V}_0^{(1)ab}$ is the array a zeroth-element-above-a-ground-screen generalized voltage vector resulting from the first approximation field penetrating the ground screen ($\vec{E}^t$ in Section 3.2.2), and $\bar{V}_0^{ex}$ is the array a zeroth-element-above-a-ground-screen generalized voltage vector resulting from $\vec{E}^{ex}$.

From (3-129) through (3-138),

$$(z^a + z_0^{aa}) I_0^{(2)a} + z_0^{ab} I_0^{(2)b} = z^a \tilde{Y}^a_{i_s} (\bar{V}_0^{ex} + \bar{V}_0^{(1)aa'} + \bar{V}_0^{(1)ab}) \tag{3-139}$$

$$z_0^{ba} I_0^{(2)a} + (z^b + z_0^{bb}) I_0^{(2)b} = z^b \tilde{Y}^b_{i_s} \bar{V}_0^{(1)bb'} \tag{3-140}$$

Equations (3-139) and (3-140) can be solved for $I_0^{(2)a}$ and $I_0^{(2)b}$. The second approximation zeroth element active impedances are determined from (3-127) and (3-128) as $V_0^{(2)a}/I_0^{(2)a}$ for array a and $V_0^{(2)b}/I_0^{(2)b}$ for array b.

Many elements are likely to reside near discontinuities in periodicy. This implies a large number of (3-139) and (3-140) computations -- one for each of these elements. The admittance row vectors, $\tilde{Y}^a_{i_s}$ and $\tilde{Y}^b_{i_s}$, are fixed for all (3-139) and (3-140) computations if all the radiating elements throughout the lens face are identi-

cal. This also applies to z^a and z^b, since $z^a(z^b)$ is the reciprocal of the i_s element of $\tilde{Y}^a_{i_s}$ ($\tilde{Y}^b_{i_s}$). The major effort, then, is in computing $\bar{V}_0^{ex}$, $\bar{V}_0^{(1)aa'}$, $\bar{V}_0^{(1)bb'}$, and $\bar{V}_0^{(1)ab}$.

Equations similar to (3-139) and (3-140) can be found for the array a and array b second approximation current distributions. These current distribution equations employ the entire isolated element generalized admittance matrices, from which $\tilde{Y}^a_{i_s}$ and $\tilde{Y}^b_{i_s}$ are extracted, with significant increase in computation time. The simulator is being designed assuming the first approximation current distributions adequately describe the current distributions for any higher approximation; i.e., a higher approximation current is assumed to differ from the first current by a complex constant scaling factor.

The third and higher port current approximations are obtained in a manner similar to that for the second approximations. The zeroth element, nth approximation, array a and array b port currents, $I_0^{(n)a}$ and $I_0^{(n)b}$, are obtained from the n-1 approximations by solving

$$(z^a + z_0^{aa})I_0^{(n)a} + z_0^{ab}\, I_0^{(n)b} = z^a\, \tilde{Y}^a_{i_s}\, (\bar{V}_0^{ex} + \bar{V}_0^{(n-1)aa'} + \bar{V}_0^{(n-1)ab}) \qquad (3\text{-}141)$$

$$z_0^{ba}\, I_0^{(n)a} + (z^b + z_0^{bb})I_0^{(n)b} = z^b\, \tilde{Y}^b_{i_s}\, \bar{V}_0^{(n-1)bb'} \qquad (3\text{-}142)$$

The free space field at the zeroth array a element arising from the n-1 approximation field penetrating the ground screen results in $\bar{V}_0^{(n-1)ab}$. This field is difficult to compute exactly. The approximation resulting from equating $\bar{V}_0^{(n-1)ab}$ and $V_0^{(1)ab}$ is being considered. Another possibility is "scaling" $\bar{V}_0^{(1)ab}$ according to

$$\bar{V}_0^{(n-1)ab} = \frac{I_0^{(n-1)b}}{I_0^{(1)b}}\, \bar{V}_0^{(1)ab} \qquad (3\text{-}143)$$

The column vectors $\bar{V}_0^{(n-1)aa'}$ and $\bar{V}_0^{(n-1)bb'}$ involve summations of the fields from L nearby elements; i.e.,

$$\bar{V}_0^{(n-1)aa'} = \sum_{\ell=1}^{L} \bar{V}_0^{(n-1)a\ell} \qquad (3\text{-}144)$$

$$\bar{V}_0^{(n-1)bb'} = \sum_{\ell=1}^{L} \bar{V}_0^{(n-1)b\ell} \tag{3-145}$$

where $\bar{V}_0^{(n-1)a\ell}$ ($\bar{V}_0^{(n-1)b\ell}$) is the contribution to the zeroth element array a (array b) generalized voltage excitation vector from the n-1th approximation current on the ℓ^{th} nearby element. These computations are facilitated by assuming the first approximation distribution of current on all nearby elements is adequate for all approximations and scaling in accordance with the higher-approximation port currents; i.e.,

$$\bar{V}_0^{(n-1)aa'} = \sum_{\ell=1}^{L} \frac{I_\ell^{(n-1)a}}{I_\ell^{(1)a}} \bar{V}_0^{(1)a\ell} \tag{3-146}$$

$$\bar{V}_0^{(n-1)bb'} = \sum_{\ell=1}^{L} \frac{I_\ell^{(n-1)b}}{I_\ell^{(1)b}} \bar{V}_0^{(1)b\ell} \tag{3-147}$$

$I_\ell^{(n)a}$ ($I_\ell^{(n)b}$) is the array a (array b) nth approximation port current at the ℓ^{th} nearby element.

3.3.2 Support Structure Scattering

The effects of hinges, ground screen edges, and other support structures on the radiating element currents can be accounted for naturally within the higher approximations. The first approximation field excites scattering currents on the support structures. These currents radiate fields that enter into the higher approximations by the addition of generalized voltage excitation vectors, $\bar{V}_0^{as}$ and $\bar{V}_0^{bs}$, to (3-141) and (3-142). These equations become

$$(z^a + z_0^{aa}) I_0^{(n)a} + z_0^{ab} I_0^{(n)b} = z^a \tilde{Y}_{i_s}^a (\bar{V}_0^{ex} + \bar{V}_0^{(n-1)aa'} + \bar{V}_0^{(n-1)ab} + \bar{V}_0^{as}) \tag{3-148}$$

$$z_0^{ba} I_0^{(n)a} + (z^b + z_0^{bb}) I_0^{(n)b} = z^b \tilde{Y}_{i_s}^b (\bar{V}_0^{(n-1)bb'} + \bar{V}_0^{(n-1)bs}) \tag{3-149}$$

The infinite array theory employed in the first approximation method naturally provides a plane wave spectra representation of the fields exciting the support structures. The numerous moment method and ray theory computer codes available then are usually directly applicable to computing the support structure scattering.

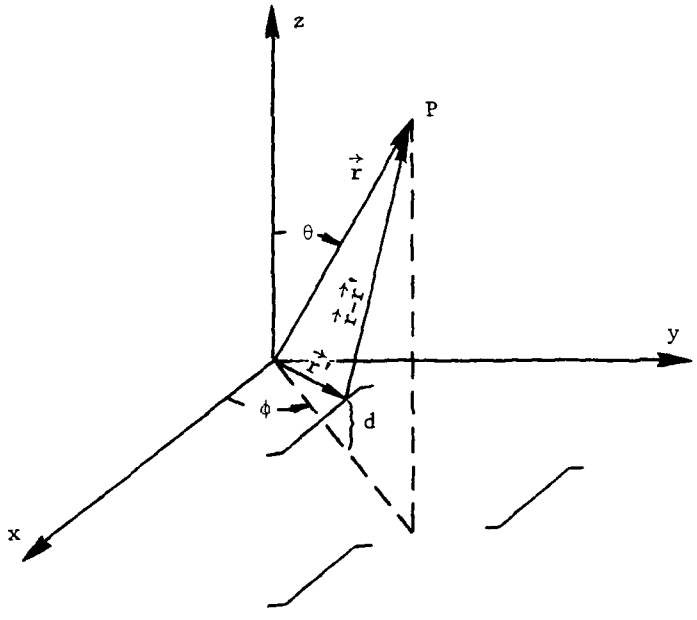

Figure 3-13. Rectilinear Planar Array of Currents a Distance d Above a Ground Screen

3.4 RADIATION PATTERN

Radiation patterns are determined from the target side radiating element currents on array a (array b with radar in transmit mode). If possible, reciprocity is employed during radar receive. If reciprocity is not permissible, as is likely with active modules, the radar receive pattern has to be analyzed directly. The array b radiating elements then lie on the feed side of the lens. Far-field radiation formulas then apply to lens sections individually, provided each section is in the far field of the receiver. In many instances, the cells defined in Section 3.1.1 may satisfy this constraint.

The first approximation currents on a cell have associated closed form radiation patterns. These are employed where ever possible. The details in computing first approximation cell and lens far-field patterns, with and without lens structural warping, are discussed below.

3.4.1 Planar Periodic Array

Radiation from one side of a cell having boundaries coinciding with its periodicity axis (Section 3.2.4) is considered here. Cells of more general shape are treated in Section 3.4.4. All radiating elements throughout the cell are identical, all are located at the nodes of a rectilinear lattice (Figure 3-7), all lie a height d above a perfect ground screen, and all can be modeled as electrically thin bent wires. A typical cell and coordinate system are shown in Figure 3-13. The position vector $\vec{r}'$ locates a point on a radiating element, $\vec{r}''$ locates its image point, and $\vec{r}$ locates a field point P. The coordinate system xy plane coincides with the infinite ground screen. The far-field vector potential for this array is given by

$$\vec{A}(\vec{r}) = \frac{e^{-jkr}}{4\pi r} \left[\int I'(\vec{r}') \, e^{jk\frac{\vec{r}\cdot\vec{r}'}{r}} \, d\vec{r}' + \int I''(\vec{r}'') \, e^{jk\frac{\vec{r}\cdot\vec{r}''}{r}} \, d\vec{r}'' \right] \quad (3\text{-}150)$$

where $I'(\vec{r}')$ is the array current, $I''(\vec{r}'')$ is the image current, and k is the wavenumber. The field point direction is given by

$$\hat{r} = \sin\theta\cos\phi\,\hat{x} + \sin\theta\sin\phi\,\hat{y} + \cos\theta\,\hat{z} \quad (3\text{-}151)$$

where a "^" indicates a unit vector. The xyz components of $\hat{r}$ are the directional cosines of $\hat{r}$.

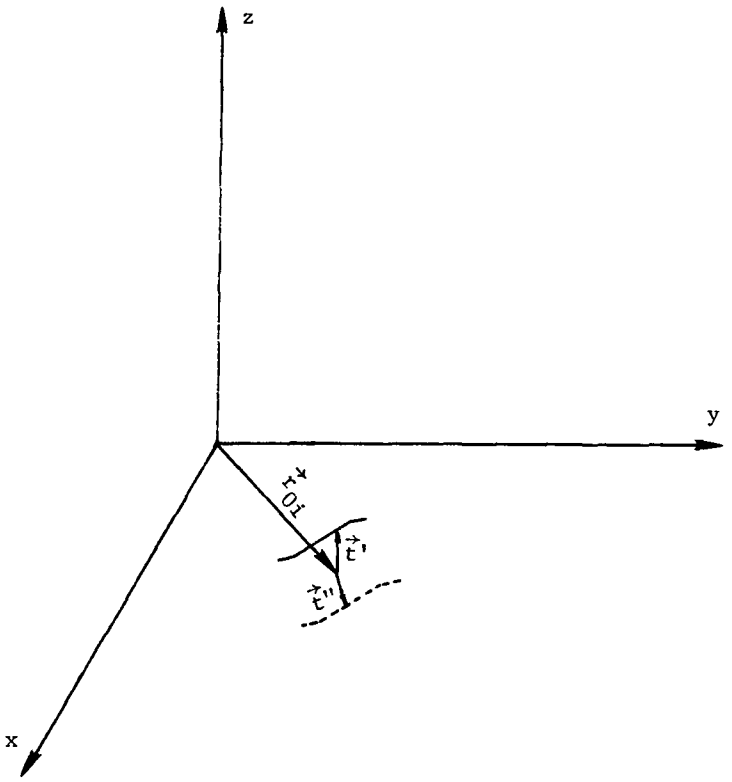

Figure 3-14. The i^{th} Element Current and Image

The array current and image are sums of the N individual radiating element currents I'_i and their images I''_i.

Equation (3-150) then becomes

$$\vec{A}(\vec{r}) = \frac{e^{-jkr}}{4\pi r} \sum_{i=1}^{N} \left[\int I'_i(\vec{r}') \, e^{jk\hat{r}\cdot\vec{r}'_i} \, d\vec{r}' + \int I''_i(\vec{r}'') \, e^{jk\hat{r}\cdot\vec{r}_i} \, d\vec{r}'' \right] \tag{3-152}$$

where $\vec{r}'_i$ locates a current source point on the i^{th} element and $\vec{r}''_i$ locates its image point; i.e.,

$$\vec{r}''_i = (\vec{r}'_i \cdot \hat{x})\hat{x} + (\vec{r}' \cdot \hat{y})\hat{y} - (\vec{r}'_i \cdot \hat{z})\hat{z} \tag{3-153}$$

as indicated in Figure 3-14. Let

$$\vec{r}'_i = \vec{r}_{oi} + \vec{t}' \tag{3-154}$$

$$\vec{r}''_i = \vec{r}_{oi} + \vec{t}'' \tag{3-155}$$

where $\vec{r}_{oi}$ locates the ground screen point corresponding to the array lattice point (the module is generally located at $\vec{r}_{oi}$), and $\vec{t}'$ and $\vec{t}''$ are as indicated in Figure 3-14. Note that $\vec{t}''$ is defined from $\vec{t}'$ by

$$\vec{t}'' = (\vec{t}' \cdot \hat{x})\hat{x} + (\vec{t}' \cdot \hat{y})\hat{y} - (\vec{t}' \cdot \hat{z})\hat{z} \tag{3-156}$$

Also $\vec{t}'$ is the same for corresponding points on the structurally identical elements. Equation (3-152) becomes

$$\vec{A}(\vec{r}') = \frac{e^{-jkr}}{4\pi r} \sum_{i=1}^{N} e^{jk\hat{r}\cdot\vec{r}_{oi}} \left[\int I'_i(\vec{r}') \, e^{jk\hat{r}\cdot\vec{t}'} \, d\vec{r}' + \int I''_i(\vec{r}'') \, e^{jk\hat{r}\cdot\vec{t}} \, d\vec{r}'' \right] \tag{3-157}$$

Assume that the current distributions on all elements throughout the cell are identical within a complex constant; i.e.,

$$I'_i = K_i I'_{ref} \tag{3-158}$$

where I'_{ref} is the reference element current and K_i is the ratio of i^{th} element to reference element port currents.

Equation (3-157) becomes (3-159)

$$\vec{A}(\vec{r}) = \frac{e^{-jkr}}{4\pi r}\left[\int I'_{ref}(\vec{r}')\, e^{jk\hat{r}\cdot\vec{t}}\, d\vec{r}' + \int I''_{ref}(\vec{r}'')\, e^{jk\hat{r}\cdot\vec{t}}\, d\vec{r}''\right]\sum_{i=1}^{N} K_i\, e^{jk\hat{r}\cdot\vec{r}_{oi}}$$

where $I''_{ref}(r'')$ is the reference element image current.

The reference element current moment can be approximated by

$\sum_{j=1}^{N_s} I'_{ref_j}\, \Delta_j \hat{\ell}_j$ where the electrically small segment lengths Δ_j and segment unit vectors $\hat{\ell}'_j$ are shown in Figure 3-4, and N_s is the total number of segments on the wire (note that the segmentation begins a half segment in from each wire end; this better models the zero current condition at these points). The corresponding image current moment becomes $-\sum_{j=1}^{N_s} I'_{ref_j}\, \Delta_j \hat{\ell}''_j$

where

$$\hat{\ell}''_j = (\hat{\ell}'_j \cdot \hat{x})\hat{x} + (\hat{\ell}'_j \cdot \hat{y})\hat{y} - (\hat{\ell}'_j \cdot \hat{z})\hat{z} \qquad (3\text{-}160)$$

Equation (3-159) then is approximated by

$$\vec{A}(\vec{r}) = \vec{e}F \qquad (3\text{-}161)$$

where the element factor $\vec{e}$ and array factor F are given by

$$\vec{e} = \frac{e^{-jkr}}{4\pi r}\sum_{j=1}^{N_s} I'_{ref_j}\, \Delta_j \left(\hat{\ell}'_j\, e^{jk\hat{r}\cdot\vec{t}_j} - \hat{\ell}''_j\, e^{jk\hat{r}\cdot\vec{t}''_j}\right) \qquad (3\text{-}162)$$

$$F = \sum_{i=1}^{N_s} K_i\, e^{jk\hat{r}\cdot\vec{r}_{oi}} \qquad (3\text{-}163)$$

respectively. The $\vec{t}'_j$ and $\vec{t}''_j$ in (3-162) correspond to $\vec{t}'$ and $\vec{t}''$ at the center points of the j^{th} segment and its image, respectively. Equation (3-161) is an expression of pattern multiplication. The underlying assumption in (3-161) is that the current distributions on any two array elements differ by only a complex constant.

The θ and ϕ components of the far radiated $\vec{E}$ and $\vec{H}$ fields are given in terms of F and the θ and ϕ components of $\vec{e}$ as

$$\begin{aligned} E_\theta &= -jk\eta e_\theta F \\ E_\phi &= -jk\eta e_\phi F \\ H_\theta &= -\frac{1}{\eta} E_\phi \\ H_\phi &= -\frac{1}{\eta} E_\theta \end{aligned} \tag{3-164}$$

where η is the free space impedance.

3.4.2 Regular Cells

The array factor F assumes a closed form expression for each feedback mode of the first approximation currents on a regularly shaped cell. A regularly shaped cell is one with boundaries that are parallel to the cell's rectilinear lattice unit vectors ($\hat{e}$ and $\hat{y}$ in Figure 3-15). Such boundaries form parallelograms. Radiation from irregularly shaped cells is treated in Section 3.4.3.

Consider a coordinate system as indicated in Figure 3-15. With respect to this system,

$\vec{r}_{oi}$ of (3-163) becomes $\vec{r}'_{mn}$ where (Section 3.2.4)

$$\vec{r}'_{mn} = md_e\hat{e} + nd_y\hat{y} \tag{3-165}$$

and

$$\hat{r}\cdot\vec{r}'_{mn} = md_e s_e + nd_y s_y \tag{3-166}$$

and the field point e and y directional cosines s_e and s_y are

$$s_e = \hat{r}\cdot\hat{e} \tag{3-167}$$

$$s_y = \hat{r}\cdot\hat{y} \tag{3-168}$$

The K_i of (3-158) become, for each first approximation feedback mode,

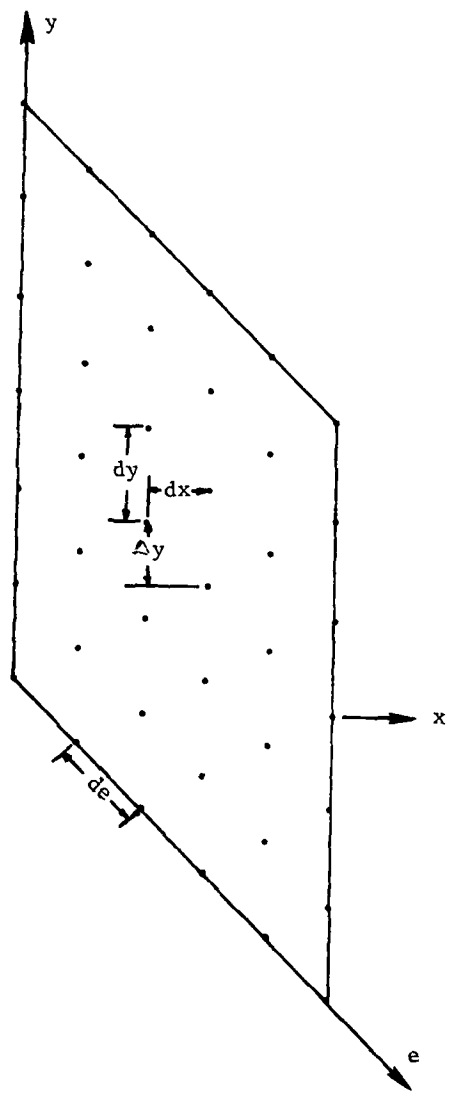

Figure 3-15. Regularly Shaped Cell

$$K_{mn} = e^{-jk(md_e\alpha_e + nd_y\alpha_y)}$$

$$= e^{-jk\vec{r}'_{mn}\cdot\vec{\alpha}} \tag{3-169}$$

where

$$\vec{\alpha} = \alpha_e\hat{e} + \alpha_y\hat{y} \tag{3-170}$$

Equation (3-163) then becomes

$$F = \sum_{m=0}^{N_e-1}\sum_{n=0}^{N_y-1} e^{jk\vec{r}'_{mn}\cdot(\hat{r} - \vec{\alpha})}$$

$$= \sum_{m=0}^{N_e-1}\sum_{n=0}^{N_y-1} e^{jm\psi_e} e^{jn\psi_y} \tag{3-171}$$

where

$$\psi_e = kd_e(s_e - \alpha_e) \tag{3-172}$$

$$\psi_y = kd_y(s_y - \alpha_y) \tag{3-173}$$

and N_e and N_y are the number of elements along constant y and constant e lattice lines, respectively, in the cell. These numbers are $N_e = 6$ and $N_y = 7$ for the Figure 3-15 cell.

The array factor can be expressed in terms of the x and y directional cosines

$$s_x = \sin\theta\cos\phi \tag{3-174}$$

$$s_y = \sin\theta\sin\phi \tag{3-175}$$

Since (Section 3.2.4)

$$\hat{e} = \frac{d_x\hat{x} - \Delta_y\hat{y}}{d_e} \tag{3-176}$$

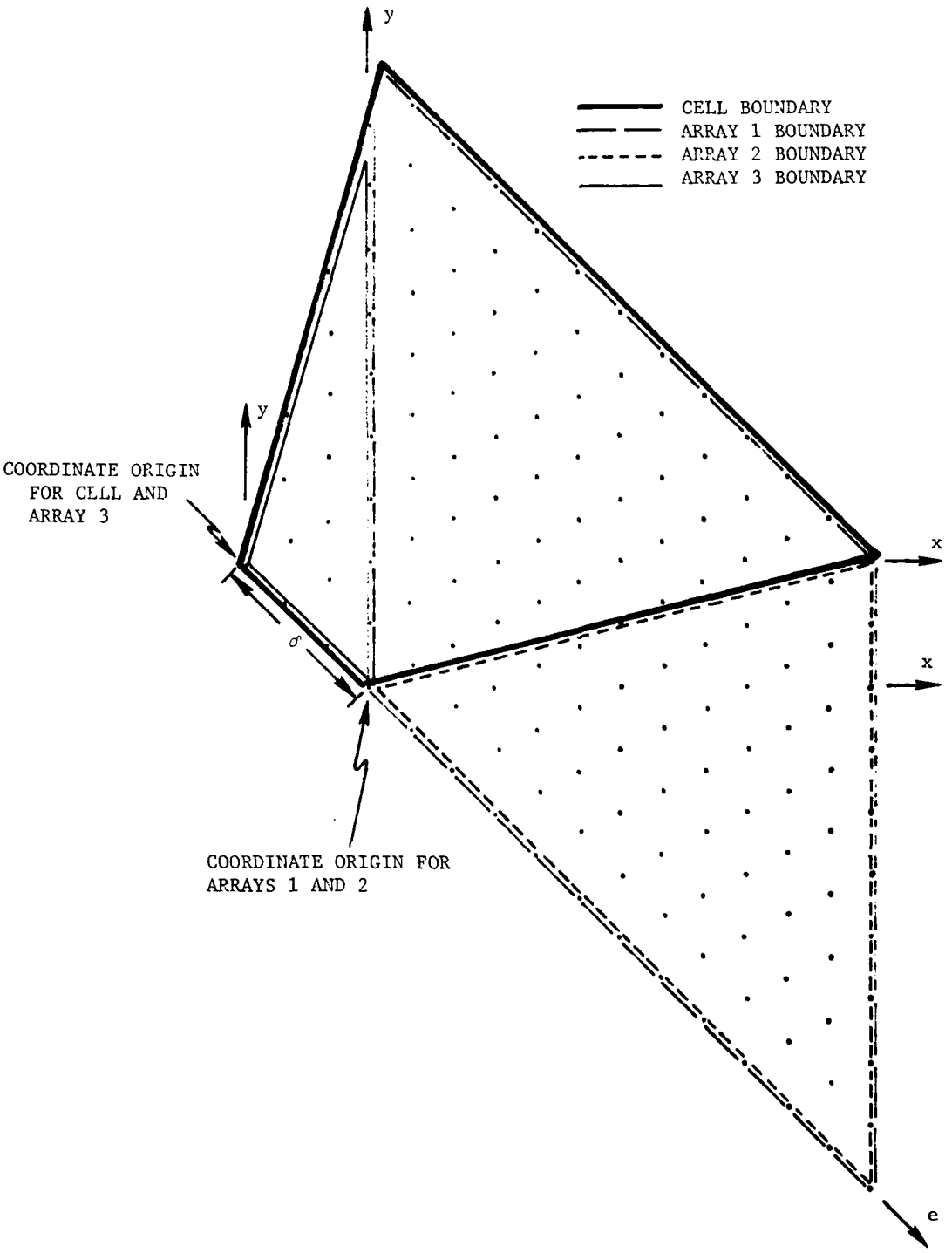

Figure 3-16. Definition of Three Arrays, Having Closed Form Array Factors, that Combine to Form Cell Array

then

$$s_e = \mathbf{r}\cdot\mathbf{e} = \frac{s_x d_x}{d_e} - \frac{s_y \Delta_y}{d_e} \tag{3-177}$$

In closed form, $F = F(s_x, s_y)$ then becomes

$$F(s_x,s_y) = e^{j(N_e-1)\psi_e/2}\, e^{j(N_y-1)\psi_y/2}\, \frac{\sin N_e\psi_e/2}{\sin \psi_e/2}\, \frac{\sin N_y\psi_y/2}{\sin \psi_y/2} \tag{3-178}$$

where

$$\psi_e = k(s_x d_x - s_y \Delta_y - \alpha_e d_e) \tag{3-179}$$

$$\psi_y = k(s_y d_y - \alpha_y d_y) \tag{3-180}$$

3.4.3 Irregular Cells

The closed form expressions for the cell array factor developed in Section 3.4.2 assume that the cell boundaries coincide with the cell lattice vectors. This restricts cell shapes to parallelograms. In general, the geometry of the cell boundaries may not coincide with the rectilinear structure. An example is shown in Figure 3-16 (heavy line). A closed form expression for the array factor for this cell is obtained by combining several array factors. Three additional arrays are indicated in Figure 3-16. Array 1 is "regular" (bounded by a parallelogram with sides coinciding with constant lattice coordinate lines). The array factor for Array 1, therefore, is given by (3-178). Arrays 2 and 3 form triangles bounded on two sides with constant lattice coordinate lines. Along each third side the y coordinate varies linearly with e coordinate. A closed form expression for this array type is derived below. The cell array factor then is given by

$$F = e^{jk\hat{r}\cdot\vec{r}_1} F_1 - e^{jk\hat{r}\cdot\vec{r}_2} F_2 + e^{jk\hat{r}\cdot\vec{r}_3} F_3 \tag{3-181}$$

where the subscript indicates the array number. The phase factors $kr\cdot r_1$, etc., are necessary to translate the corresponding array coordinate origins, references for array factors F_1, etc., to the cell coordinate origin. In the Figure 3-16 example,

$$\vec{r}_1 = \vec{r}_2 = \delta\hat{e} \text{ and } \vec{r}_3 = 0$$

Array factors for array shapes such as Array 2 and Array 3 of Figure 3-16 are of the form

$$F = \sum_{m=0}^{N_e-1} \left[e^{jm\psi_e} \sum_{n=0}^{N_y(m)-1} e^{jn\psi_y} \right] \tag{3-182}$$

This equation is similar to (3-171) except that N_y in (3-182) is now a function of m (i.e., $N_y = N_y(m)$). A linear behavior, expressed by

$$N_y(m) = \varepsilon_0 + \varepsilon_1 m \tag{3-183}$$

results in a closed form expression for (3-182). The inner summation in (3-182) becomes

$$\sum_{n=0}^{N_y(m)-1} e^{jn\psi_y} = \frac{e^{jN_y(m)\psi_y} - 1}{e^{j\psi_y} - 1} \tag{3-184}$$

This results in

$$F = \frac{1}{e^{j\psi_y} - 1} \left[\sum_{m=0}^{N_e-1} e^{j(N_y(m)\psi_y + m\psi_e)} - \sum_{m=0}^{N_e-1} e^{jm\psi_e} \right] \tag{3-185}$$

which reduces further to

$$F = F(s_x, s_y) = \frac{1}{e^{j\psi_y} - 1} \left[e^{j[t_0\psi_y + (N_e-1)\psi']} \frac{\sin N_e\psi'}{\sin \psi'} - e^{j(N_e-1)\psi_e/2} \frac{\sin (N_e\psi_e/2)}{\sin (\psi_e/2)} \right] \tag{3-186}$$

where

$$\psi' = (\varepsilon_1 \psi_y + \psi_e)/2 \tag{3-187}$$

and ψ_e and ψ_y are given by (3-179) and (3-180).

Note that when $\varepsilon_1 = 0$, N_y is a constant ($=\varepsilon_0$) and (3-186) reduces to (3-178) as expected.

3.4.4 Flat Lens

The far-field radiation pattern of a flat lens face is considered here. Curved lens faces, as may occur from structural deployment errors or from severe temperature gradients, are considered in Section 3.4.5.

The lens patterns are with respect to a lens coordinate system, termed "global," having z axis directed outward from the lens plane. The relationship between the global coordinate system and the local coordinate system for the v^{th} cell is shown in Figure 3-17. The g subscript refers to the global system and the v subscript to the cell system. The v^{th} cell is positioned $\vec{r}_{gv}$ from the global system and rotated an angle ϕ_v in the lens plane as indicated.

The lens pattern is obtained by combining the contributions from all the cells. Closed form cell pattern expressions with respect to local cell coordinate systems have been developed in Sections 3.4.2 and 3.4.3. These expressions must be modified to refer to the global coordinate system. The array factor of the v^{th} cell $F_v(s_x, s_y)$ is given by

$$F_v(s_x, s_y) = e^{jk\hat{r}\cdot\vec{r}_{gv}} F(s_x, s_y) \tag{3-188}$$

where $F(s_x, s_y)$ is (3-178) or of the type (3-181) and

$$s_x = \hat{r}\cdot\hat{x}_v \tag{3-189}$$

$$s_y = \hat{r}\cdot\hat{y}_v \tag{3-190}$$

The global system rectangular components of the field point unit vector $\hat{r}$, in column vector form, are given by

$$\hat{r}_g = \begin{bmatrix} \hat{r}\cdot\hat{x}_g \\ \hat{r}\cdot\hat{y}_g \\ \hat{r}\cdot\hat{z}_g \end{bmatrix} = \begin{bmatrix} \sin\theta\cos\phi \\ \sin\theta\cos\phi \\ \cos\theta \end{bmatrix} \tag{3-191}$$

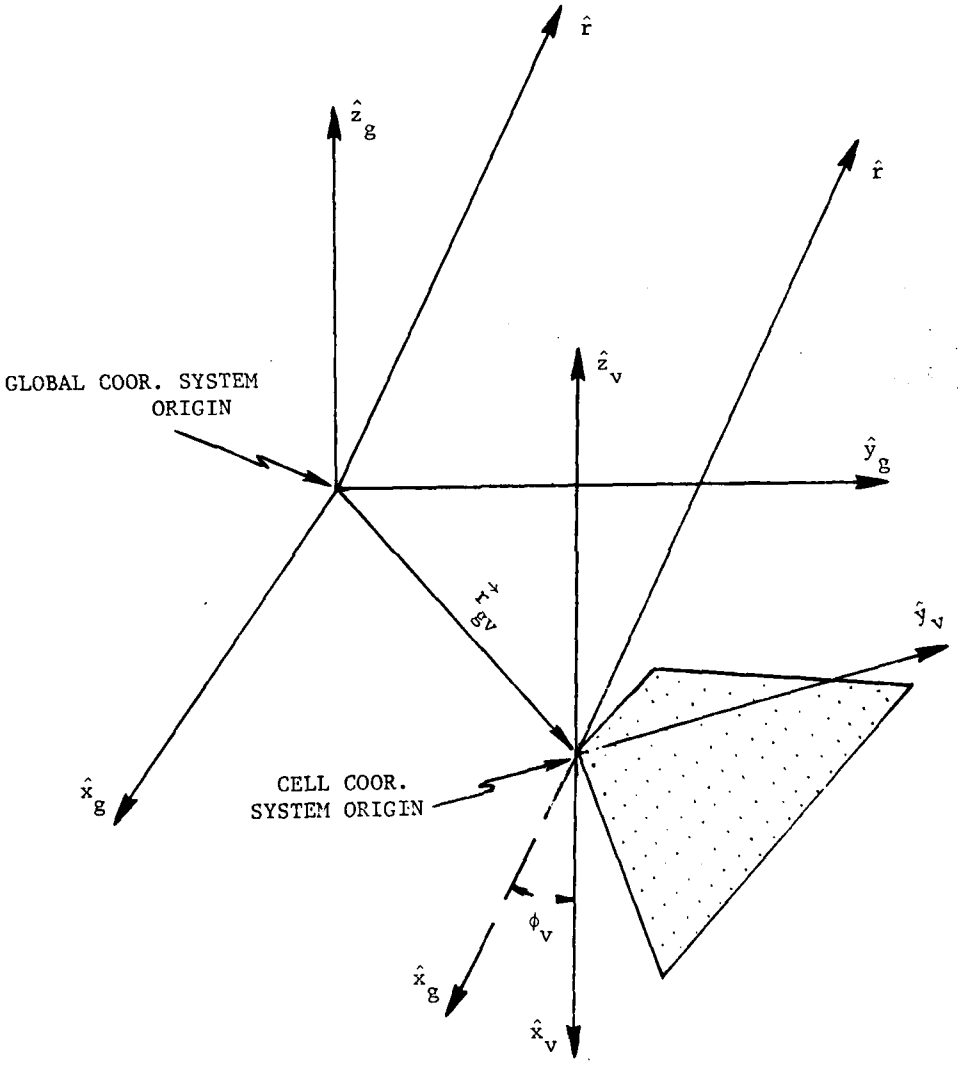

Figure 3-17. Cell Lying in Plane of Lens

In the local coordinate system of the v^{th} cell, $\hat{r}$ has rectangular components given by

$$\hat{r}_v = \begin{bmatrix} \hat{r}\cdot\hat{x}_v \\ \hat{r}\cdot\hat{y}_v \\ \hat{r}\cdot\hat{z}_v \end{bmatrix} = [R_v]\,\hat{r}_g \tag{3-192}$$

where $[R_v]$ is the coordinate system rotation matrix. For flat cells, the z axes of the global and local coordinate systems coincide resulting in

$$[R_v] = \begin{bmatrix} \cos\phi_v & \sin\phi_v & 0 \\ -\sin\phi_v & \cos\phi_v & 0 \\ 0 & 0 & 1 \end{bmatrix} \tag{3-193}$$

Equation (3-162) for the element factor $\vec{e}$ and (3-178) or equations of type (3-181) for the array factor F employ $\hat{r}$ with components given by $\hat{r}_v$ in determining the v^{th} cell contribution to the lens pattern.

The lens fields (3-164) are computed from the θ and ϕ components of the element factor, e_θ and e_ϕ. Here θ and ϕ are with respect to the global system. Since $\hat{\ell}'_j$ and $\hat{\ell}''_j$ in (3-162) are generally known in local system coordinates, a determination of e_θ and e_ϕ requires that $\hat{\theta}$ and $\hat{\phi}$ be expressed in local coordinates. In column vector form, the $\hat{\theta}$ and $\hat{\phi}$ global system rectangular components are respectively

$$\hat{\theta}_g = \begin{bmatrix} \hat{\theta}\cdot\hat{x}_g \\ \hat{\theta}\cdot\hat{y}_g \\ \hat{\theta}\cdot\hat{z}_g \end{bmatrix} = \begin{bmatrix} \cos\theta\cos\phi \\ \cos\theta\sin\phi \\ -\sin\theta \end{bmatrix} \tag{3-194}$$

$$\hat{\phi}_g = \begin{bmatrix} \hat{\phi}\cdot x_g \\ \hat{\phi}\cdot y_g \\ \hat{\phi}\cdot z_g \end{bmatrix} = \begin{bmatrix} -\sin\phi \\ \cos\phi \\ 0 \end{bmatrix} \tag{3-195}$$

The corresponding v^{th} cell rectangular components are

$$\hat{\theta}_v = [R_v]\hat{\theta}_g \tag{3-196}$$

$$\hat{\phi}_v = [R_v]\hat{\phi}_g \tag{3-197}$$

where, for flat cells, $[R_v]$ is given by (3-193).

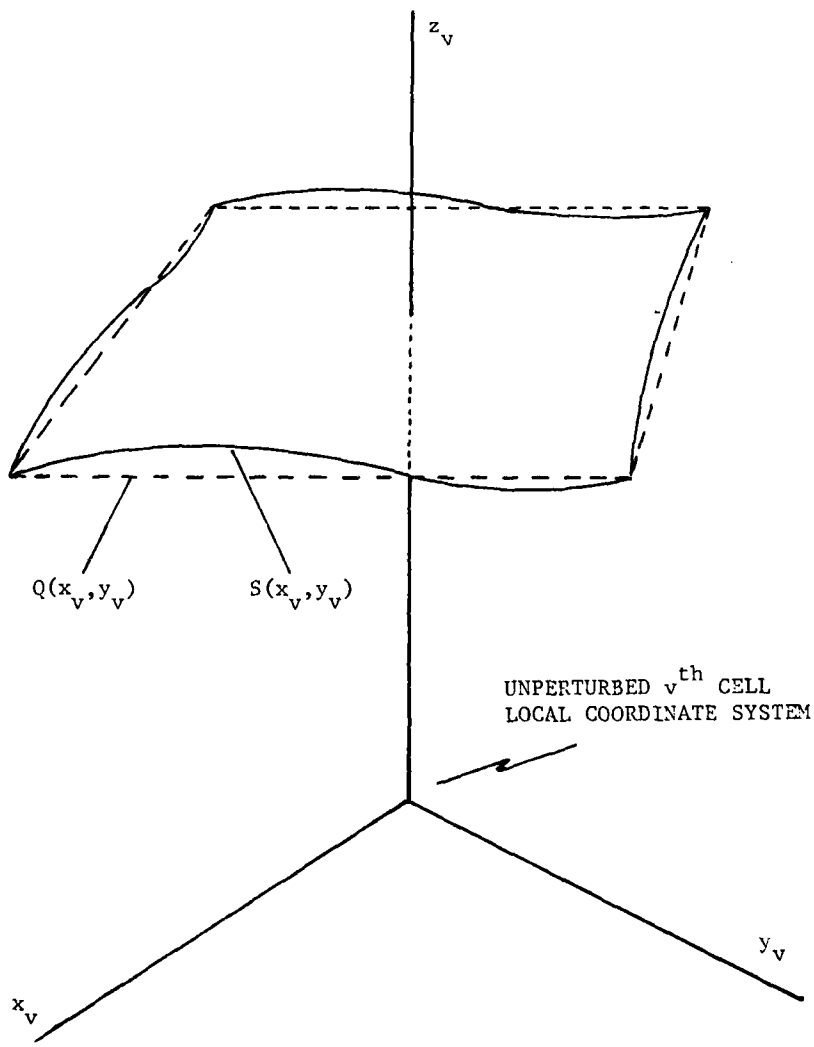

Figure 3-18. Warped Lens Surface S(x,y) with Quadrilateral Approximation Q(x,y)

3.4.5 Nonflat Lens

The pattern expressions -- (3-162), (3-178), and (3-181) -- assume a flat lens array. Departures from flatness can be caused by the adverse space envrionment and possible antenna mechanical malfunctions or imperfections. An example of the former would be array warping caused by thermal gradients across the lens surface induced by alternate light and shadow areas. An example of the latter would be an imperfect mechanical deployment of the lens in space. The development in this section generalizes work done by Coffey and Carver.[15]

The total lens warping is represented in a piecewise manner using the cells defined in Sections 3.4.2 and 3.4.3. A warped array is shown in Figure 3-18. If the warp is smooth and slowly varying, as in thermal expansion, the array surface can be modeled by a continuous function, $S(x_v,y_v)$. Discontinuous warps, such as imperfect antenna panel unfolding, can be modeled by piecewise continuous functions.

If the array edges are connected by straight lines (the dotted lines in Figure 3-18), the resulting surface is a quadrilateral, $Q(x_v,y_v)$, that approximates $S(x_v,y_v)$ linearly in the arguments x_v and y_v. The functional form for $Q(x_v,y_v)$ is

$$Q(x_v,y_v) = b_0 + b_1x_v + b_2y_v + b_3x_vy_v \tag{3-198}$$

here the coefficients b_0, b_1, b_2, and b_3 are unknowns. The x_v,y_v cross-term, b_3, is a measure of the twist in the warped surface. The unknown coefficients of $Q(x_v,y_v)$ could be determined by choosing four "representative" array elements locations (e.g., the elements closest to the corners of the array) and obtaining four linear equations in the four coefficient unknowns. Different representative elements will lead to different choices of $Q(x_v,y_v)$.

There should be little variation in the various quadrilaterals for small warps. A least-squares analysis could be performed on all array element locations to obtain a "best" quadrilateral approximation. It is believed that such an analysis will not be necessary.

A simple expression for the array factor for a quadrilateral surface is not presently available. Consequently, a further approximation must be made. A planar surface, $P(x_v,y_v)$, of the form

$$P(x_v,y_v) = a_0 + a_1x_v + a_2y_v \tag{3-199}$$

is made to "best fit" the quadrilateral $Q(x_v,y_v)$ by minimizing the integral

AD-A093 493 ATLANTIC RESEARCH CORP ROME NY F/G 17/9
SPACE-BASED RADAR ARRAY SYSTEM SIMULATION AND VALIDATION,(U)
SEP 80 H K SCHUMAN, D R PFLUG, L D THOMPSON F30602-79-C-0116
UNCLASSIFIED RADC-TR-80-294 NL

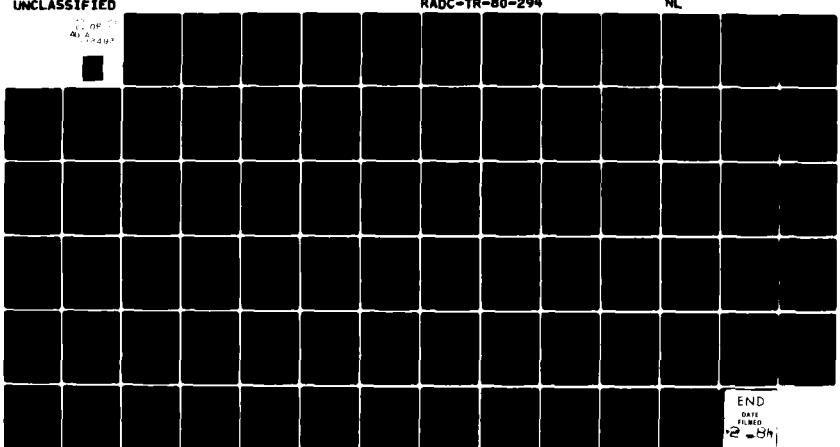

END
DATE FILMED
2-81
DTIC

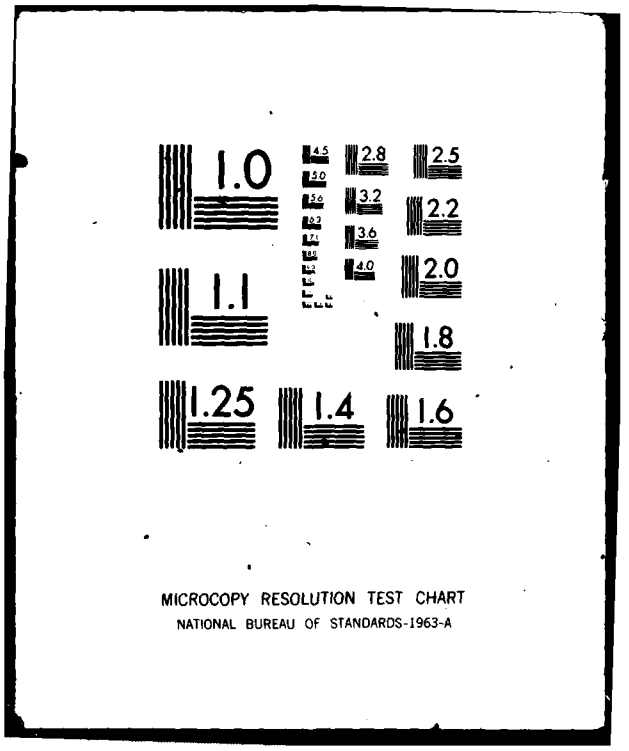

MICROCOPY RESOLUTION TEST CHART
NATIONAL BUREAU OF STANDARDS-1963-A

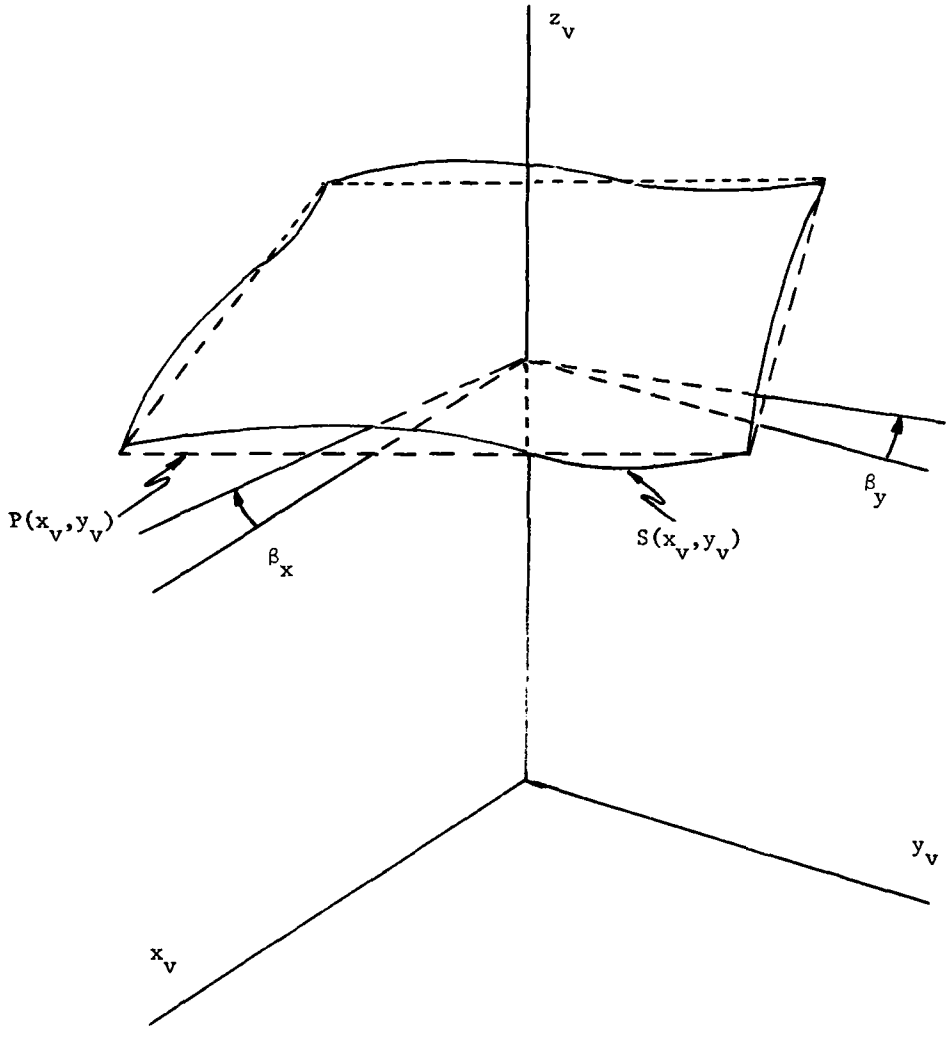

Figure 3-19. Planar Approximation, $P(x_v,y_v)$ to Warped Surface, $S(x_v,y_v)$

$$\int |Q - P| dxdy \tag{3-200}$$

The minimization process leads to the following optimum choices for the coefficients in (3-199):

$$\begin{aligned} a_0 &= b_0 \\ a_1 &= b_1 \\ a_2 &= b_2 \end{aligned} \tag{3-201}$$

The plane, $P(x_v,y_v)$, containing the optimum coefficients will, in general, be tilted with respect to the x_v,y_v plane (Figure 3-19). The tilt is measured by the polar angles β_x and β_y. The equations that determine the tilt angles can be deduced from knowledge of $P(x_v,y_v)$.

$$\begin{aligned} \tan \beta_x &= a_1 \\ \tan \beta_y &= a_2 \end{aligned} \tag{3-202}$$

The overall result is that the warped section of the array can be approximated by a lens array cell tilted in the local unperturbed cell coordinate system an amount measured by the tilt angles. Element periodicity is assumed to still exist on the tilted cell although this periodicity may differ from that of the unperturbed cell. Closed form array factor expressions are not employed if the elements are not periodically located.

The pattern functions must be generalized to include the case of a "tilted" planar array. Let $\vec{r}''_{mn}$ extend from the origin of the v^{th} unperturbed cell local coordinate system to the mn^{th} ground screen lattice point on the corresponding tilted cell (Figure 3-20). Then

$$\vec{r}''_{mn} = a_0\hat{z}_v + \vec{r}^{\,t}_{mn} \tag{3-203}$$

where

$$\vec{r}^{\,t}_{mn} = x_{mn}\hat{x}_v + y_{mn}\hat{y}_v + (a_1x_{mn} + a_2y_{mn})\hat{z}_v \tag{3-204}$$

and $\hat{x}_v$, $\hat{y}_v$, and $\hat{z}_v$ are the cartesian unit vectors of the v^{th} unperturbed cell local coordinate system. $\vec{r}^{\,t}_{mn}$ locates the mn^{th} lattice point in the tilted cell with respect to a local tilted cell coordinate origin.

The vector $\vec{r}^{\,t}_{mn}$ defines the tilted cell. The tilted cell lattice vectors and a suitable tilted cell local coordinate system can be determined from $\vec{r}^{\,t}_{mn}$. The flat

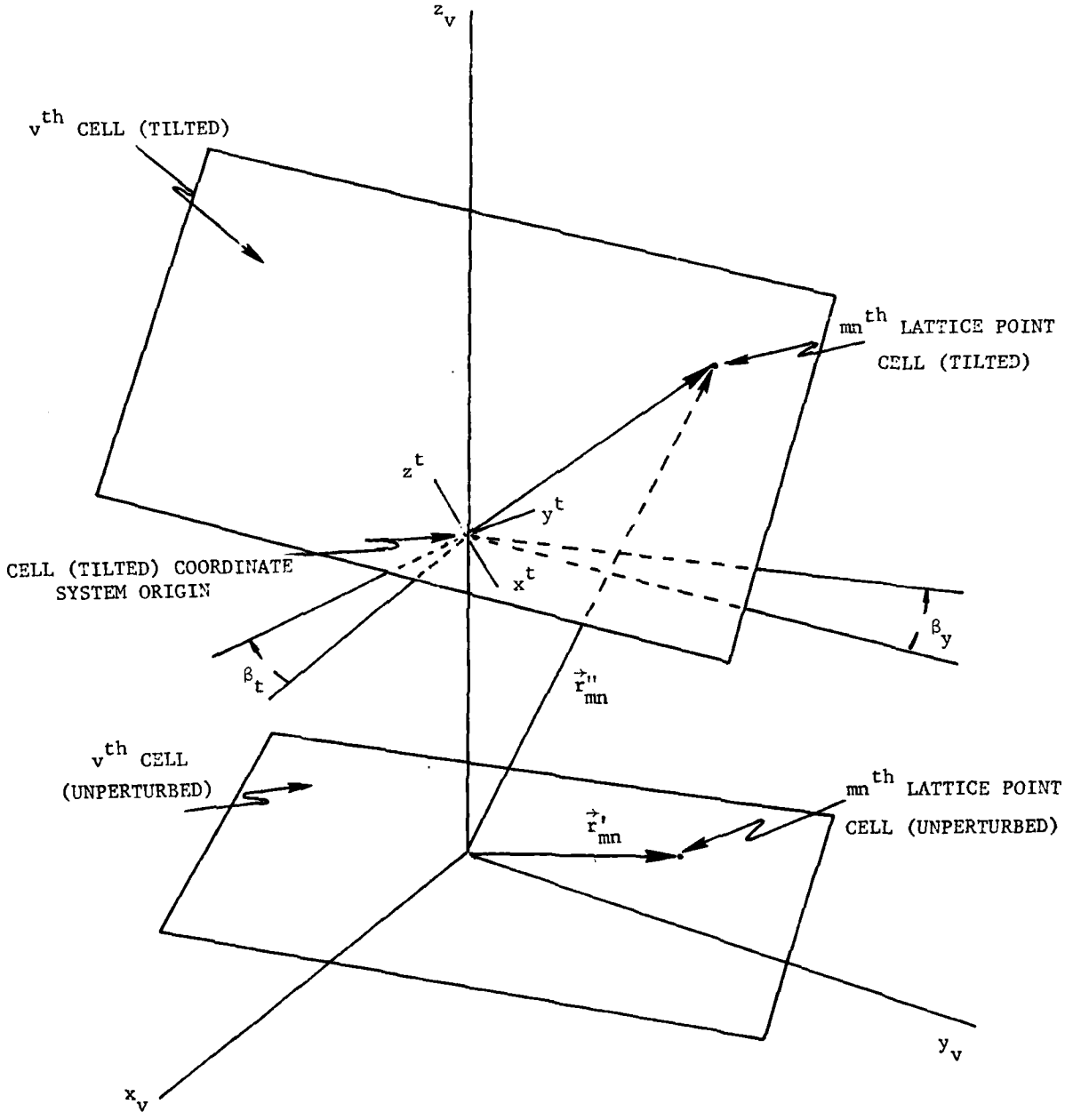

Figure 3-20. Unperturbed Cell and Tilted Cell Approximation to a Warp

cell radiation pattern expressions developed in Sections 3.4.2 and 3.4.3 now are applicable to the tilted cell. The contribution of the tilted cell to the lens pattern then can be obtained by a generalization of the Section 3.4.4 development. This is carried out below.

The mn^{th} lattice point in the unperturbed cell is defined by

$$\vec{r}'_{mn} = md_e \hat{e}_v + nd_y \hat{y}_v \tag{3-205}$$

The quantities in (3-205) are the same as those in (3-165) with the v subscripts implied for e and y in (3-165). From Section 3.2.4,

$$\vec{r}'_{mn} = md_x \hat{x}_v + (nd_y - m\Delta y)\, \hat{y}_v \tag{3-206}$$

The x_{mn} and y_{mn} in (3-204) are the coordinates of the mn^{th} lattice point in the unperturbed cell. From (3-206), therefore,

$$x_{mn} = md_x \tag{3-207}$$

$$y_{mn} = nd_y - m\Delta y \tag{3-208}$$

and (3-204) becomes

$$\vec{r}^{\,t}_{mn} = md_x \hat{x}_v + (nd_y - m\Delta y)\hat{y}_v + [a_1 md_x + a_2(nd_y - m\Delta y)]\, \hat{z}_v \tag{3-209}$$

The y-directed lattice vector of the tilted cell is defined by

$$d^t_y \hat{y}^t = \vec{r}^{\,t}_{m,n+1} - \vec{r}^{\,t}_{mn} \tag{3-210}$$

where d^t_y is the tilted cell y-directed interelement spacing and $\hat{y}^t$ is the tilted cell y-directed lattice unit vector. Similarly, the e directed lattice vector of the tilted cell is defined by

$$d^t_e \hat{e}^t = \vec{r}^{\,t}_{m+1,n} - \vec{r}^{\,t}_{mn} \tag{3-211}$$

with similar definitions for d^t_e and $\hat{e}^t$. Equations (3-202), (3-209), (3-210), and (3-211) combine to yield

$$d^t_y = d_y/\cos\beta_y \tag{3-212}$$

$$d^t_e = \sqrt{d_x^2/\cos^2\beta_x + y^2/\cos^2\beta_y - 2d_x \Delta y \tan\beta_x \tan\beta_y} \tag{3-213}$$

$$\hat{y}^t = \cos\beta_y \hat{y}_v + \sin\beta_y \hat{z}_v \tag{3-214}$$

$$\hat{e}^t = \frac{1}{d_e^t} \left[d_x \hat{x}_v - \Delta y \hat{y}_v + (d_x \tan\beta_x - \Delta y \tan\beta_y) \hat{z}_v \right] \tag{3-214}$$

The x and y cartesian unit vectors in the local tilted cell coordinate system are obtained readily from

$$\hat{x}^t = \vec{A} / \sqrt{\vec{A} \cdot \vec{A}} \tag{3-216}$$

$$\hat{z}^t = \hat{x}^t \times \hat{y}^t \tag{3-217}$$

where

$$\vec{A} = \hat{e}^t - (\hat{y}^t \cdot \hat{e}^t) \hat{y}^t \tag{3-218}$$

Equations (3-212) through (3-218) define the lattice parameters and local coordinate system of the tilted cell. The radiation from a tilted cell then can be determined from the expressions of Sections 3.4.2 and 3.4.3.

A tilted cell lattice structure may differ from its original, unperturbed lattice structure; e.g., an unwarped cell with a rectangular lattice ($\Delta y = 0$) has, after warping, a tilted cell approximation with, from (3-213) and 3-215),

$$\hat{e}^t = \cos \beta_x \, \hat{x}_v + \sin \beta_x \, \hat{z}_v \tag{3-219}$$

From (3-215) and (3-220),

$$\hat{y}^t \cdot \hat{e}^t = \sin \beta_y \sin \beta_x \tag{3-220}$$

The tilted cell lattice is, therefore, not generally rectangular; i.e., $\hat{y}^t \cdot \hat{e}^t \neq 0$.

A tilted cell contribution to the lens far-field pattern is obtained by extending (3-188) to

$$F_v(S_x^t, S_y^t) = e^{jk\hat{r} \cdot (\vec{r}_{gv} + a_0 \hat{z})} F(s_x^t, s_y^t) \tag{3-221}$$

where $\vec{r}_{gv}$ locates the unperturbed cell local coordinate origin and $F(s_x^t, s_y^t)$ is the array factor of the tilted cell with respect to the tilted cell coordinate system. The factor $F(s_x, s_y)$ is given by (3-178) or equations of type (3-181) with s_x and s_y replaced, respectively, by

$$s_x^t = \hat{r} \cdot \hat{x}^t \tag{3-222}$$

$$s_y^t = \hat{r} \cdot \hat{y}^t \tag{3-223}$$

Since $\hat{r}$ will be specified with respect to the global system coordinates (i.e., via the column vector $\bar{r}_g$ of (3-191)) and, since $\hat{r}$ with respect to the unperturbed cell coordinates is $\bar{r}_v$ of (3-192), then, with respect to the tilted cell coordinates, the column vector representation for $\hat{r}$ is

$$\bar{r}_v^t = [R^t]\,[R]\bar{r}_g \tag{3-224}$$

where $[R^t]$ is the tilted cell rotation matrix given by

$$[R^t] = \begin{bmatrix} \hat{x}_v^t \cdot \hat{x}_v & \hat{x}_v^t \cdot \hat{y}_v & \hat{x}_v^t \cdot \hat{z}_v \\ \hat{y}_v^t \cdot \hat{x}_v & \hat{y}_v^t \cdot \hat{y}_v & \hat{y}_v^t \cdot \hat{z}_v \\ \hat{z}_v^t \cdot \hat{x}_v & \hat{z}_v^t \cdot \hat{y}_v & \hat{z}_v^t \cdot \hat{z}_v \end{bmatrix} \tag{3-225}$$

The expression for the element factor $(\vec{e})$ for a tilted cell is given by (3-162) with $\hat{r}$ having components given by $\bar{r}_v^t$. Since $\hat{\ell}_j'$ and $\hat{\ell}_j''$ are known with respect to the tilted cell coordinate system, a determination of e_θ and e_ϕ requires that $\hat{\theta}$ and $\hat{\phi}$ be expressed in tilted cell coordinates. In column vector form, these coordinates become

$$\bar{\theta}_v^t = [R^t]\,[R]\bar{\theta}_g \tag{3-226}$$

$$\bar{\phi}_v^t = [R^t]\,[R]\bar{\phi}_g \tag{3-227}$$

where $\bar{\theta}_g$ and $\bar{\phi}_g$ are defined by (3-194) and (3-195). Equations (3-196) and (3-197) were employed in deriving (3-226) and (3-227).

SECTION 4
IMPLEMENTATION

The SBR RF simulation successive approximation method software is subdivided into two sections, based upon level of approximation. One section implements the First Approximation Method (FAM), which makes extensive use of infinite array theory (Section 3.2). The second implements the Higher Approximation Method (HAM), which employs previous approximation results in a conventional isolated element moment method approach to calculating the edge effects and effects of nonperiodicities on current distributions and antenna patterns (Section 3.3).

4.1 PROGRAM FUNCTIONAL DESCRIPTION

4.1.1 First Approximation Method

The first approximation analysis is performed for each cell. Data for array a are read in and the element data are calculated in subroutine GEOMET (Figure 4-1). GEOMET is called again to calculate array b element data after array b data are read in.

The program loops over the incident plane waves from 1 to NPWAVE. An inner loop then begins over the feedback modes. The feedback mode counters are calculated for both array a and array b. The phase functions for the total impressed field are calculated at each array reference element.

Subroutine ZMATX is called with array b data to calculate the array b impedance matrix, [Z], for an infinite array above an infinite perfect ground screen and [ZF] for an infinite array in free space. Subroutine SCAN is called to calculate the array b admittance matrix by inverting [Z] and calculating the active impedance. The array b reference element current for unit port voltage excitation is saved. The reference element port current is taken from the LSB^{th} column of [Z], where LSB is the number of the current segment containing the antenna element feedpoint for array b elements.

ZMATX is called again with array a data to calculate the array a above a ground screen impedance matrix [Z]. The impedance matrix for array a in free space [ZF] is also calculated in ZMATX and is written to a file. Matrix [Z] for array a is sent to SCAN to calculate the admittance matrix for array a and the active impedance for array a. The LSA^{th} column of [Z] is saved. It is the element current for unit port excitation.

For a zero feedback loop, matrix [Z] for array a is sent to SCIA to calculate the array a generalized voltage and current vectors. The reference element port current, SCIAEX, is also calculated.

Array a and array b reference element port currents are then calculated for the zero feedback loop using SCIAEX.

If there is feedback and if the number of feedback modes is zero, the array a impedance matrix for free space [ZF] is read from the file. It is sent to SCAN to calculate the array a reference element free space admittance matrix and element active impedance.

The array a impedance matrix for free space [ZF] and the array a active impedance are sent to subroutine MUTUAL to calculate the mutual impedance between array b and array a through the imperfect ground plane. MUTUAL also calculates the array a generalized voltage and current vectors arising from current on array b. The mutual impedance is used to calculate the feedback mode array a and array b references element port currents.

When there is no feedback, the call to SCAN for the free space active impedance and the call to MUTUAL are bypassed.

The program continues by calculating the reference element port feedback voltages. For feedback, the voltage array is corrected for array b port current excitation. For no feedback, the voltage and current arrays are set to zero.

Array a and array b generalized current vectors then are adjusted for the correct array port voltages. The current and voltage arrays for array a and array b are written to file. This ends the feedback loop.

Subroutine CELPAT is called to calculate the array b current moments for the reference elements and the pattern of the antenna cell under analysis. The individual cell patterns are stored on a file for integration into the total lens pattern.

Array a reference element voltage and current induced for each incident plane wave are written to file. This ends the plane wave loop.

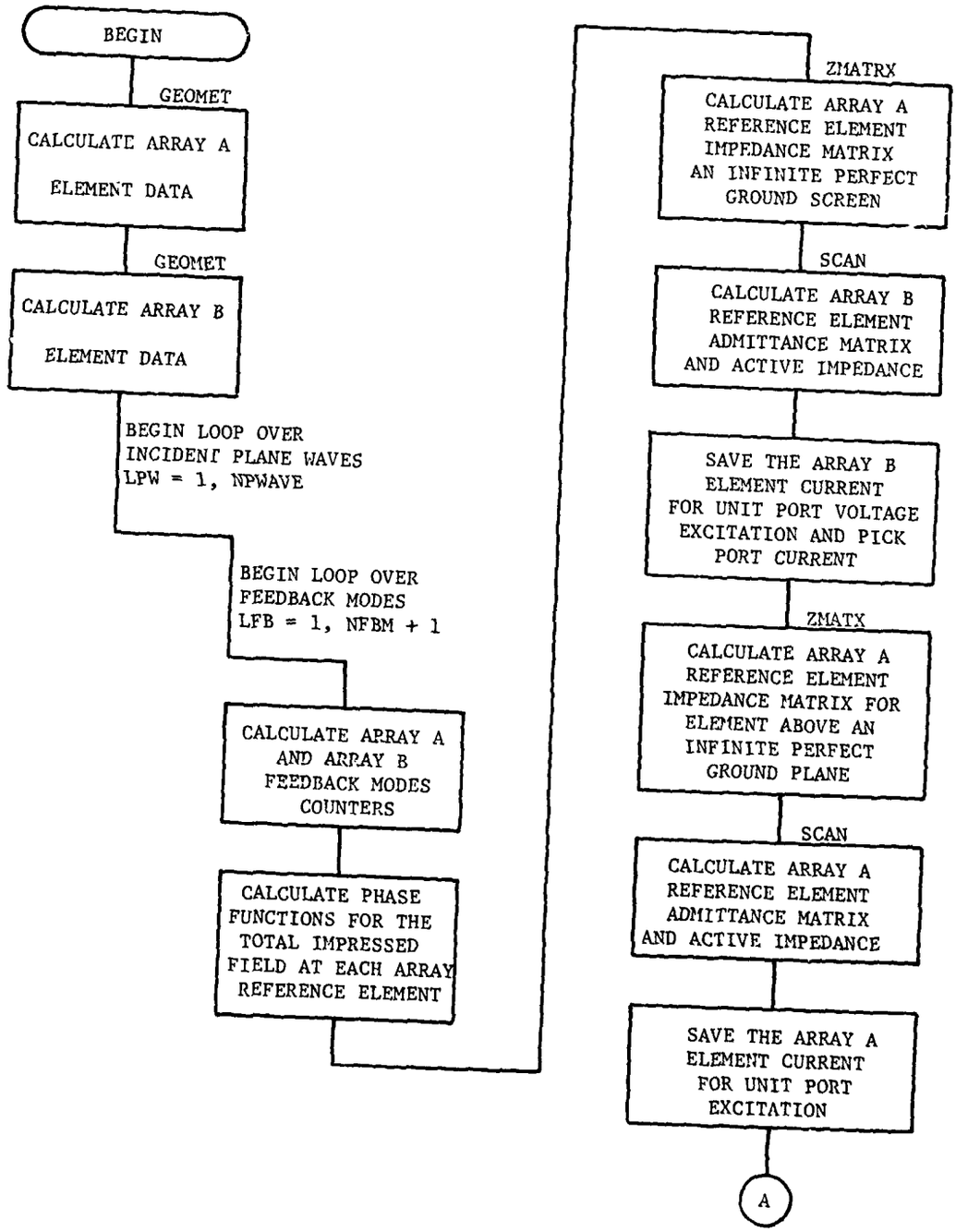

Figure 4-1. FAM Flow Chart

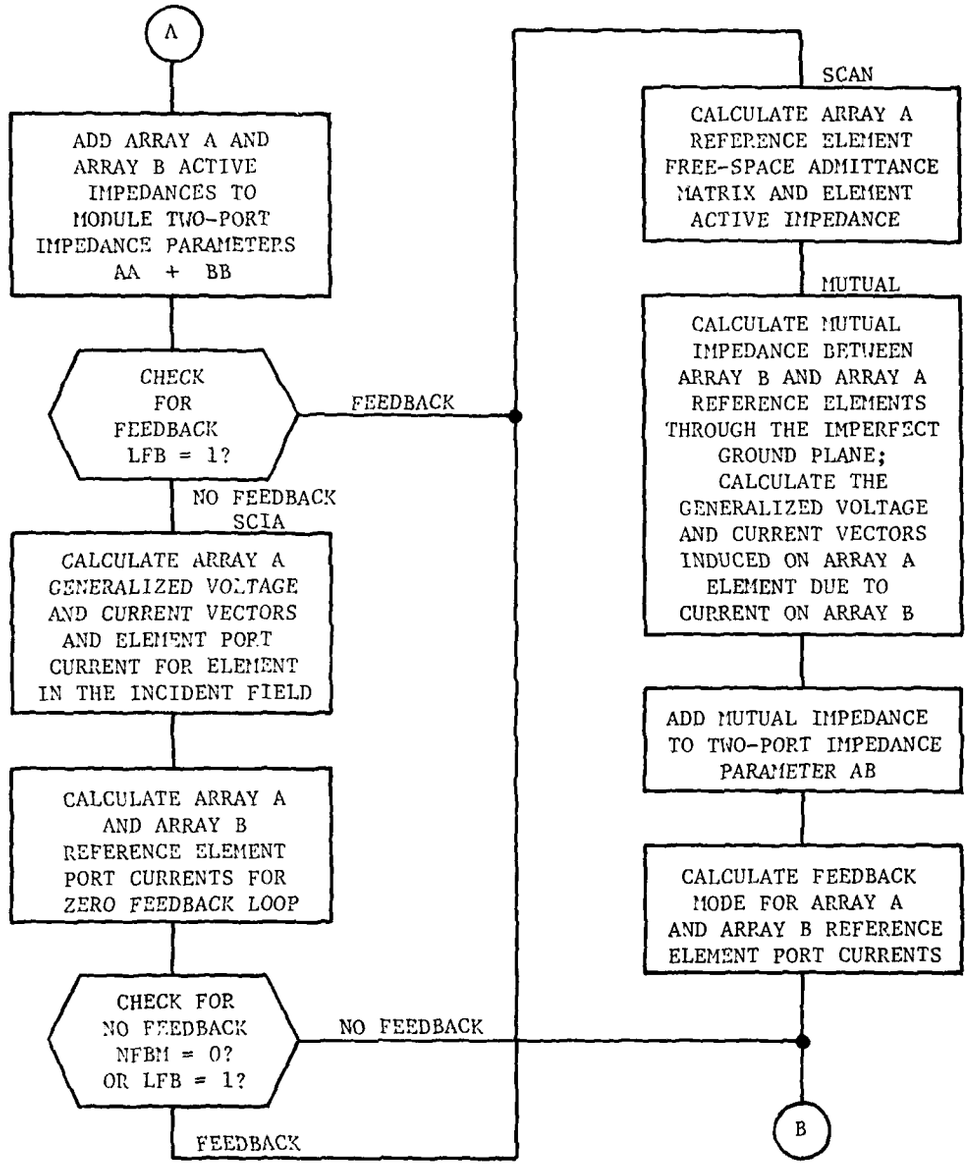

Figure 4-1. FAM Flow Chart (continued)

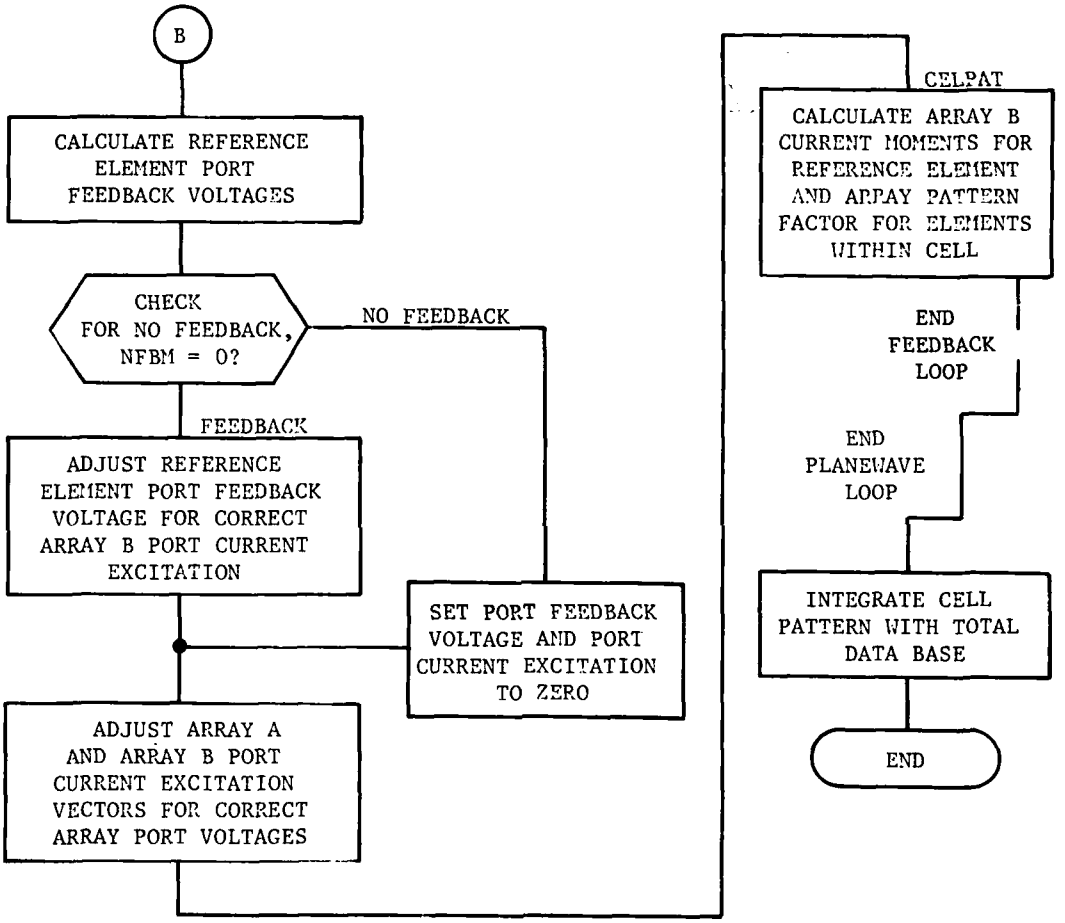

Figure 4-1. FAM Flow Chart (continued)

4.1.2 Higher Approximation Method

The higher approximation method (HAM) calculates corrections to the first approximation of the lens patterns and current amplitudes to account for edge effects and missing elements, or any nonperiodicities in the array lattice. HAM will be the implementation of the theory discussed in Section 3.3.

HAM begins the calculation of the second approximation with a loop over the nonperiodicities in the lens (Figure 4-2). For each nonperiodicity, HAM loops over the elements in the neighborhood of the nonperiodicity.

The physical characteristics of the radiating elements on array a and array b are read in. Next, the Z-parameters of the module are input. The program then calculates the generalized admittance row matrices for array a and array b elements above a perfect ground plane. The input impedances are calculated from the array a and array b elements' admittances which are extracted from the admittance row matrices.

The module port admittance matrix relating voltages induced along array a and array b elements to module port currents is calculated using the impedance matrices and the Z-parameters.

The generalized voltage for the array a element induced by the first approximation currents on array b is calculated using the first approximation prediction of mutual coupling through the ground screen.

Next, the generalized voltage induced on array a element by excitation field is calculated.

The program then loops over the neighboring elements. In this loop, the generalized voltage, induced on the array a element by first approximation currents on the neighboring array a element is calculated. This generalized voltage is summed to obtain the generalized voltage. The generalized voltage, induced on array b element by first approximation currents on the neighboring element is calculated and summed to obtain the generalized voltage. This ends the loop over neighboring elements.

The generalized voltages at the array a element are summed to obtain the voltage. This voltage is used to calculate the second approximation port currents.

The module port currents for the second approximation are stored and the loop over the elements in the neighborhood of the nonperiodicity ends, completing the second approximation calculation.

For higher approximations, the code assumes the current distributions will change by a complex constant. The complex constant is the ratio of the 2nd to the 1st approximations of the module's port currents. Therefore, the higher approximation begins by adjusting the voltage induced at the array b element by the ratio of the 2nd to the 1st approximation module port currents on the array a side of the lens.

The higher approximation generalized voltages are calculated by looping over all the elements in the neighborhood of the chosen element. The second approximation port currents for the module are used to adjust the 1st approximation generalized current vectors. The adjusted currents are then used to calculate the second approximation generalized voltage vectors for the chosen element. The third approximation port currents are then calculated using the second approximation generalized voltages. The third approximation port currents for the elements are stored and used to calculate new current moments. The current moments are used to calculate a correction field pattern. When the loop over the elements near nonperiodicities is completed, the third approximation correction field pattern is also completed.

The higher approximation correction calculations are complete upon completion of the loop over all the nonperiodicities on the SBR RF array lens.

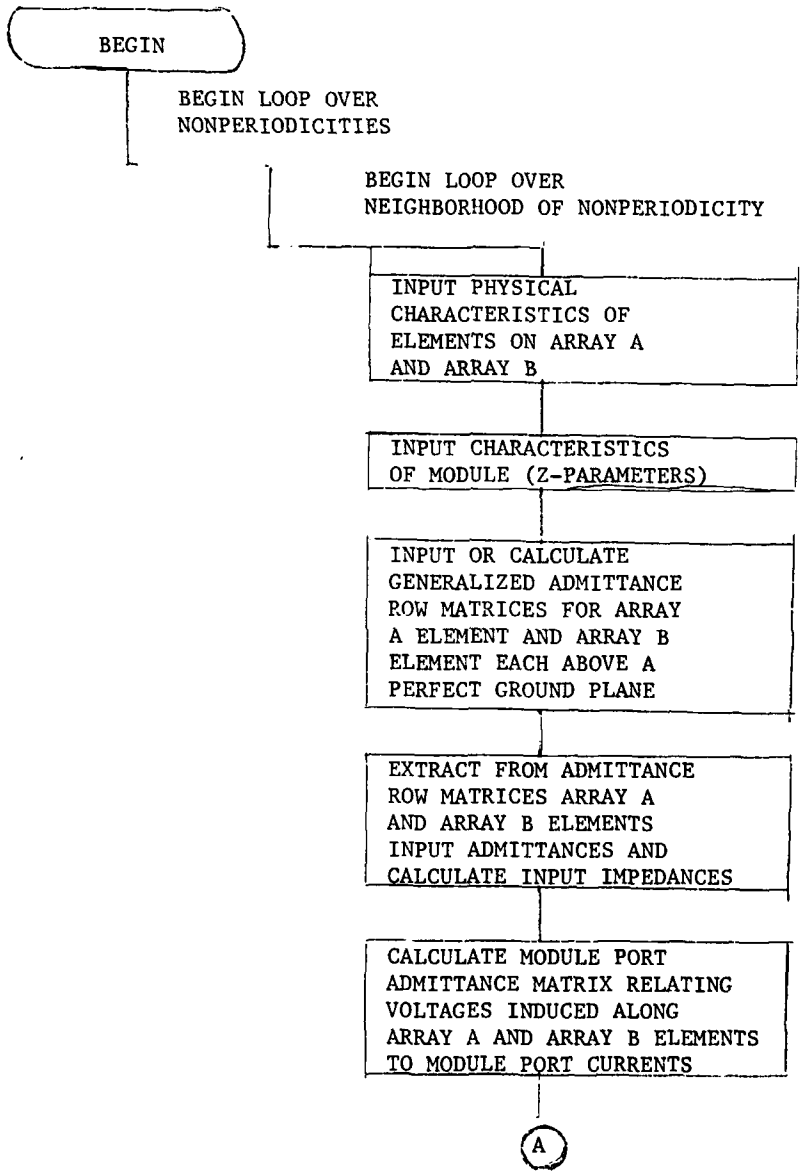

Figure 4-2. HAM Flow Chart

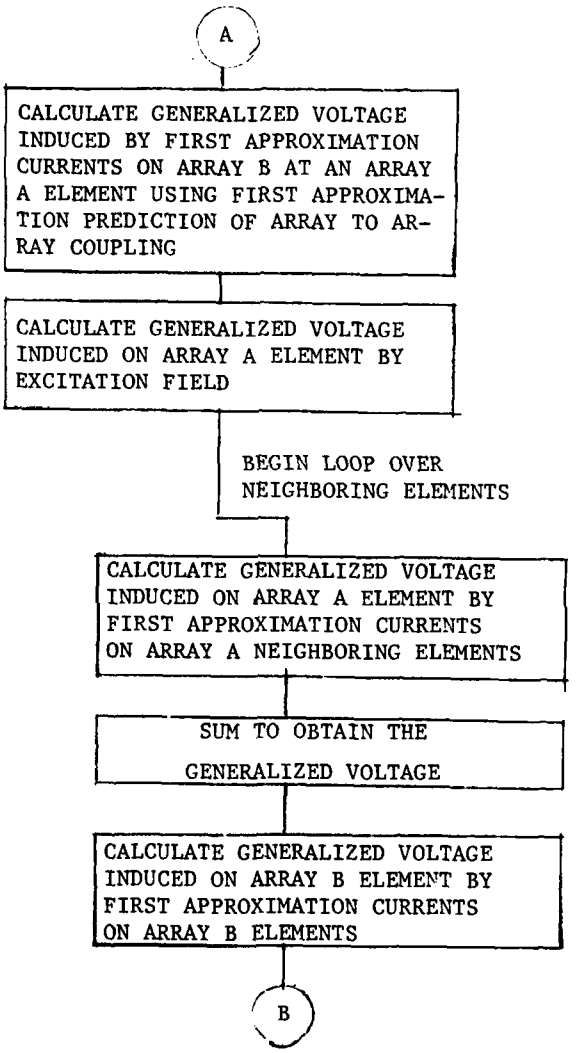

Figure 4-2. HAM Flow Chart (continued)

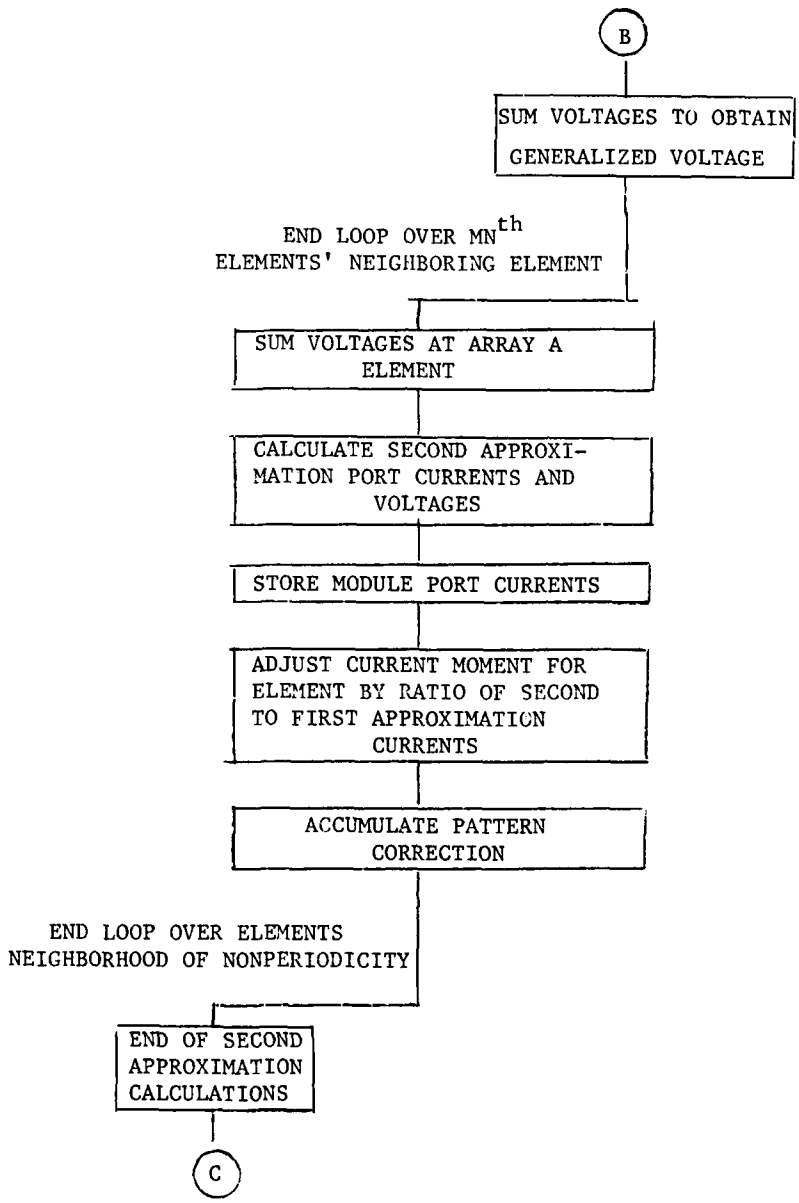

Figure 4-2. HAM Flow Chart (continued)

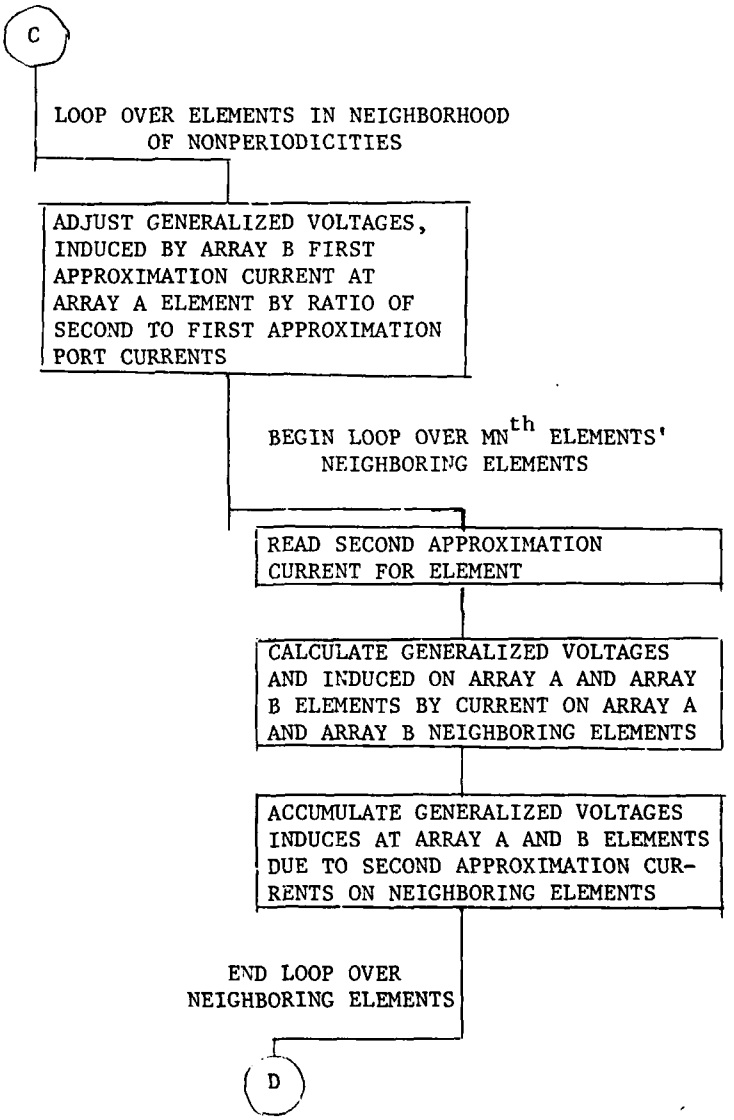

Figure 4-2. HAM Flow Chart (continued)

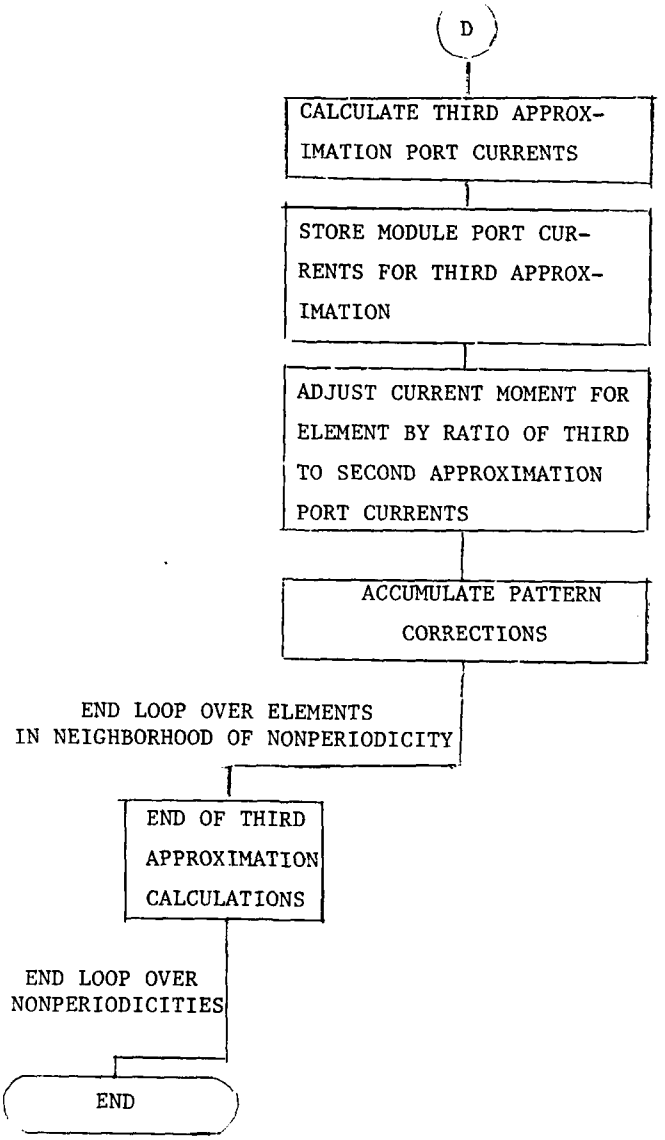

Figure 4-2. HAM Flow Chart (continued)

4.2 DATA FLOW

4.2.1 Data Flow for FAM

FAM - First Approximation Method Main Program

Inputs

ALPHAX, ALPHAY	Module phase shifts
AMP	Amplitude of external field over cell
CELLID	Alphanumeric label which characterizes the antenna cell under analysis
D	Height of array b above the ground plane
DA	Height of array a above the ground plane
DELTA(NBF), DELTAA(NBFA)	Arrays of lengths of wire current segments $\{\Delta\}$
DX, DY	Array b interelement spacing
DXA, DYA	Array a interelement spacing
FREQ, K	Radiation frequency and wave number
LBA(NBFA,3), LB(NBF,3)	Arrays of vectors parallel to array a and array b wire current segments
L, LSA, LSB	Number of the current segment containing antenna element feedpoint for array a and array b elements
NA, NB	Number of elements on array a and array b of the lens
NBFA, NBF	Number of basis functions which describe the currents on the array a and array b elements
NBFM	Number of feedback modes used in mutual coupling calculation
NPWAVE	Number of external plane waves exciting array a
PMAX, QMAX	Control parameters for the calculation of the impedance matrix for array b
PMAXA, QMAXA	Control parameters for the calculation of the impedance matrix for array a
PMAXM, QMAXM	Control paremeters for the calculation of the array b to array a mutual impedance
(POLX, POLY, POLZ)	Polarization vector of external field
RBCA(NBFA,3), RBC(NBF,3)	Array of position vectors $\vec{R}$ pointing to the center of array a or array b element current segments from array element feedpoint
(SX, SY, SZ)	Direction cosines of propagation direction of external field
TPERP, TPARA	Perpendicular and parallel ground plane transmission coefficients
YDELA, YDEL	Array a and array b skew parameters

ZMODAA, ZMODAB ZMODBA, ZMODBB	Module 2-port impedance parameters

Outputs

IAAA(NBFA) IAAB(NBFA) IAEX(NBFA	Array a reference element generalized current vectors
IBBB(NBF)	Array b generalized current vector
VAAA VAAB(NBF VAEX(NBF)	Array a voltages
VBBB	Array b port voltage

GEOMET - Calculates Array Element Data

Inputs

FREQ	Radiation frequency
JCODE	Connector code
NFP	Number of feedpoint
NS	Number of segments
NW	Number of wires
R	Input radius
XB, YB, ZB, XE, YE, ZE	Beginning and end points
XF, YF, ZF	Feedpoint location

Outputs

DELTA(NBF)	Segment length
K	Wave number
LB(NBF,3)	Segment unit vector
NFS(5)	Array containing basis function number for each feed segment
NWS(NBF)	Segment wire number
RAD(NBF)	Radius
RBC(NBF,3)	Vector to center of segment

MUTUAL - Caluculates the Array b to Array a Mutual Coupling Through an Infinite Imperfect Ground Plane

Inputs

D	Height of array b above the ground plane
DA	Height of array a above the ground plane

DELTA(NBF)	Array b lengths of wire current segments
DELTAA(NBFA)	Array a lengths of wire current segments
DX, DY	Array b interelement spacing
IBBB(NBF)	Array of current segments containing array b feedpoint
K	Wave number
LB(NBF,3)	Array of vectors parallel to array b wire current segments
LBA(NBFA,3)	Array of vectors parallel to array a wire current segments
LSB	Number of the current segment containing antenna element feedpoint for array b
NBF	Number of basis functions for array b
NBFA	Number of basis functions for array a
PMAXM, QMAXM	Control parameters
PTPL	Flag to indicate pulse or point matching
RBC(NBF,3)	Array of position vectors pointing to center of array b element current segments from array b element feedpoint
RBCA(NBFA,3)	Array of position vectors pointing to center of array a element current segments from array a element feedpoint
TSXB, TSYB	Array b phase factors
YDEL	Skew parameter for array b
Z(NBFA, NBFA)	Array a admittance matrix

Outputs

IAAB(NBF)	Array a reference element generalized current vector due to VAAB excitation
VAAB(NBF)	Generalized voltage vector on array a due to penetration of ground screen by field radiated by array b currents
ZMUTAB	Mutual impedance between array b and array a reference elements through the imperfect ground plane

SCAN - Calculates Array Reference Element Admittance Matrix and Active Impedance

Inputs

L	The number of the current segment containing antenna element feedpoint for array elements
NBF	Number of basis functions
Z(NBF, NBF)	Impedance matrix

Outputs

Z(NBF, NBF)	Inverted impedance matrix; the admittance matrix
ZSCAN	Active impedance

SCIA - Calculates Array Generalized Voltage and Current Vectors and Element Port Current for Element in the Incident Field

Inputs

DELTA(NBF)	Array of lengths $\{\Delta\}$ of wire current segments
K	Wave number
L	Number of the current segment containing antenna element feedpoint for array element
LB(NBF,3)	Array of vectors $[\vec{\ell}]$ parallel to array wire current segments
NBF	Number of basis functions
(POLX, POLY, POLZ)	Polarization vector of external field
RBC(NBF,3)	Array of position vectors $[\vec{R}]$ pointing to center of array element current segments from array element feedpoint
Z(NBF, NBF)	Admittance matrix

OUTPUTS

IAEX(NBF)	Short circuit current vector
SCIAEX	Short circuit source current for reference element
VAEX(NBF)	Total excitation vector (including reflection) for reference element

ZMATX - Calculates the Impedance Matrix

Inputs

D	Height above the ground plane
DELTA(NBF)	Array of lengths $\{\Delta\}$ of wire current segments
DX, DY	Interelement spacing
K	Wave number
LB(NBF,3)	Array of unit vectors $[\vec{\ell}]$ parallel to wire current segments
NBF	Number of basis functions
PTPL	Flag to indicate 0 = point matching 1 = pulse matching
RAD(NBF)	Radius
RBC(NBF,3)	Array of position vectors $[\vec{R}]$ pointing to center of element current segments.
WLEN	Wave length
YDEL	Skew parameter

Outputs

Z(NBF, NBF)	Impedance matrix for an array above a perfect ground screen
ZF(NBF, NBF)	Impedance matrix for an array in free space

CELLPAT - Cell Pattern Calculations

Inputs

RGV(3)	Global coordinates of cell
PHICG	Rotation of cell relative to GCS
PHIEC	Rotation of element relative to CCS
NARY	Number of arrays within cell
NY(30)	Number of rows in y direction for each array
NX(30)	Number of columns in x direction for each array
NO(30)	Number of elements in first column of irregular array
IAS(30)	Add-subtract factor for each array
RREFC(30,3)	Coordinates of reference element of each array
DX(30)	x separation for each array
DY(30)	y separation for each array
DELTAY(30)	Skew in y direction for each array
RBC(NBF,3)	Array position vectors for segments of array a element
IBBB(NBF)	Generalized current vector for array b elements

Outputs

THETA	Polar angles to field points
PHI	Azimuth to field points
ETHETA	Theta component of E field
EPI	Phi component of E field

4.2.2 Data Flow for HAM

Main Program

Inputs

ALPHAX, ALPHAY	Module phase shifts
AMP	Amplitude of external field over cell
CELLID	Alphanumeric label which characterizes the antenna cell under analysis

D	Height of array b above the ground plane
DA	Height of array a above the ground plane
DX, DY	Array b interelement spacing
DXA, DYA	Array a interelement spacing
FREQ, K	Radiation frequency and wave number
IAAA(NBFA) IAAB(NBFA) IAEX(NBFA)	Array a reference element generalized current vectors for first approximation
IBBB(NBF)	Array b generalized current vector for first approximation
LBA(NBFA,3), LB(NBF,3)	Arrays of vectors $\vec{\ell}$ parallel to array a and array b wire segments
L, LSA, LSB	Number of the current segment containing antenna element feedpoint for array a and array b elements
NA, NB	Number of elements on array a and array b of the lens
NBFA, NBF	Number of basis functions which describe the currents on the array a and array b elements
NFBM	Number of feedback modes used in mutual coupling calculation
(POLX, POLY, POLZ)	Polarization vector of external field
RBCA(NBFA,3), RBC(NBF,3)	Array of position vectors $\vec{R}$ pointing to the center of array a or array b element current segments from array element feedpoint
(SX, SY, SZ)	Direction cosines of propagation direction of external field
VAAA VAAB(NBF) VAEX(NBF)	Array a voltages
VBBB	Array b port voltage
(XLOC, YLOC, ZLOC)	Location of mn^{th} element on cell
YDELA, YDEL	Array a and array b skew parameters
ZMODAA, ZMODAB, ZMODBA, ZMODBB	Module 2-port impedance parameters

Outputs (Subscript j denotes order of approximation)

IAAAj (NBFA)	Array a generalized current vector
IBBBj (NBFA)	Array b generalized current vector
$\Delta E\theta j$ $\Delta E\phi j$	Electric field corrections provided by higher order approximations of voltages and currents
VAAAj	Array a port voltage for 00 element
VBBBj	Array b port voltage for 00 element

SECTION 5

RESULTS - FIRST APPROXIMATION METHOD CURRENTS AND ACTIVE IMPEDANCE

Simulation results obtained to date have been limited to infinite array analysis. Active impedance and current distributions have been compared with published results on planar, rectangular lattice, and dipole arrays.[11,12,13] Simulation results are presently being compared with moment method analyses of large, triangular, spaced-dipole arrays. The center element impedance and current have been compared with the first approximation method (FAM). Several of these comparisons are presented in this section. The effect of varying the orientation of the dipoles in an infinite triangular array is presented, as is a design of a single-port turnstile radiator for use in an infinite triangular array. These results demonstrate the versatility of the simulator. Convergence curves are given in terms of minimum number of required plane wave modes (truncated doubly infinite summation in (3-16)) and number of subsections (order of $[Z^{gs}]$).

5.1 INFINITE ARRAY COMPARISONS

Stark[11] analyzed an infinite rectangular array of thin $\lambda/2$ strip dipoles over a perfect ground screen. Active impedances were computed. A single sinusoidal current distribution on each element was assumed since this is exact for vanishingly thin wires and since such an approximation proved valid in calculating impedances of isolated dipoles not exceeding $\lambda/2$ in length. These results compared well with Carter's large finite array analysis[14] for active impedances near the center of the array; however, Carter also assumed the same single sinusoidal current distribution per element.

VanKoughnett and Yen[12] observed that since the dipoles were almost touching in the collinear direction the current distribution may significantly deviate from a single sinusoid even for very thin dipoles. They analyzed the same array in a manner which permitted computing the current distribution to any desired degree of accuracy. The resulting active impedances displayed a variation with scan that was similar to Stark's results; however, the variation was considerably more pronounced and the broadside impedance values significantly differed.

VanKoughnett and Yen's method is applicable only to elements with small spacings in the collinear direction. Chang[13] removed this restriction by applying a "five-term expansion" as well as a multiple mode sinusoidal expansion to the rectangular infinite array of dipoles.

The results from the above papers selected for comparison with the first approximation method (FAM) were obtained with the configuration of Figure 5-1 where

a = dipole radius

d = dipole length

h = array height above ground screen

d_x = periodicity in x direction

d_y = periodicity in y direction

The excitations were unit amplitude voltages progressively phased for radiation in a specified direction. The dimensions for three problems that were considered for this configuration are indicated in Table 5-1. The voltage sources were phased for a variety of E-plane, H-plane, and diagonal plane scan angles. Both current distributions and active impedances were computed. The results from Problems 1 and 2 apply to Chang's results. The results from Problem 3 apply to VanKoughnett and Yen's results.

The zero scan (broadside radiation) reference element current distribution for Problem 1 is shown in Figure 5-2. Six FAM results appear. Each result applies to one of six combinations of maximum plane wave expansion numbers p_{max} and q_{max} and number of segments N_s used in computing the infinite array generalized impedance matrix $[Z^{gs}]$ of Section 3.2.2. Equation (3-16) shows the doubly infinite summation in p and q needed to compute the ij^{th} element of the $N_s \times N_s$ matrix $[Z^{gs}]$. These summations are truncated according to $|p| \leq p_{max}$ and $|q| \leq q_{max}$. The p_{max}, q_{max}, and N_s for the FAM results in Figure 5-2 are listed below.

Curve No.	N_s	p_{max}	q_{max}
1	11	15	40
2	11	15	30
3	11	15	20
4	21	15	20
5	21	15	40
6	21	15	30

The required p_{max} and q_{max} increases with increasing d_x/a and d_y/a respectively. For Chang's results (Problems 1 and 2) d_x is almost 5 times d_y. Therefore, p_{max} was chosen smaller than q_{max}. The Problem 1 current distribution results (Figure 5-2) appear converged for 21 segments per half wavelength. The curves for 11 segments have not yet converged. Curves 1 and 2 are further from Chang's results than curve 3 even though the value of q is higher for curves 1 and 2 than for 3. Additional convergence results are given in Section 5.5.

The principal plane scan active admittances for Problem 1 are plotted in Figure 5-3. For these results $p_{max} = 20$, $q_{max} = 70$ and $N_s = 21$.

The element current for the full wavelength dipole array of Problem 2, scanned for broadside radiation is shown in Figure 5-4. The FAM results used $p_{max} = 15$, $q_{max} = 50$ and $N_s = 21$. As with Problem 1, close agreement between FAM and Chang's method is indicated.

The E-plane and H-plane active impedances for Problem 3 are compared with VanKoughnett and Yen in Figures 5-5 (resistance) and 5-6 (reactance). The resistance is in close agreement throughout the 0° (broadside) to 45° scan range. The agreement in reactance is within approximately 15% for near broadside scan. This agreement deteriorates for larger scan angles.

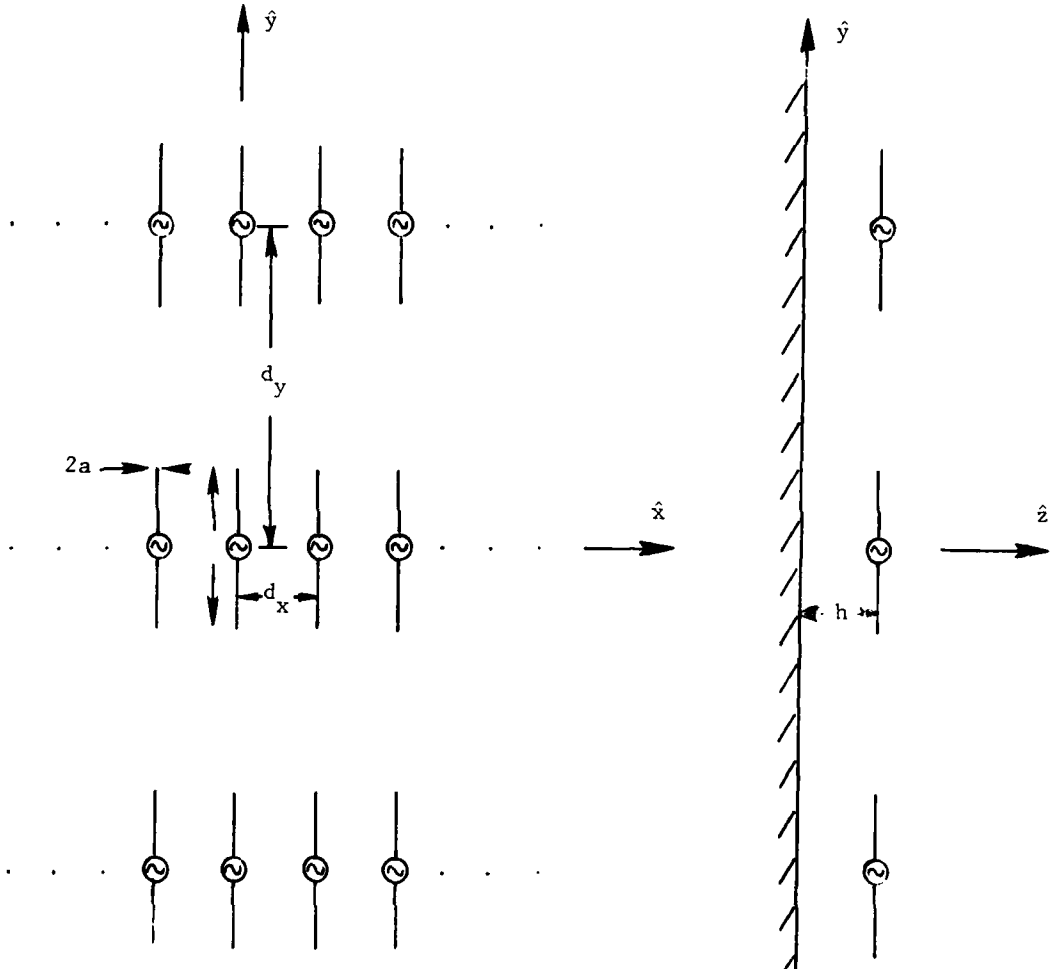

a. Front View

b. Side View

Figure 5-1. Infinite Planar Dipole Array Above a Perfect Ground Screen

TABLE 5-1

INFINITE ARRAY PROBLEMS

	Problem 1	Problem 2	Problem 3
a	0.007022	0.007022	0.00796
d	0.5	1.	0.5
h	0.25	0.25	0.25
d_x	0.25	0.25	0.5
d_y	1.2	2.2	0.5

All dimensions in wavelengths

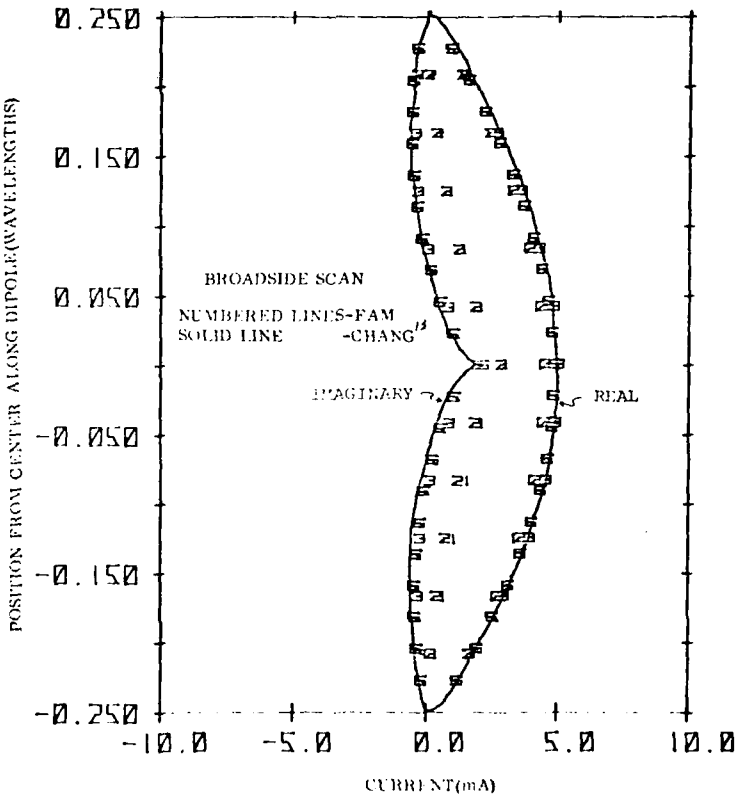

Figure 5-2. Element Current for Problem 1 of Table 5-1

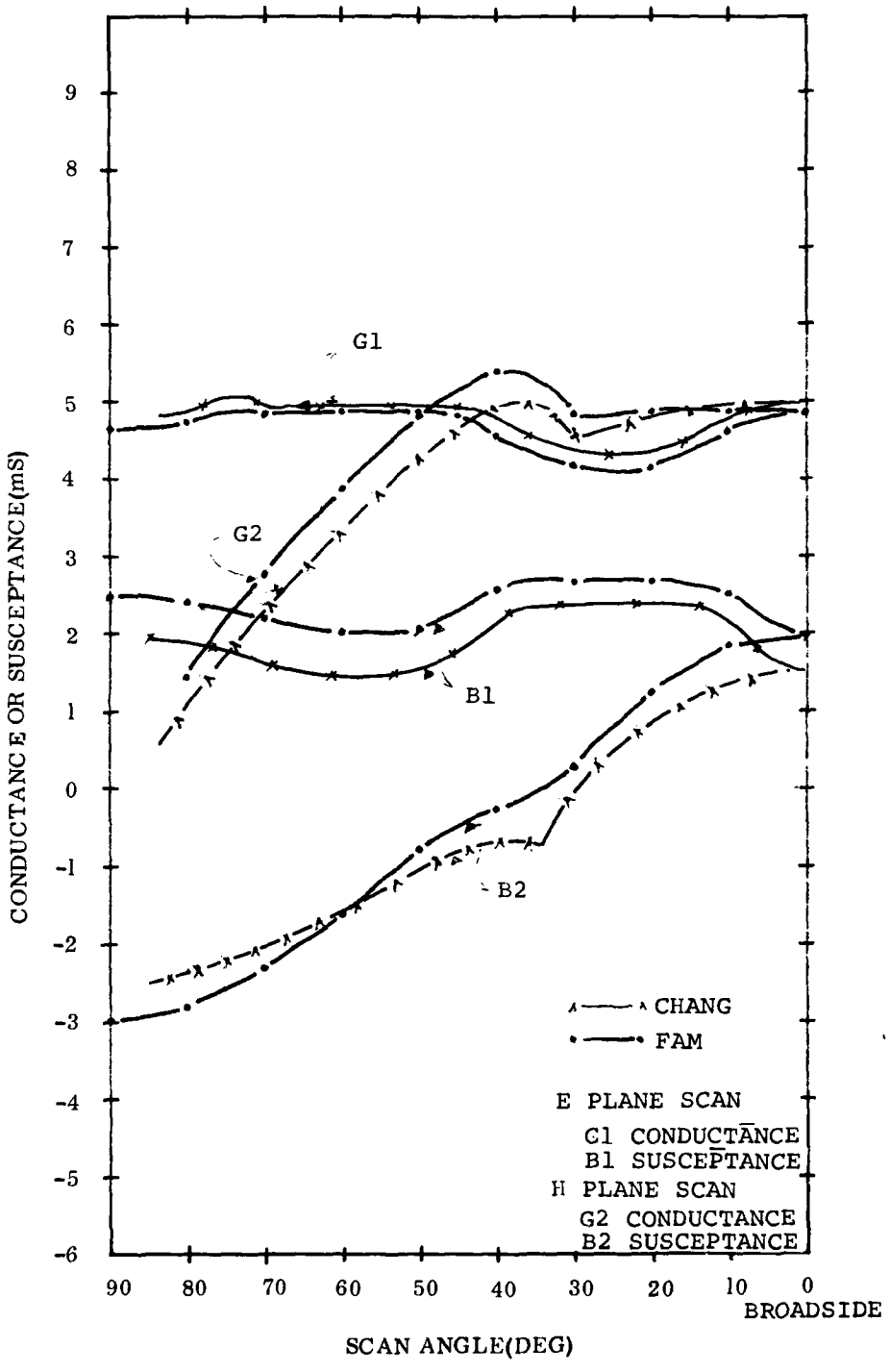

Figure 5-3. Active Admittances for Problem 1 of Table 5-1

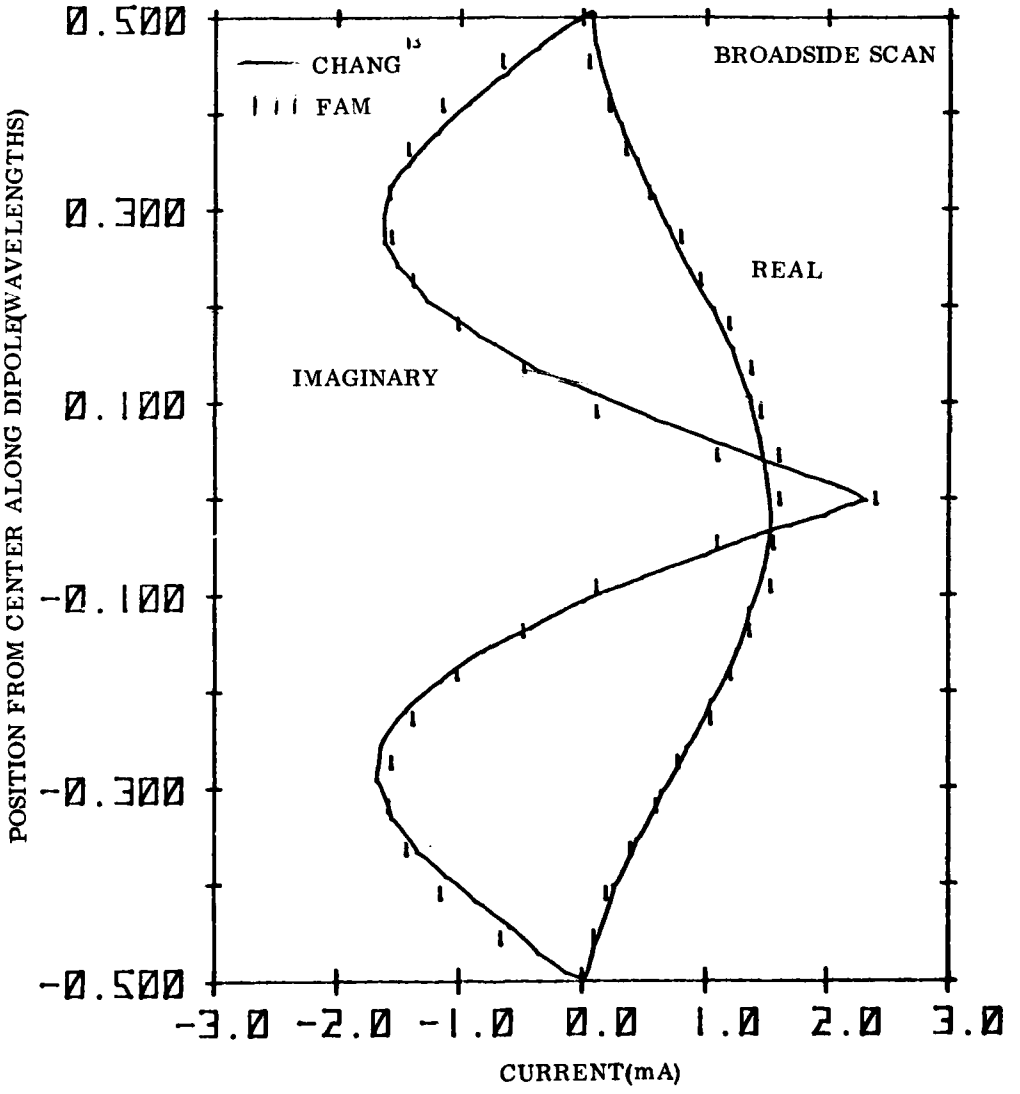

Figure 5-4. Element Current for Problem 2 of Table 5-1

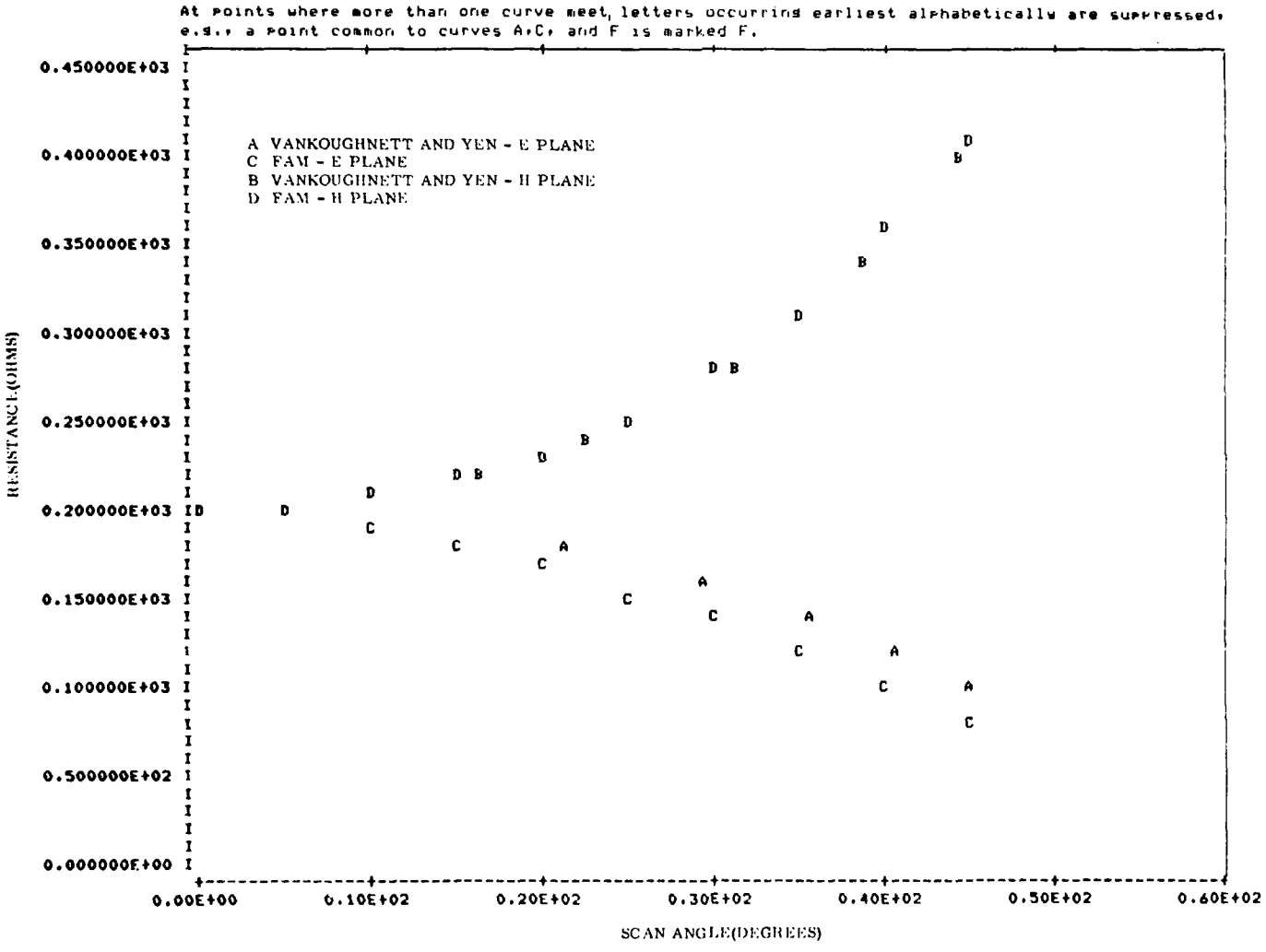

Figure 5-5. Active Resistance for Problem 3 of Table 5-1

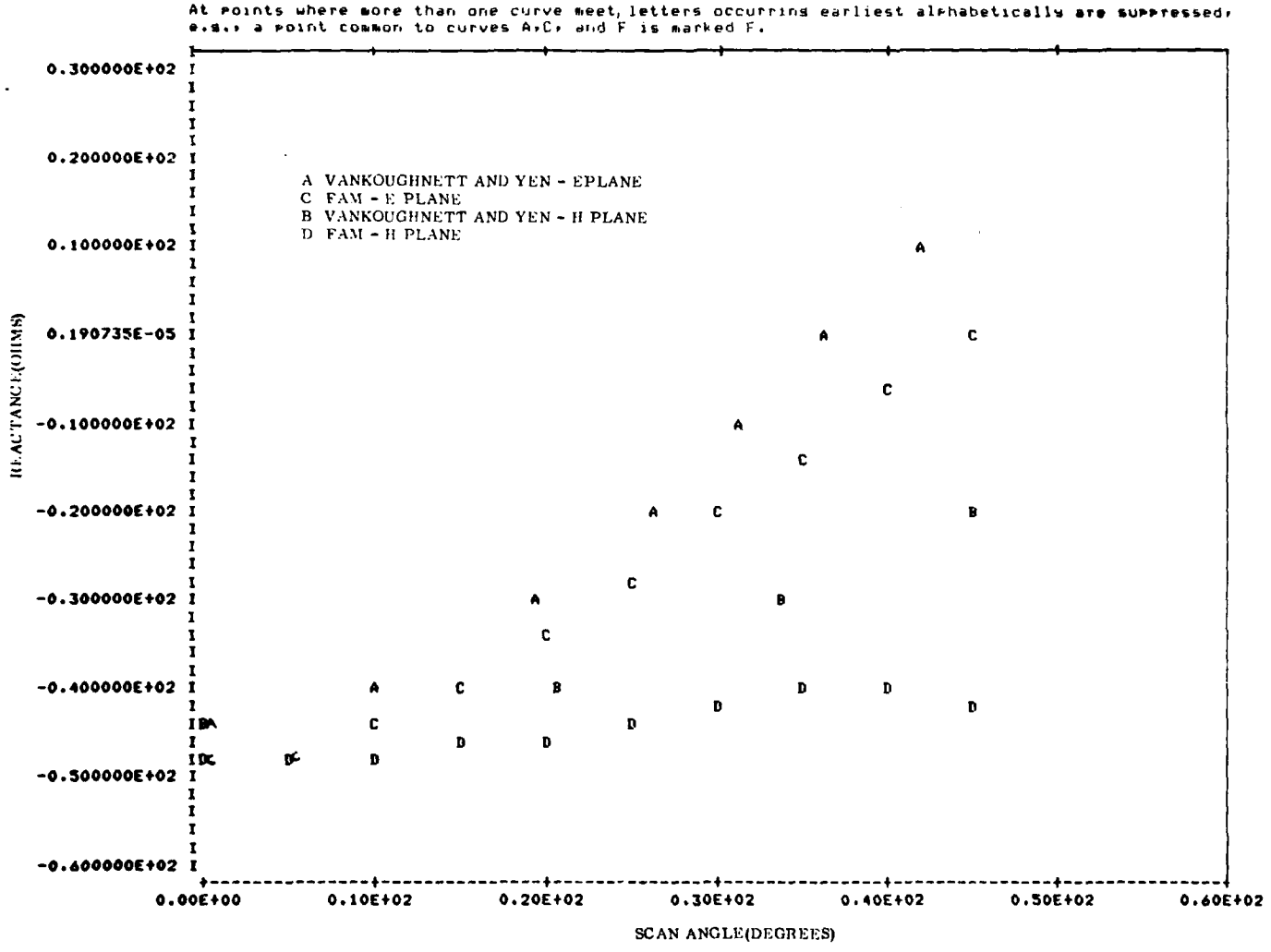

Figure 5-6. Active Reactance for Problem 3 of Table 5-1

5.2 FINITE ARRAY COMPARISONS

Thin wire moment method computer codes are applicable to finite arrays of arbitrarily bent wire radiators over infinite perfectly conducting ground screens. Two of these codes GEMACS[18] and AMP[19] are available as an aid in validating the simulator.

The results in Section 5.1 apply only to rectangular lattices. Since triangular lattices are of particular interest, the configuration chosen for comparing FAM with finite array moment methods is that of Figure 5-7. A 19-element dipole array is indicated. Each dipole is centrally excited with progressively phased voltage sources. The parameter values are

$d = 0.5\lambda$

$a = 0.01\lambda$

$d_x = 0.715\lambda$

$d_y = 0.826\lambda$

$\Delta_y = 0.413\lambda$

$h = 0.25\lambda$

Consider the standard spherical coordinates r, θ, ϕ with respect to the right hand x, y, z coordinates indicated in Figure 5-7 where z is outward normal to the array plane and the origin is at the reference element (m = n = o) center. The phasing of the V_{mn} voltage sources can be related to main beam angular directions θ_α, ϕ_α (scan angles) by letting $\vec{r}'_{mn}$ denote the mn^{th} element center position vector. Then, with reference to Figure 5-7 and the discussion in Section 3.2.4, (3-95) results in

$$V_{mn} = e^{-jk\hat{r}\cdot\vec{r}'_{mn}} = e^{-jk(md_x\alpha_x + (nd_y - m\Delta y)\alpha_y)} \qquad (5\text{-}1)$$

where α_x and α_y are the scan directional cosines

$\alpha_x = \cos\phi_\alpha \sin\theta_\alpha$

$\alpha_y = \sin\phi_\alpha \sin\theta_\alpha$

and $\hat{r}$ is the unit vector for the main beam field point position vector. Equation (5-1) provides the element excitations for any scan direction. The "principal" scans are

H-plane: $\alpha_y = 0$ ($\phi_\alpha = 0$)

E-plane: $\alpha_x = 0$ ($\phi_\alpha = \pi/2$)

Diagonal plane: $\alpha_x = \alpha_y$ ($\phi_\alpha = \pi/4$)

FAM treats the Figure 5-7 problem as an infinite array. The active impedances for the principal scan planes for this problem, as computed by FAM, are shown in Figures 5-8 (resistance) and 5-9 (reactance). The scan angle is θ_α. The computational variables were $N_s = 23$ and $p_{max} = q_{max} = 60$. The discontinuities in these curves occur at grating lobe singularities; i.e., at scan angles for which there exist integers p and q such that q_z, given by (3-97), vanishes. (A discussion on grating lobe singularities appears in the paragraph following (3-58) and in the paragraph containing (3-61).) The H-plane grating lobe singularity occurs at $\theta_\alpha = 23.49°$, the E-plane singularity occurs at $\theta_\alpha = 29.22°$, and the diagonal plane singularity occurs at $\theta_\alpha = 59.75°$. The locations of grating lobe singularities depend only upon lattice spacings.

The broadside scan current on the reference element (m = n = 0) of the Figure 5-7 finite array as computed by the GEMACS moment method code is shown in Figure 5-10. Also shown are the GEMACS current with the array extended to include 37 dipoles (same interelement spacings) and the infinite array FAM current.

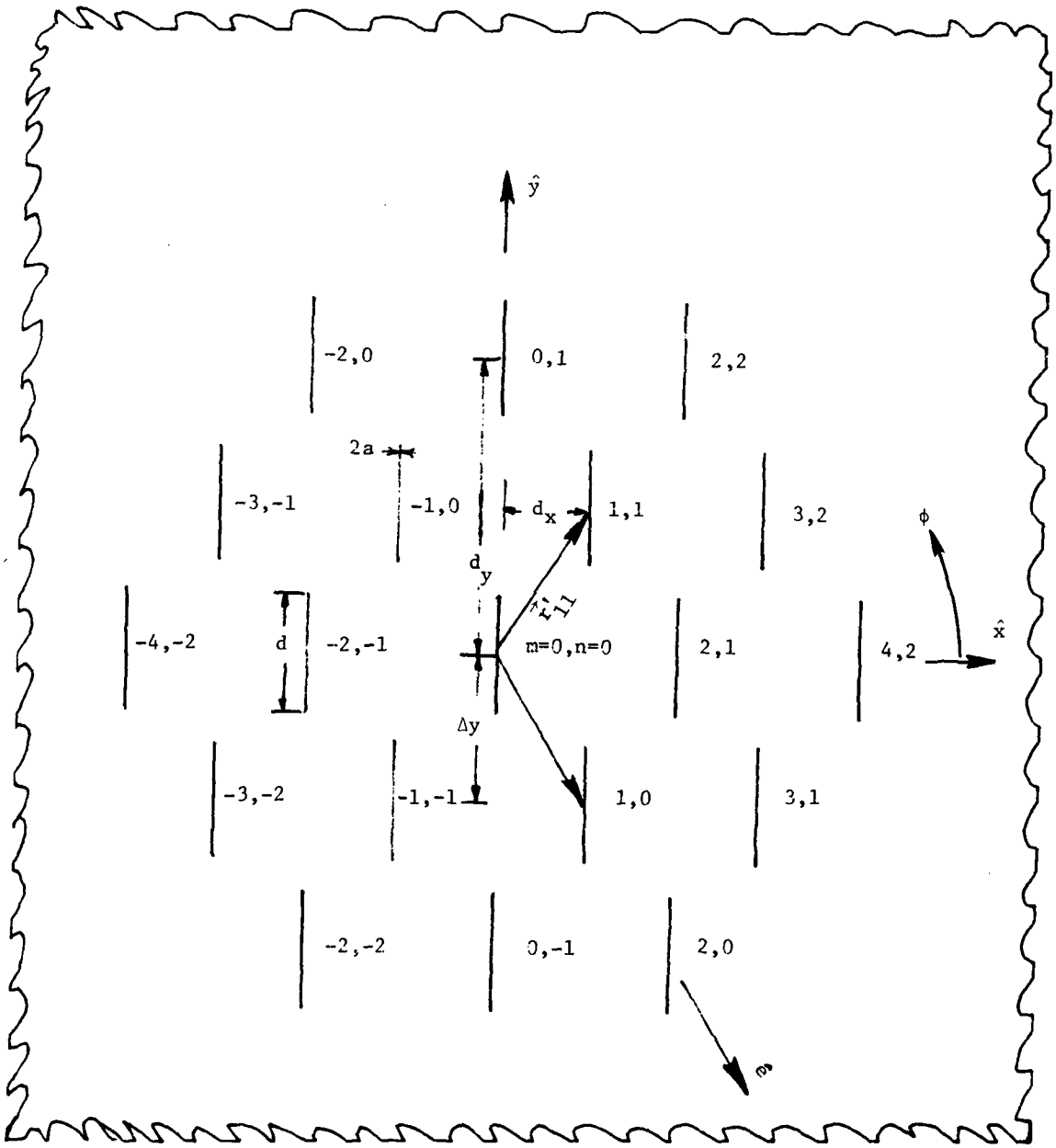

Figure 5-7. Finite triangular lattice dipole array a height h above an infinite ground screen. Identifying m,n indices are indicated. A voltage source V_{mn} centrally excites each dipole.

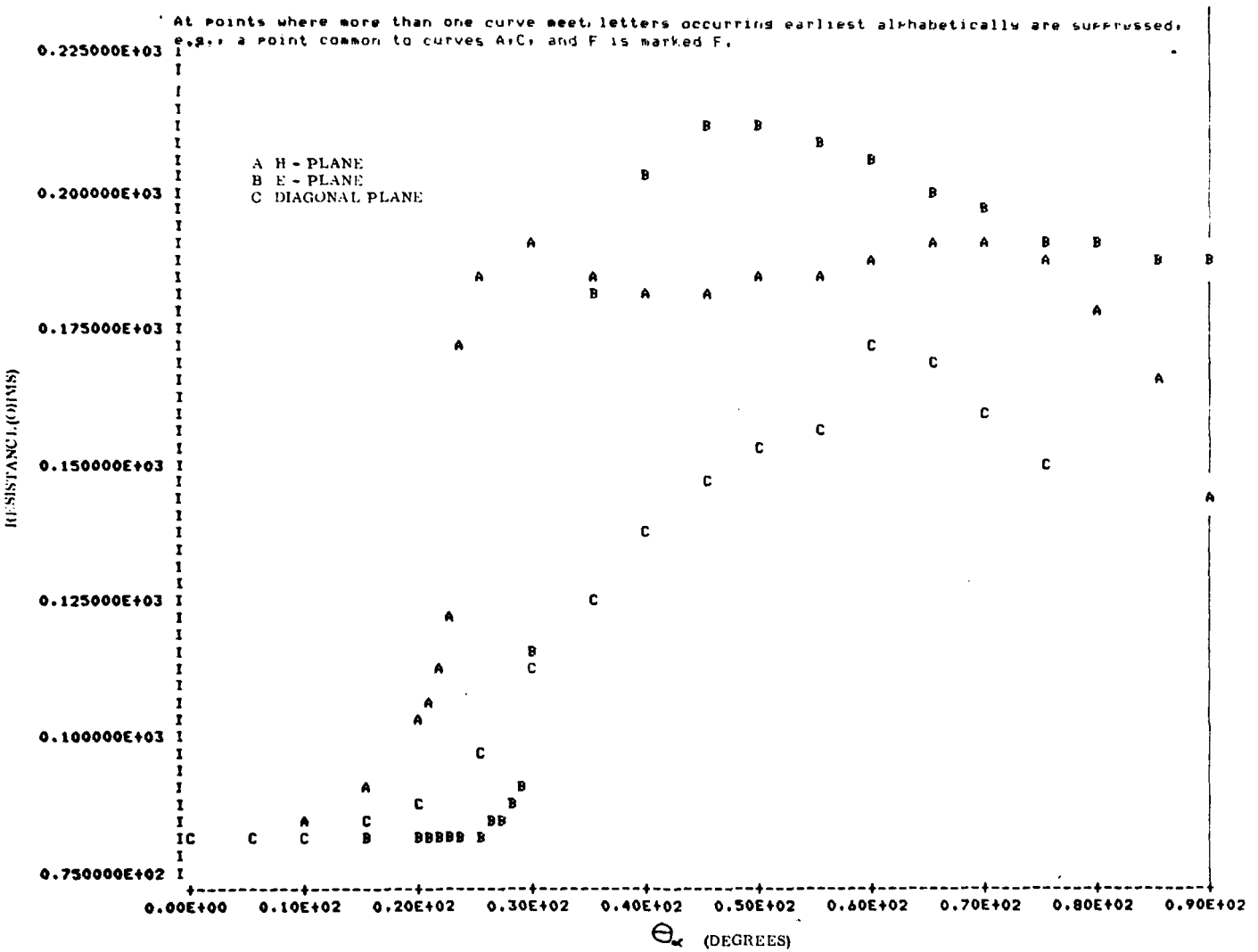

Figure 5-8. Active Resistance vs. Scan Angle for Figure 3-7 Problem Treated as an Infinite Array

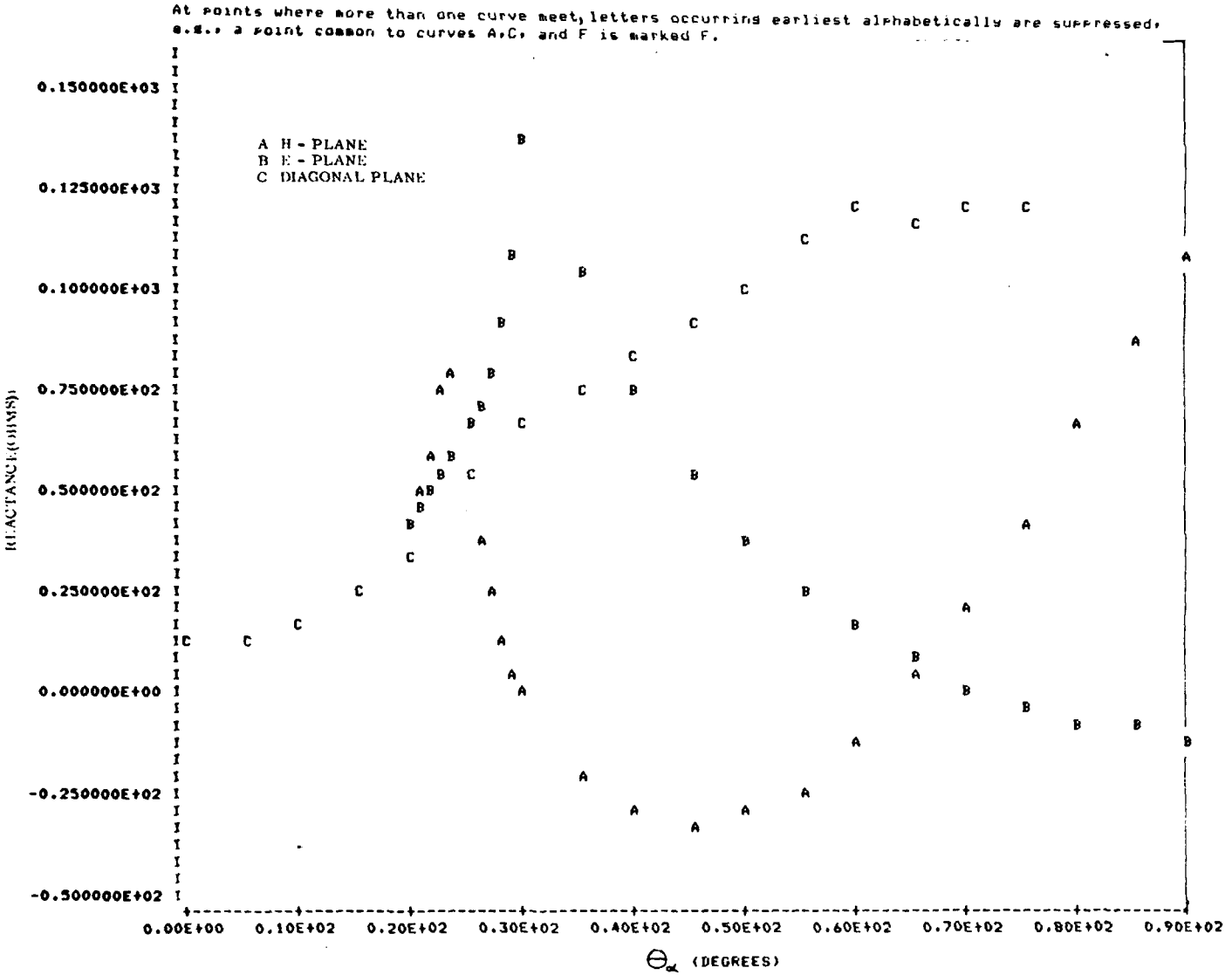

Figure 5-9. Active Reactance vs. Scan Angle for Figure 5-7 Problem Treated as an Infinite Array

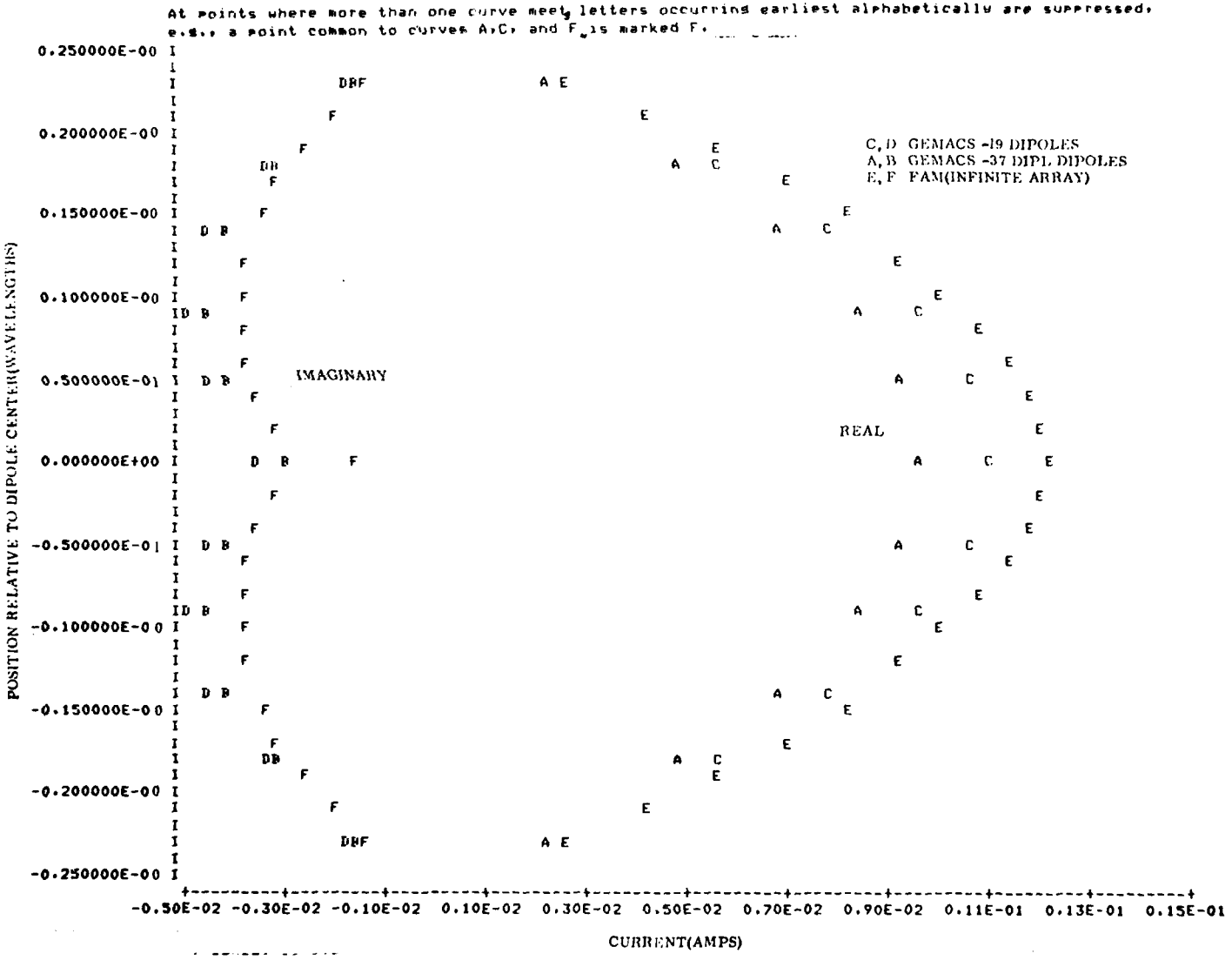

Figure 5-10. Current on the Center Element of the Figure 5-7 Array Excited for Broadside Radiation

5.3 ELEMENT ROTATION IN THE ARRAY PLANE

The effects of rotating all dipole array elements in the array plane (about the z axis) are of interest. The reference element currents and active impedances were obtained using FAM for rotation angles (Figure 5-11) ψ = 0°, 15°, 30°, 45°, 60°, and 90°. This was done at both broadside scan and θ_α = 20°, ϕ_α = 0° scan. Two lattices were considered: the Figure 5-7 triangular lattice and a $d_x = d_y = 0.8\lambda$ rectangular lattice. The active impedances are given in Table 5-2. The reference element currents are plotted in Figures 5-12 to 5-19. These results indicate greater element rotation induced impedance and current variations for the 20 degree scan than for broadside and for the rectangular lattice than for triangular.

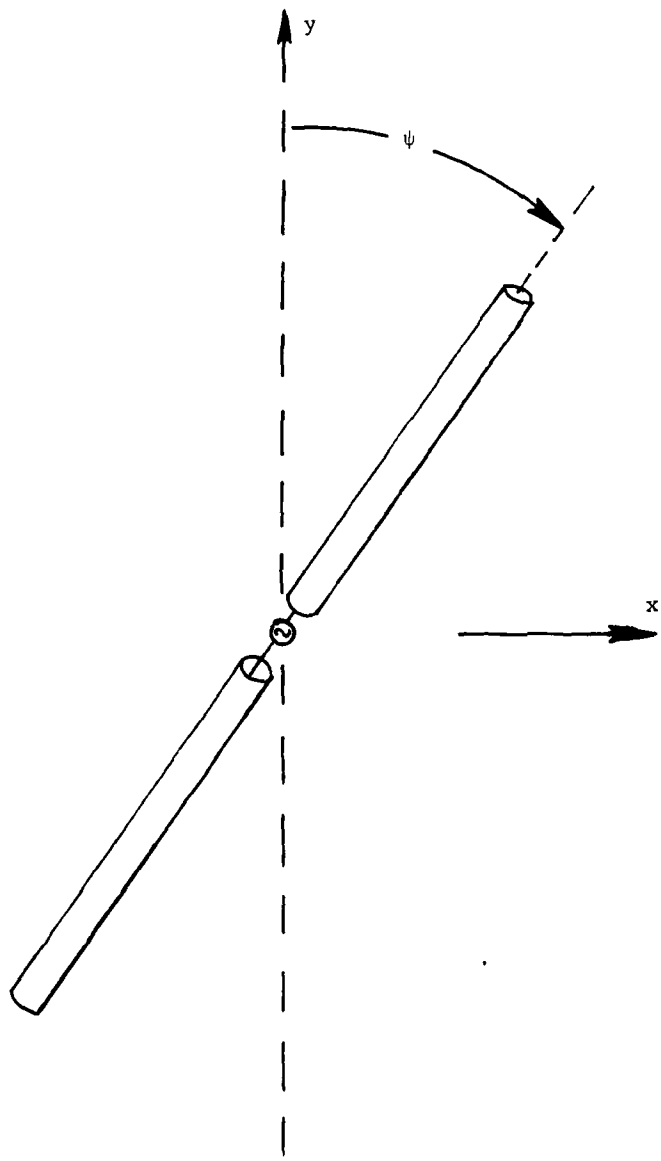

Figure 5-11. Rotation of Dipole Radiator in Array Plane

TABLE 5-2

ACTIVE IMPEDANCES FOR ROTATED ELEMENT ARRAYS

Lattice	Scan Angle θ_α(Degrees)(ϕ_α=0°)	Rotation Angle ψ(Degrees)	Impedance(Ohms)
Triangular	0	0	78.87 + j 8.614
		15	78.4 + j 7.773
		30	77.99 + j 7.147
		45	78.41 + j 7.803
		60	78.87 + j 8.607
		90	77.86 + j 6.806
	20	0	99.48 + j41.17
		15	96.74 + j39.13
		30	90.9 + j35.51
		45	85.35 + j33.52
		60	81.56 + j34.5
		90	78.73 + j37.95
Rectangular	0	0	78.71 + j24.42
		15	77.36 + j21.7
		30	75.2 + j17.19
		45	74.26 + j15.17
		60	75.19 + j17.18
		90	78.72 + j24.44
	20	0	166.6 + j12.52
		15	158.7 + j15.66
		30	140.1 + j23.63
		45	118.3 + j32.58
		60	99.78 + j39.53
		90	83.98 + j44.4

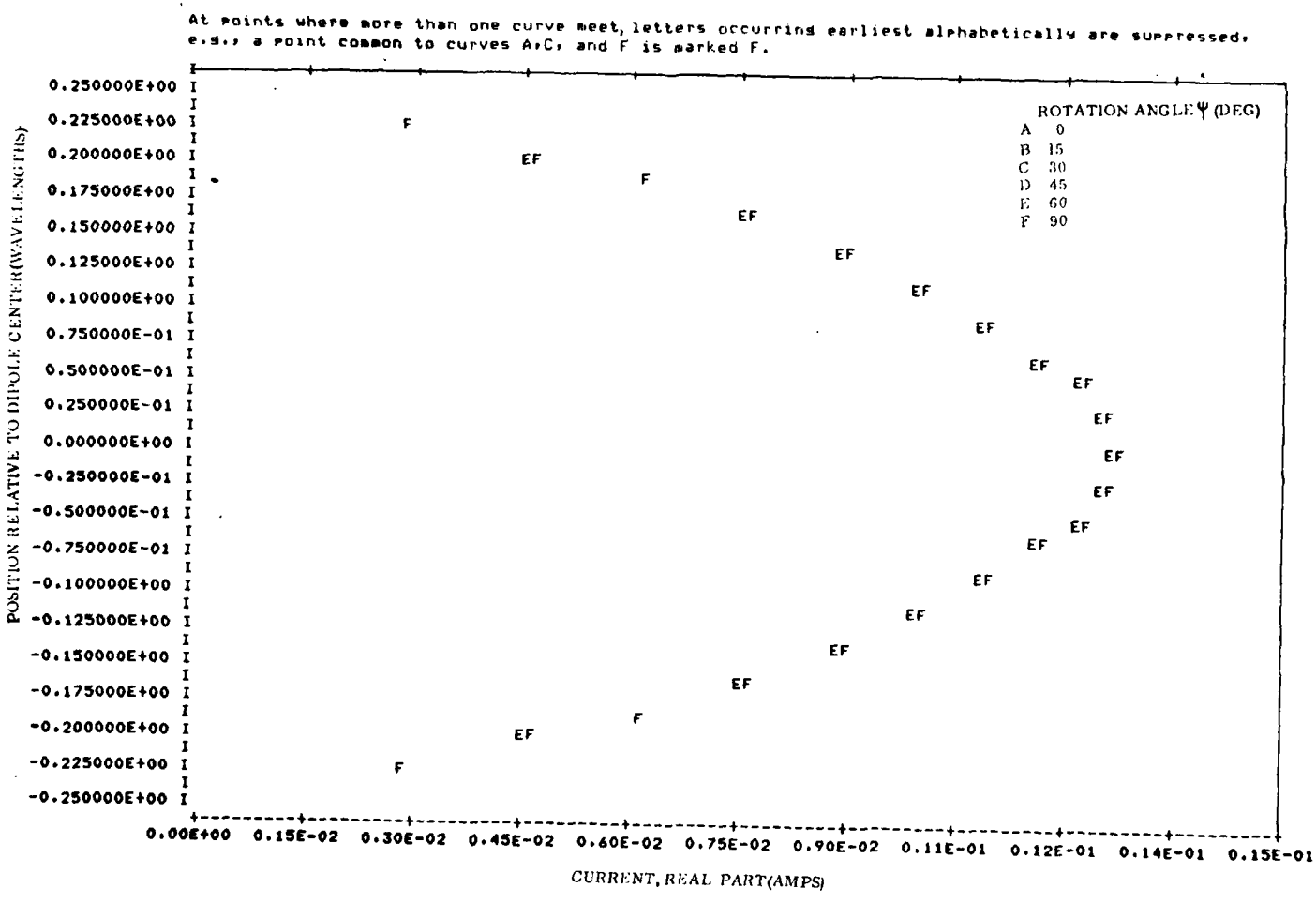

Figure 5-12. Real Part of Reference Dipole Current for Triangular Lattice (Figure 5-7) for Several Dipole Orientations and Broadside Scan ($\theta_\alpha = 0°$)

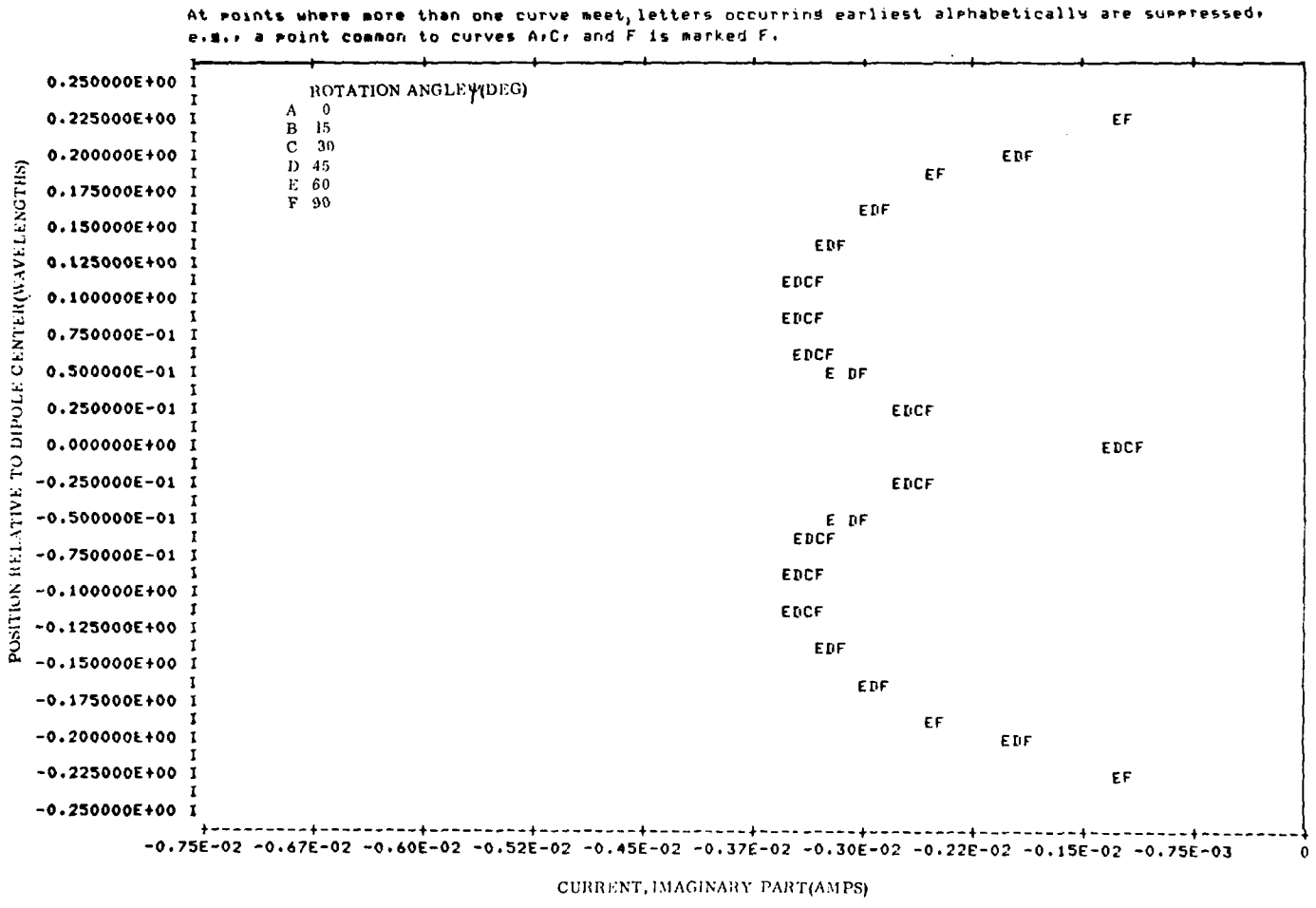

Figure 5-13. Imaginary Part of Reference Dipole Current for Triangular Lattice (Figure 5-7) for Several Dipole Orientations and Broadside Scan ($\theta_\alpha = 0°$)

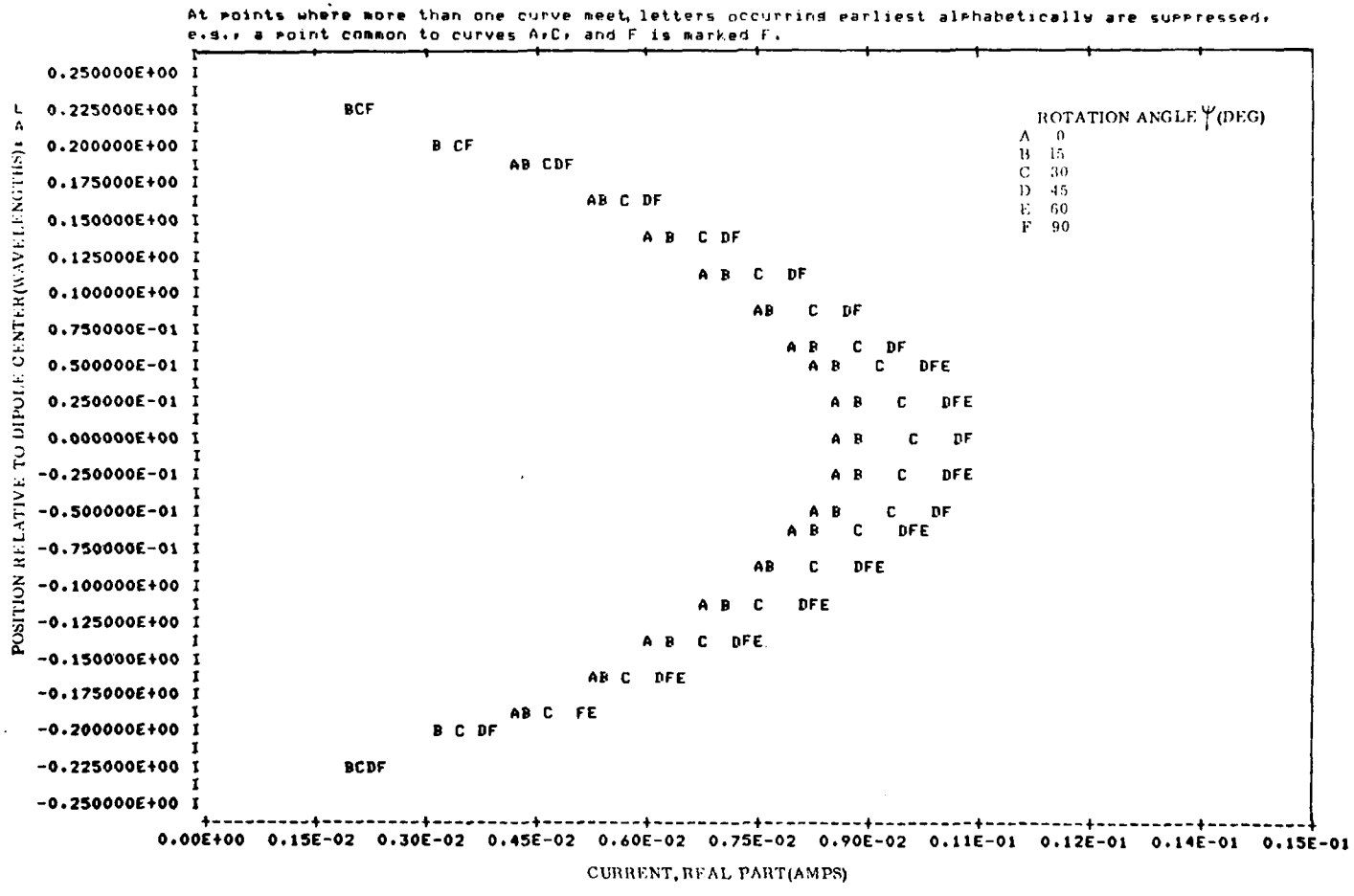

Figure 5-14. Real Part of Reference Dipole Current for Triangular Lattice (Figure 5-7) for Several Dipole Orientations and $\theta_\alpha = 20°$, $\phi_\alpha = 0°$ Scan

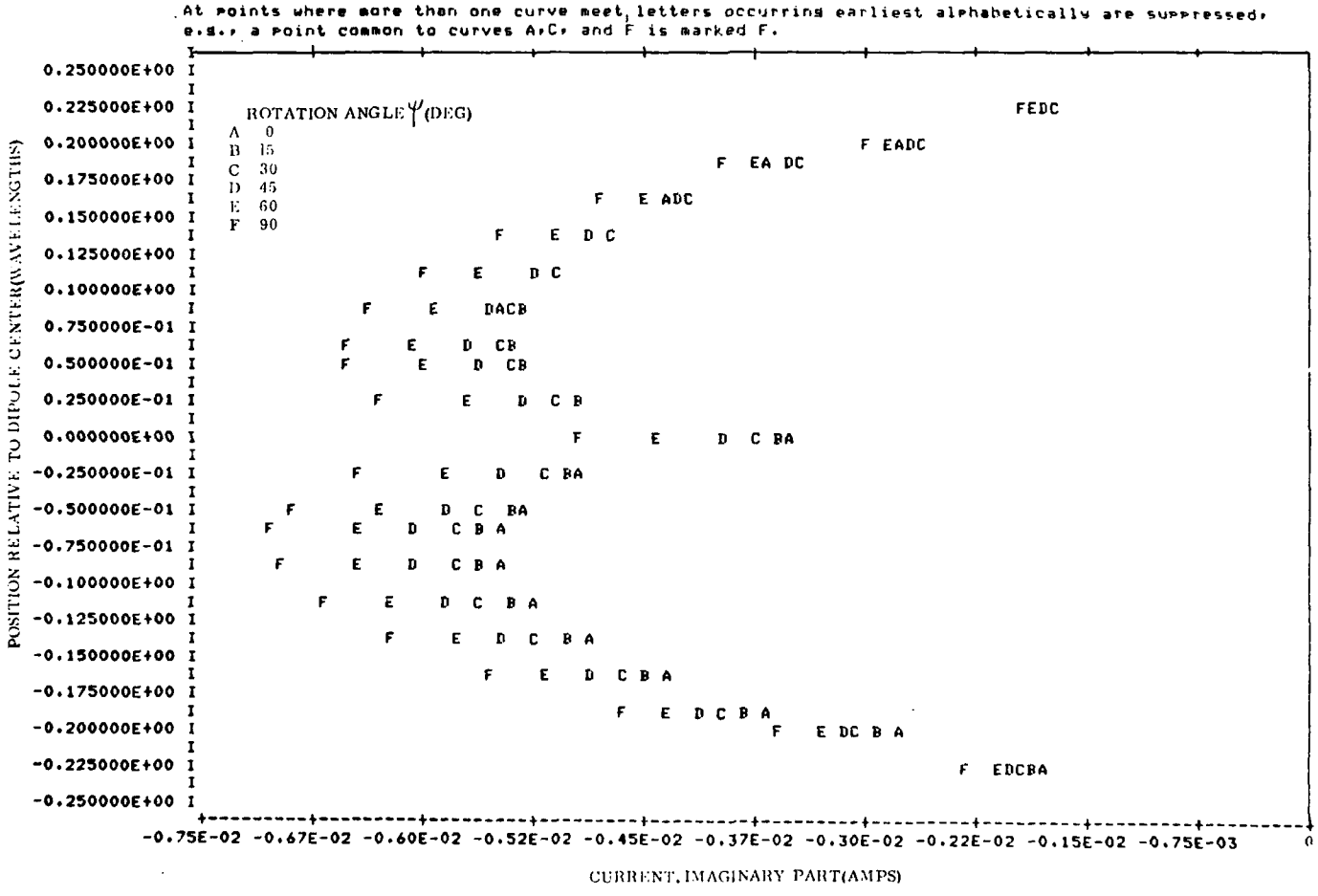

Figure 5-15. Imaginary Part of Reference Dipole Current for Triangular Lattice (Figure 5-7) for Several Dipole Orientations and θ_α =20°, ϕ_α = 0° Scan

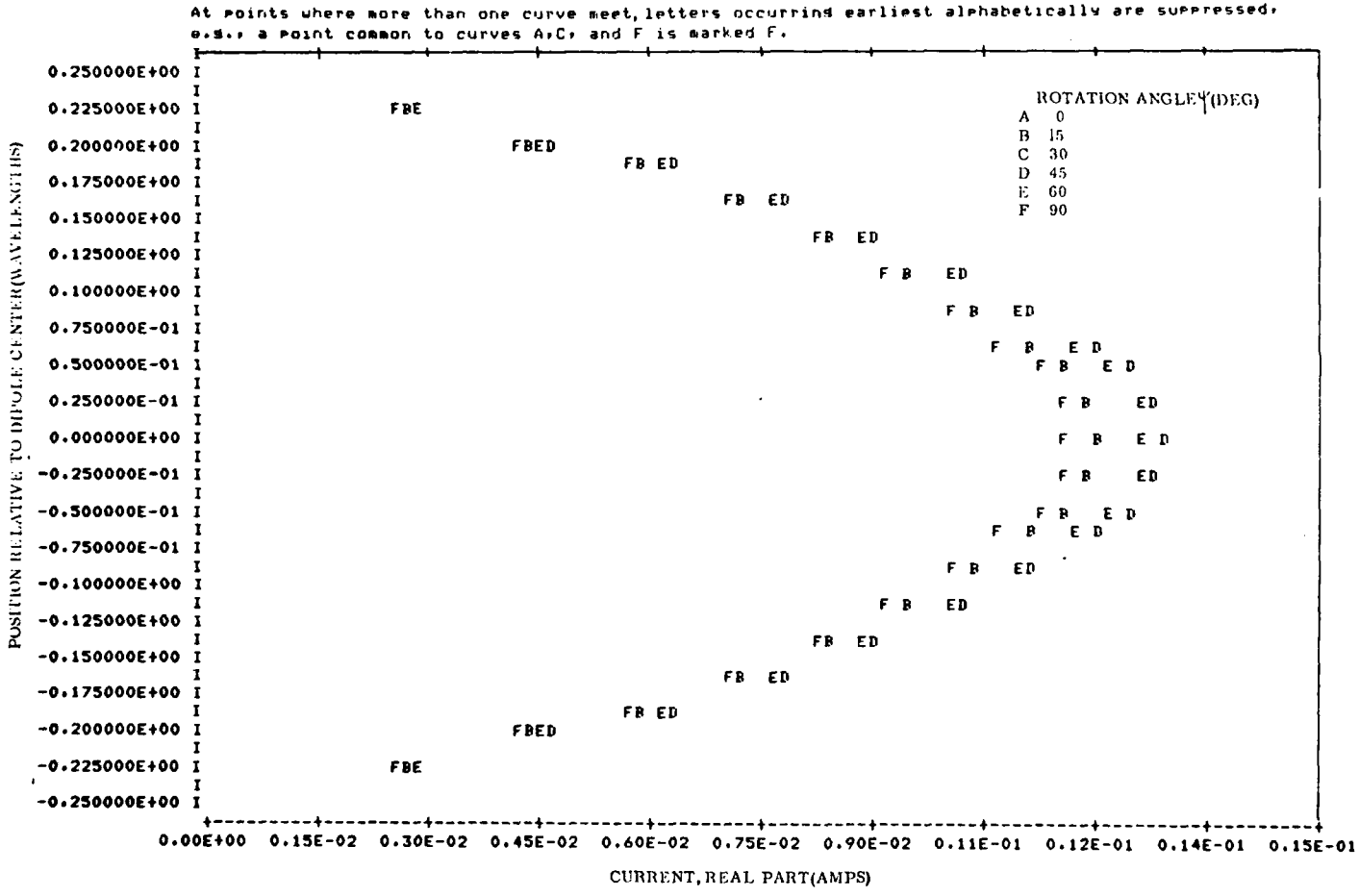

Figure 5-16. Real Part of Reference Dipole Current for Rectangular Lattice ($d_x = d_y = 0.8\lambda$) for Several Dipole Orientations and Broadside Scan ($\theta_\alpha = 0°$)

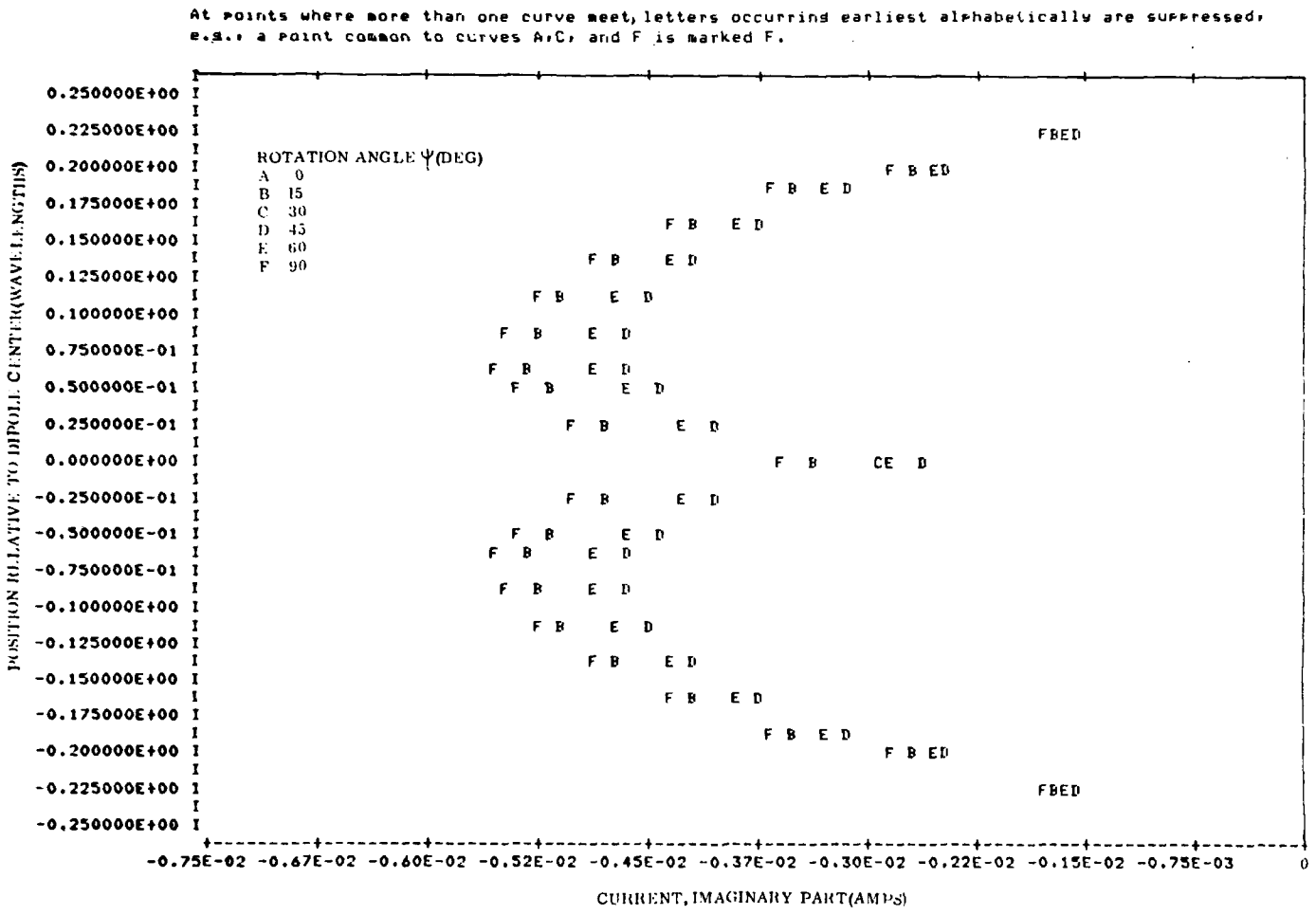

Figure 5-17. Imaginary Part of Reference Dipole Current for Rectangular Lattice ($d_x = d_y = 0.8\lambda$) for Several Dipole Orientations and Broadside Scan ($\theta_\alpha = 0°$)

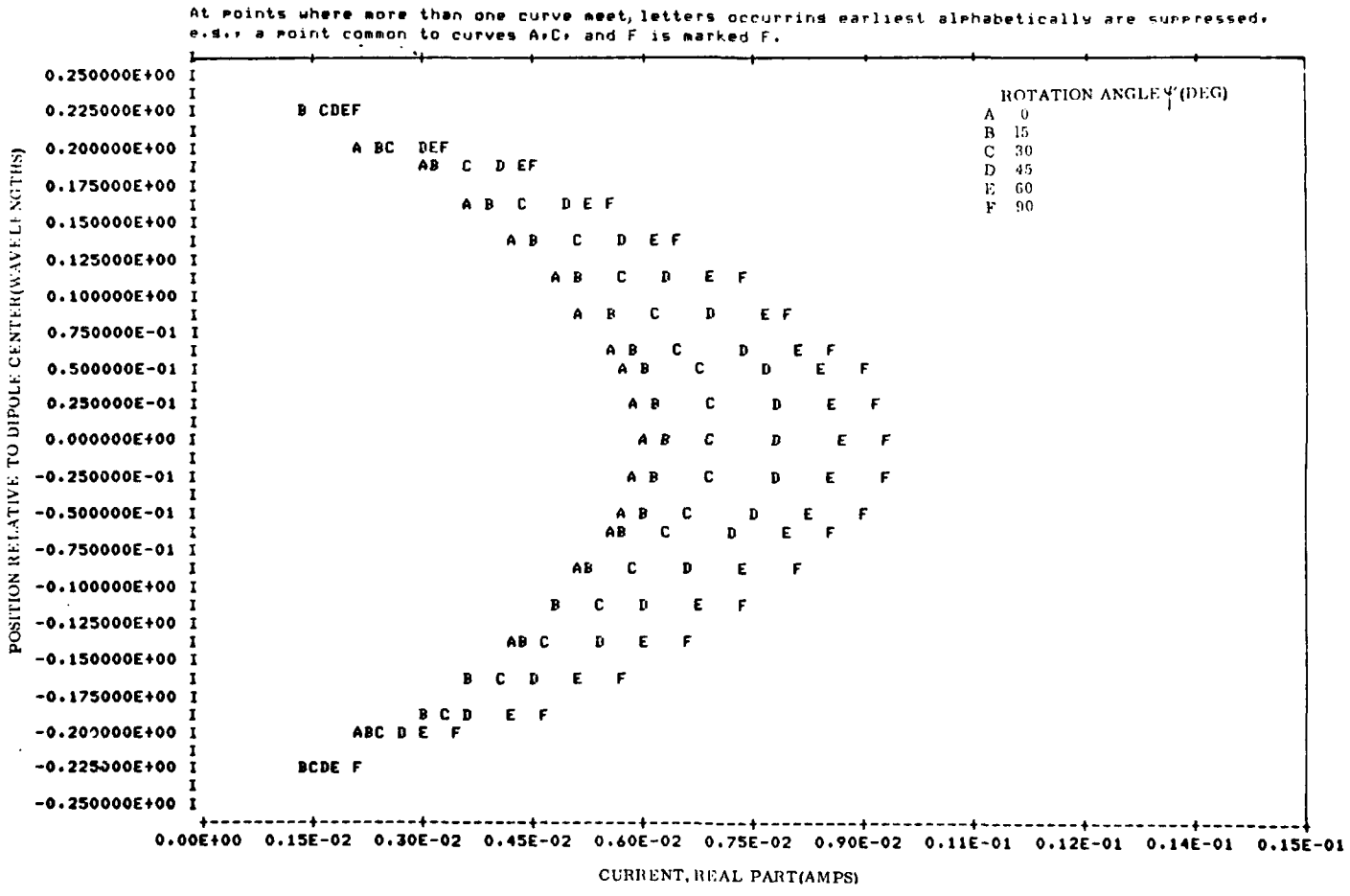

Figure 5-18. Real Part of Reference Dipole Current for Rectangular Lattice ($d_x = d_y = 0.8\lambda$) for Several Dipole Orientations and $\theta_\alpha = 20°$, $\phi_\alpha = 0°$ Scan

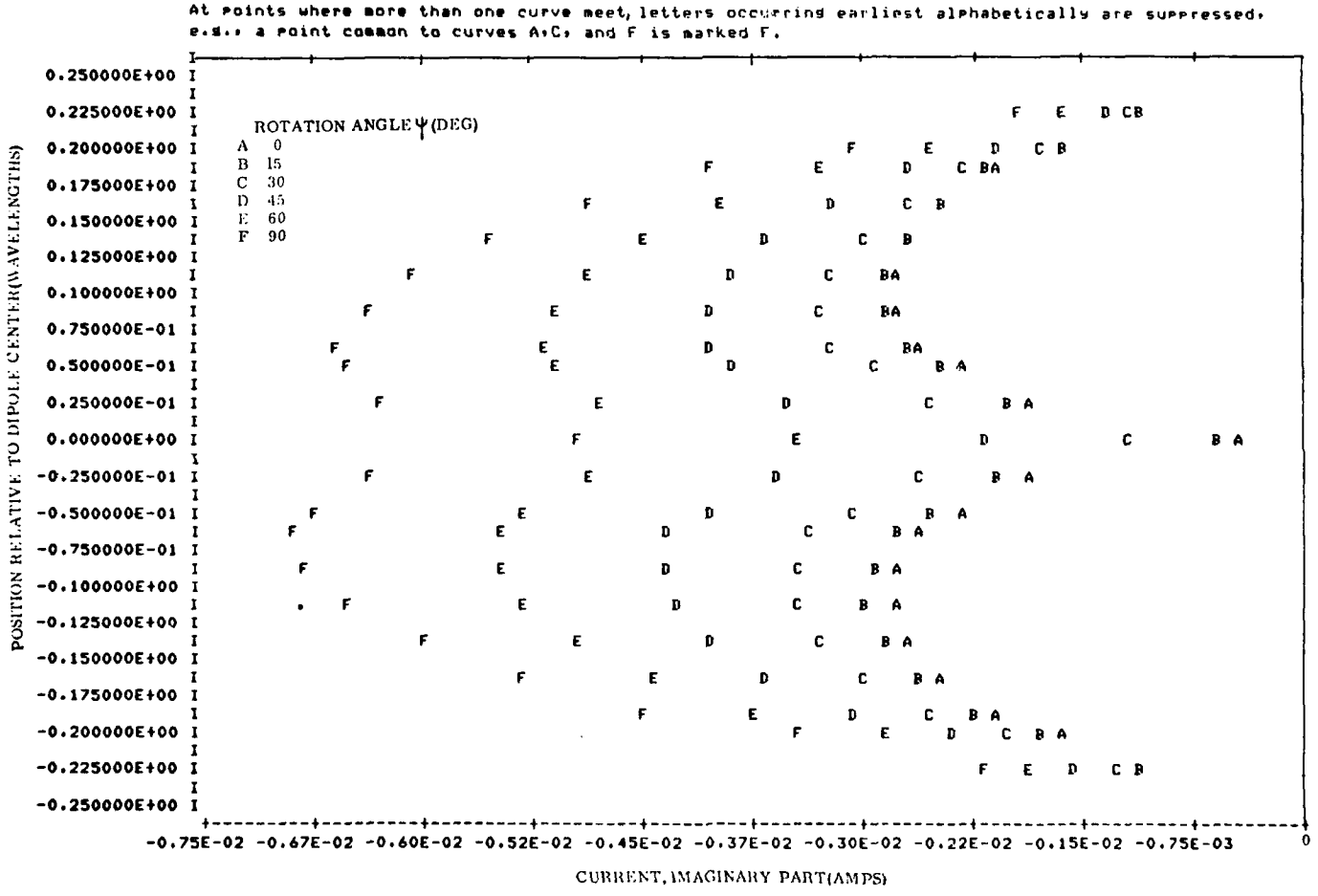

Figure 5-19. Imaginary Part of Reference Dipole Current for Rectangular Lattice ($d_x = d_y = 0.8\lambda$) for Several Dipole Orientations and θ_α =20°, ϕ_α = 0° Scan

5.4 TURNSTILE RADIATORS

The first approximation method was applied to the design of a turnstile radiator (crossed dipoles excited for circular polarization) for use as an array element. Reactance loads were determined to effect the 90 degree phasing between horizontal and vertical arms. This design avoids having to excite the radiator with the conventional two-port source. The array element is shown in Figure 5-20. The array lattice was that of Figure 5-7. Only broadside array phasing was considered, resulting in symmetric current about the axes of both dipoles. The need to model the short excited arm was avoided by passing the source through the junctions. This resulted in the equivalent problem of Figure 5-21.

The reference element current as computed by FAM, with the complex impedance loads $Z_H = Z_V = 0$ is shown in Figures 5-22 and 5-23.

The current under non-zero load conditions is easily determined by FAM as discussed in Section 3.2.7. Also, by considering the radiator as a multiport - one port for each load and excitation - and using FAM to obtain the port parameters relating these values of Z_H and Z_V were determined such that the currents at the load ports were equal in amplitude and in phase quadrature between horizontal and vertical arms. The resulting complex loads are

$$Z_H = 0. + j32 \tag{5-2}$$

$$Z_V = -0.2 - j48.8 \tag{5-3}$$

Since, for energy considerations, purely reactive loads are desirable the small real part of Z_V was set to zero prior to computing the reference element current. This current is plotted in Figures 5-24 and 5-25. The active impedance for this radiating element in the Figure 5-7 lattice infinite array is 74.4 + j10.9 ohms.

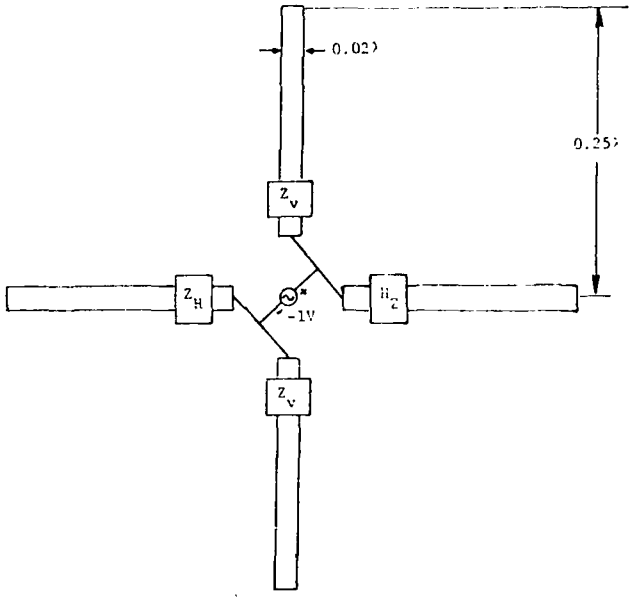

Figure 5-20. Loaded Crossed Dipoles with Single Feed Port

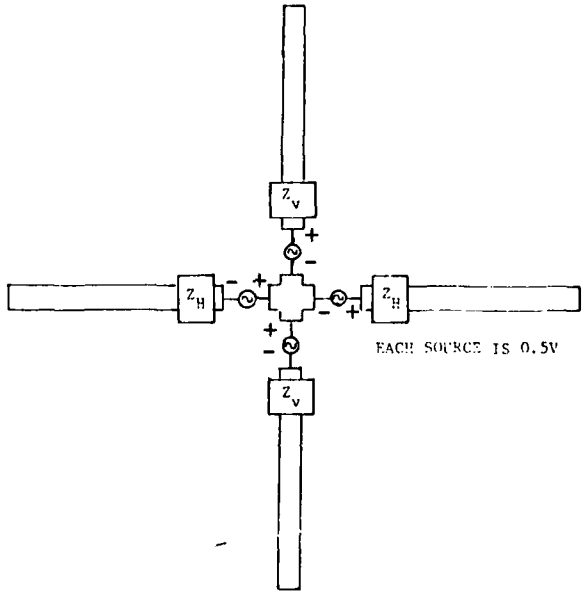

Figure 5-21. Loaded Crossed Dipoles with Equivalent Feed
This Model is Equivalent to the Figure 5-20
Single Feed Port Radiator

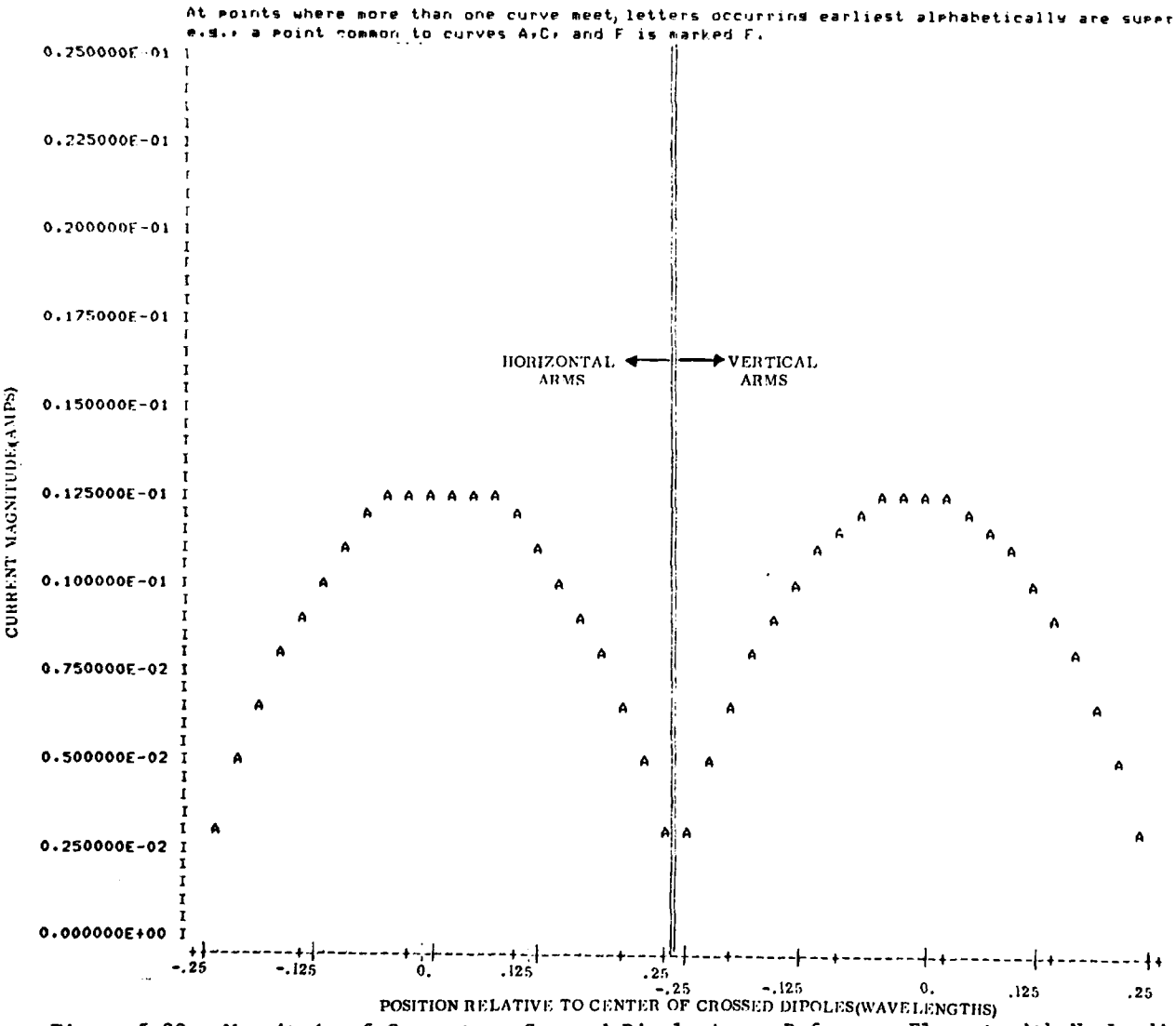

Figure 5-22. Magnitude of Current on Crossed Dipole Array Reference Element with No Loading

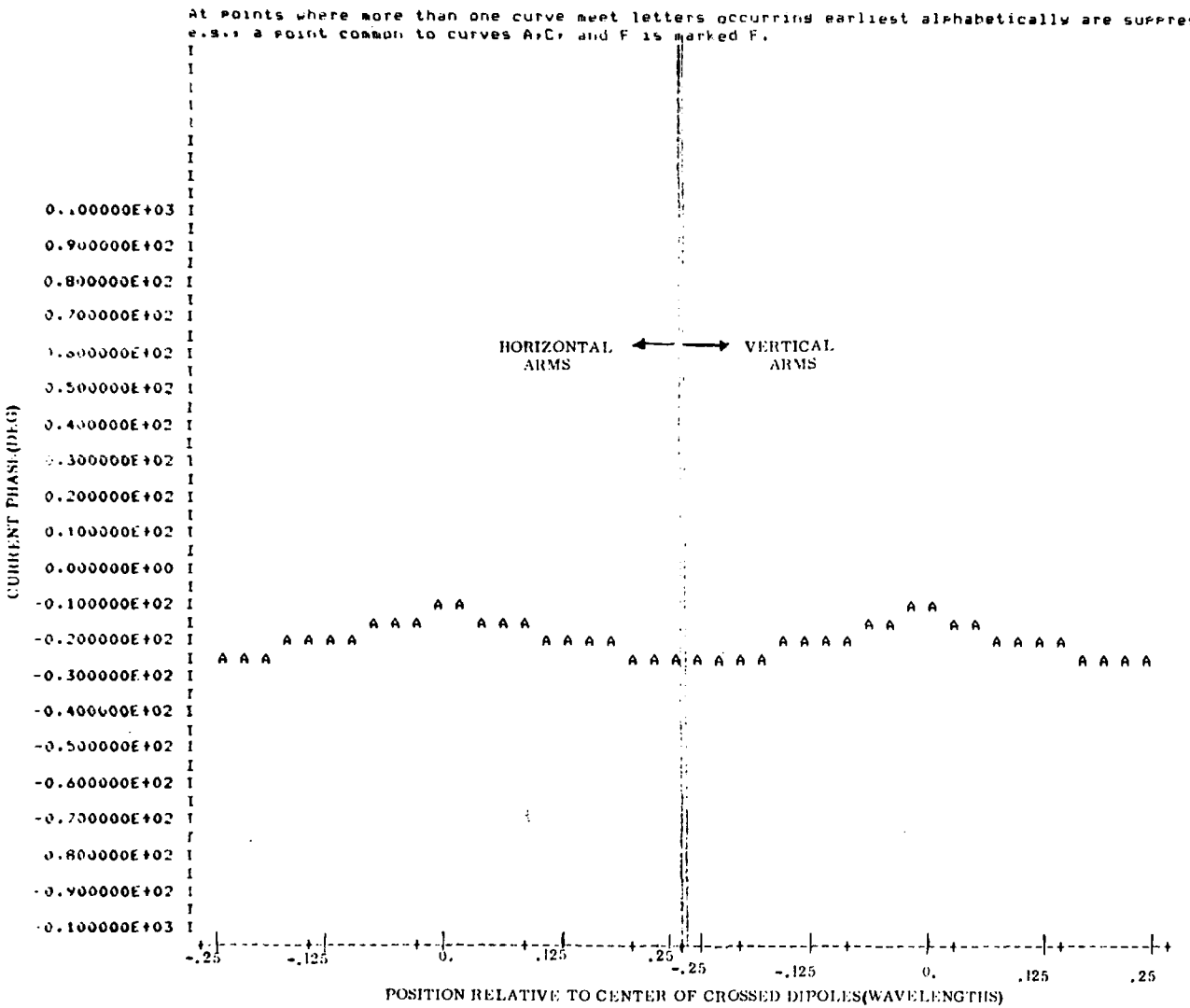

Figure 5-23. Phase of Current on Crossed Dipole Array Reference Element with No Loading

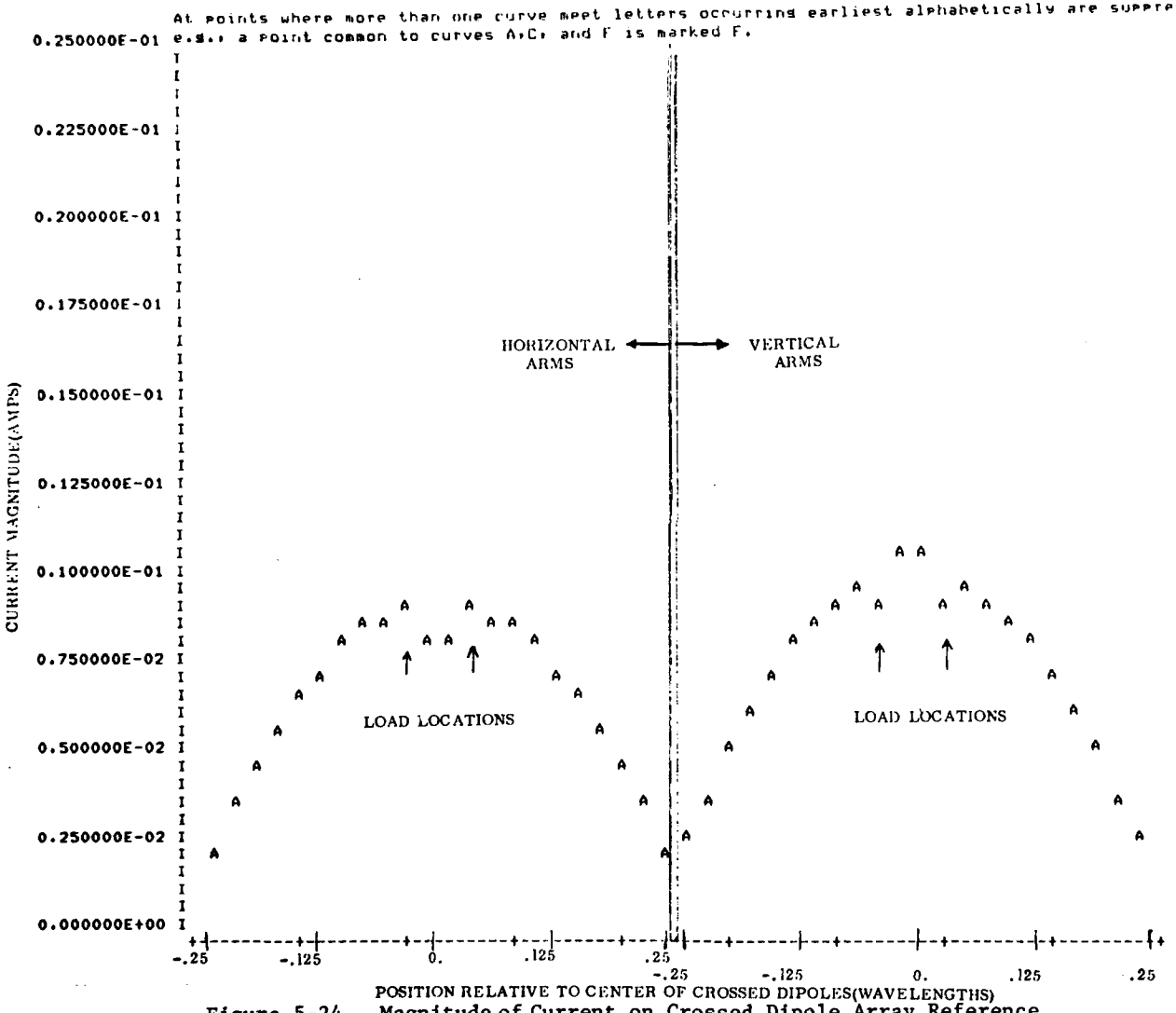

Figure 5-24. Magnitude of Current on Crossed Dipole Array Reference Element with Loading for Circular Polarization

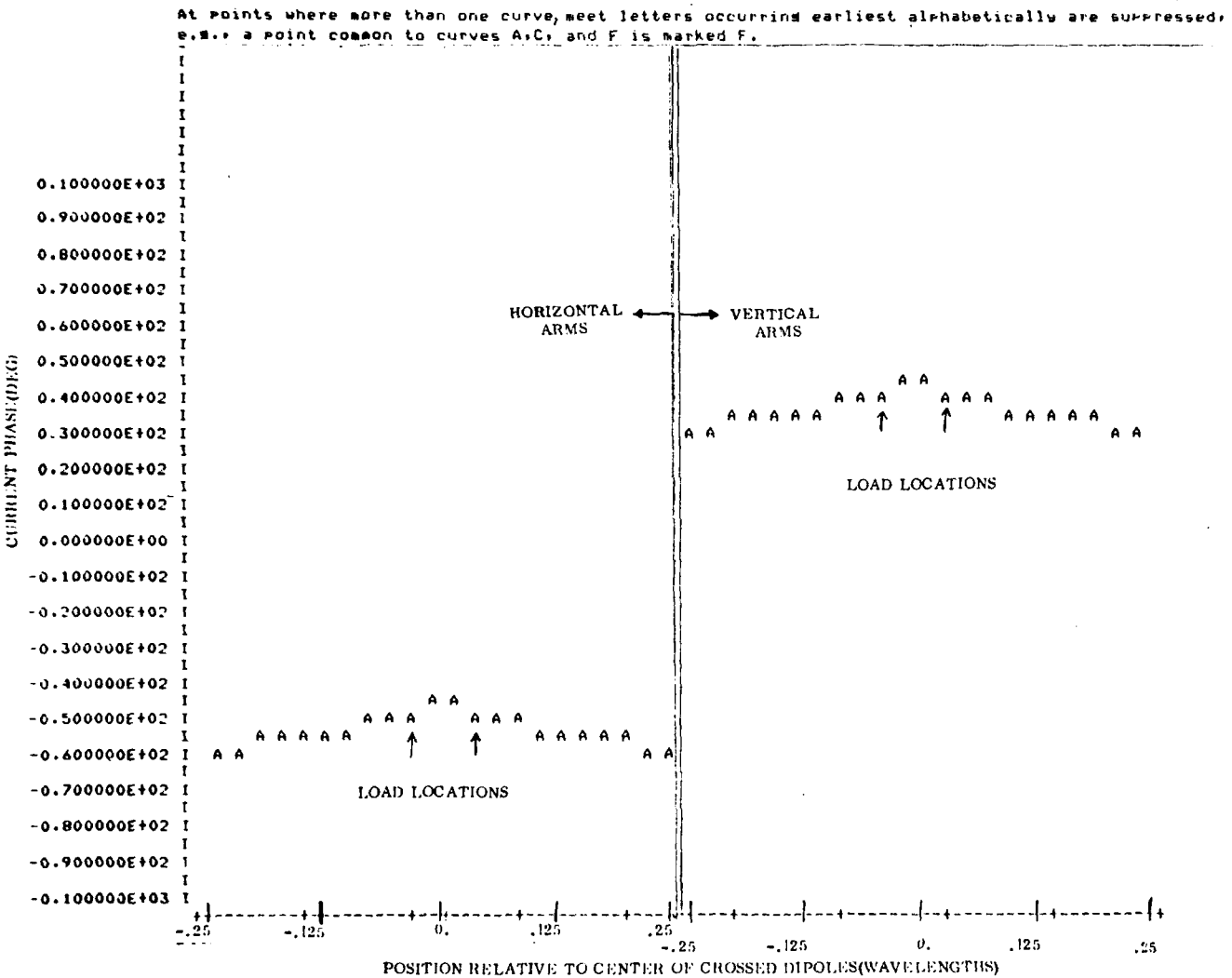

Figure 5-25. Phase of Current on Crossed Dipole Array Reference Element with Loading for Circular Polarization

5.5 CONVERGENCE

Each element of the generalized impedance matrix $[Z^{gs}]$, given by (3-61), involves a doubly infinite summation in integers p and q. Adequate truncation of this summation depends on its rate of convergence. As discussed in Section 5.1, p_{max} and q_{max} must be determined such that the exclusion of all p and q for which $|p| > p_{max}$ and $|q| > q_{max}$ in the summation provides an accurate result. Each pq term in the summation represents a plane wave. Beyond the first few values of $|p| \div |q|$ these waves are evanescent; they exponentially decay away from the array plane. The summation term corresponding to an evanescent wave is imaginary since the energy imparted to these waves is entirely reactive. The principal parameters which impact p_{max} and q_{max} for wire radiators lying in the array plane are d_x/a and d_y/a. The larger these ratios of interelement spacing to wire radius the slower the convergence of the summation.

The reactance of a "self-impedance" (diagonal) element of $[Z^{gs}]$ was computed for values of $p_{max} = q_{max} \leq 150$ and several values of $d_x/a = d_y/a$ (square lattice). Convergence rates are apparent from these results by plotting (Figures 5-26 to 5-29)

$$\varepsilon(M) = \left|\frac{X(M) - X(150)}{X(150)}\right| \tag{5-4}$$

versus M where X(M) = imaginary part of a diagonal element of $[Z^{gs}]$ determined with $p_{max} = q_{max} = M$. Figures 5-26 to 5-29 each correspond to a different wire radius and each display six curves. Each curve corresponds to a different interelement spacing. Curve C in Figure 5-26 and Curve A in Figure 5-28 correspond to the same ratio 50, of interelement spacing to radius. As expected, these two curves exhibit similar convergence rates.

The size of $[Z^{gs}]$ is N_s^2 where N_s is the number of segments dividing a wire radiator. Convergence of the reference element wire current with increasing N_s is shown in Figures 5-30 to 5-33. Figures 5-30 and 5-31 correspond to the Figure 5-7 triangular lattice dipole array and $p_{max} = q_{max} = 60$. Figures 5-32 and 5-33 correspond to the Figure 5-7 array with the exception that the wire radius was reduced to $a = 0.005\lambda$ and $p_{max} = q_{max} = 80$. Convergence is quite slow in both cases. It was pointed out[20] that the use of pulse expansion functions in the moment method formulation in conjunction with an exact representation for the $\vec{E}$-field operator is likely the cause of the slow convergence. The convergence is expected to be significantly

improved by computing the $\vec{E}$-field via a partial difference approximation. Approximately seven subsections per wavelength is expected to then be adequate. This modification is presently being implemented.

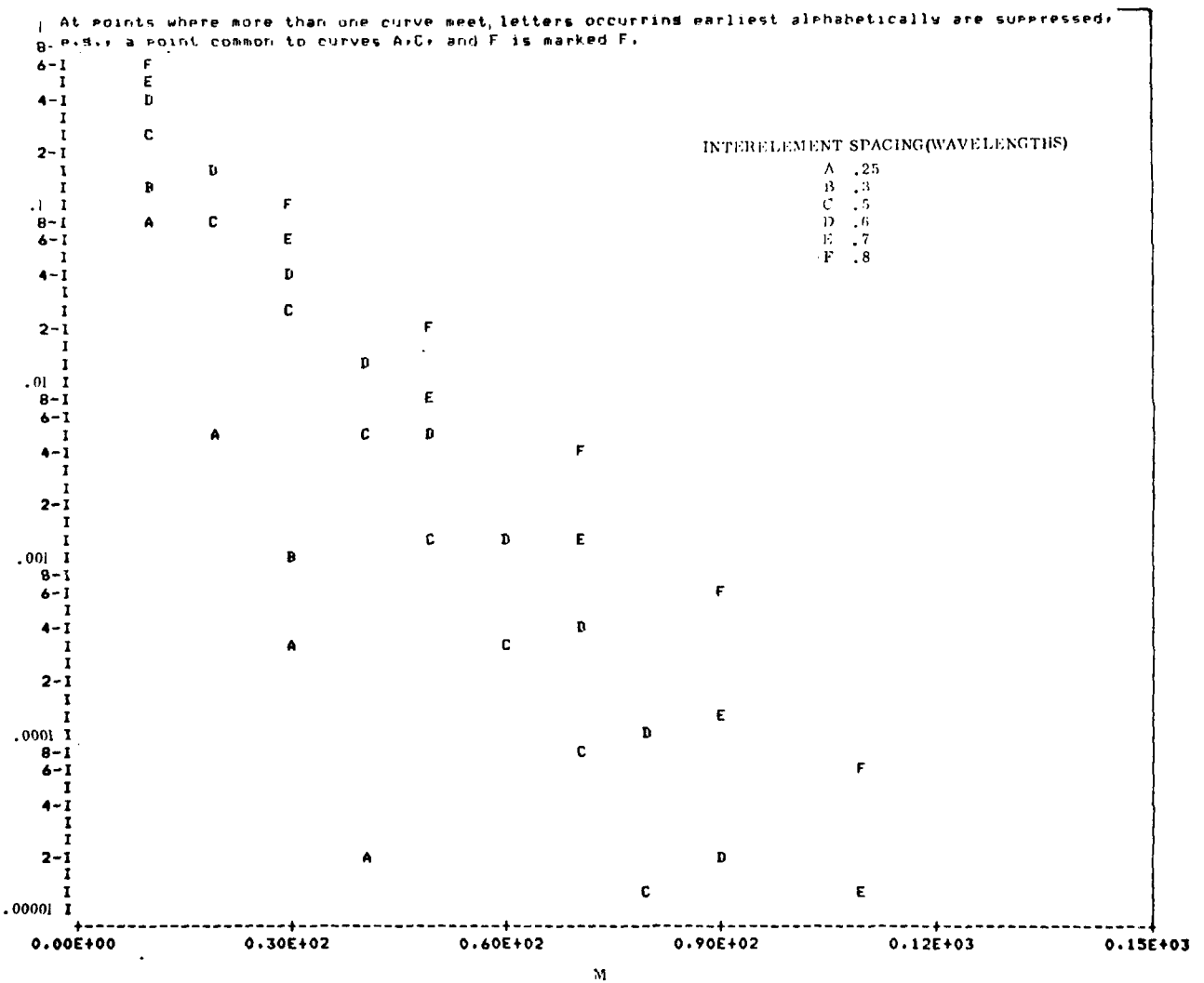

Figure 5-26. Convergence of Diagonal Element of $[Z^{gs}]$ for Wire Radius = 0.01λ

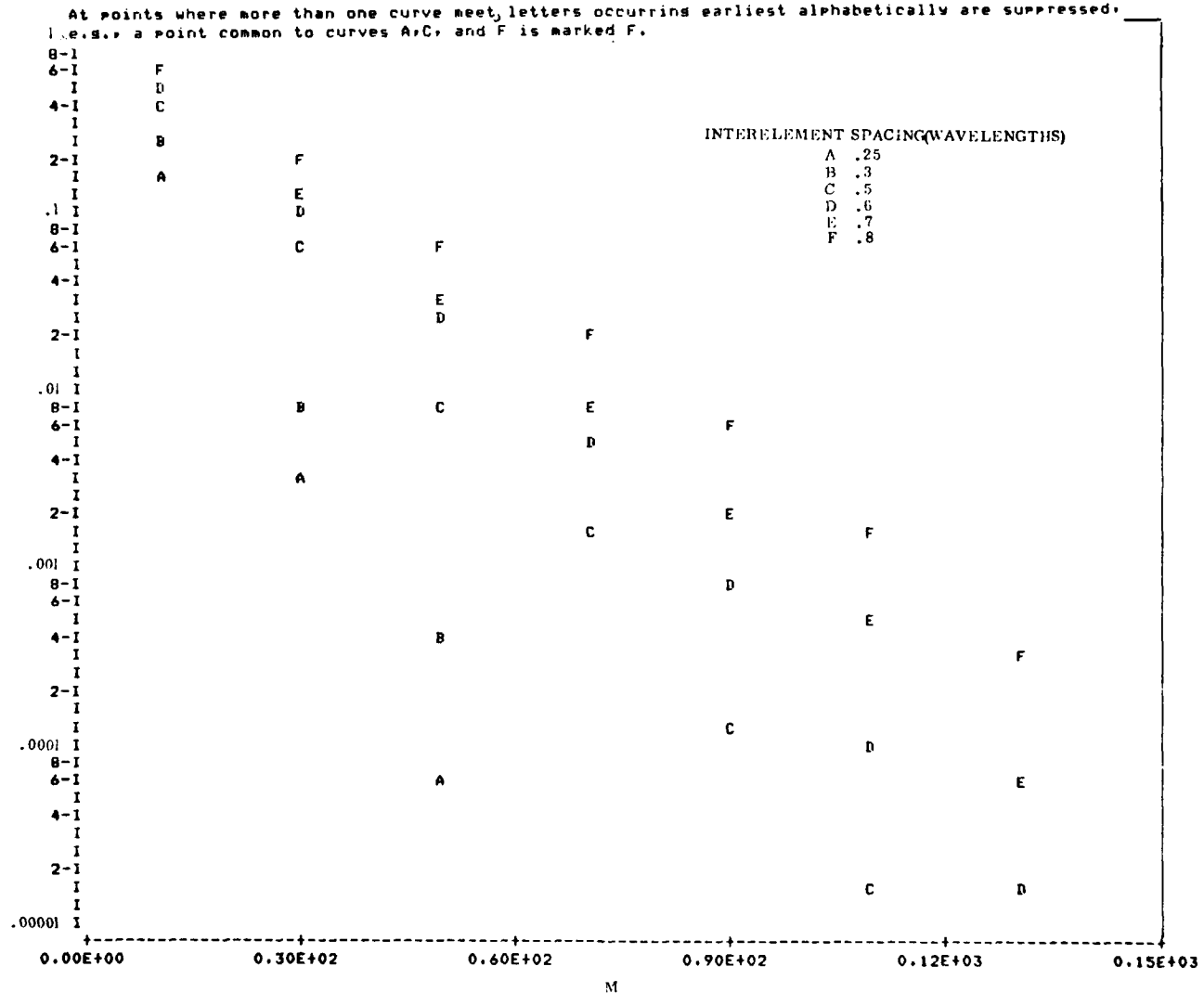

Figure 5-27. Convergence of Diagonal Element of $[Z^{gs}]$ for Wire Radius = 0.007λ

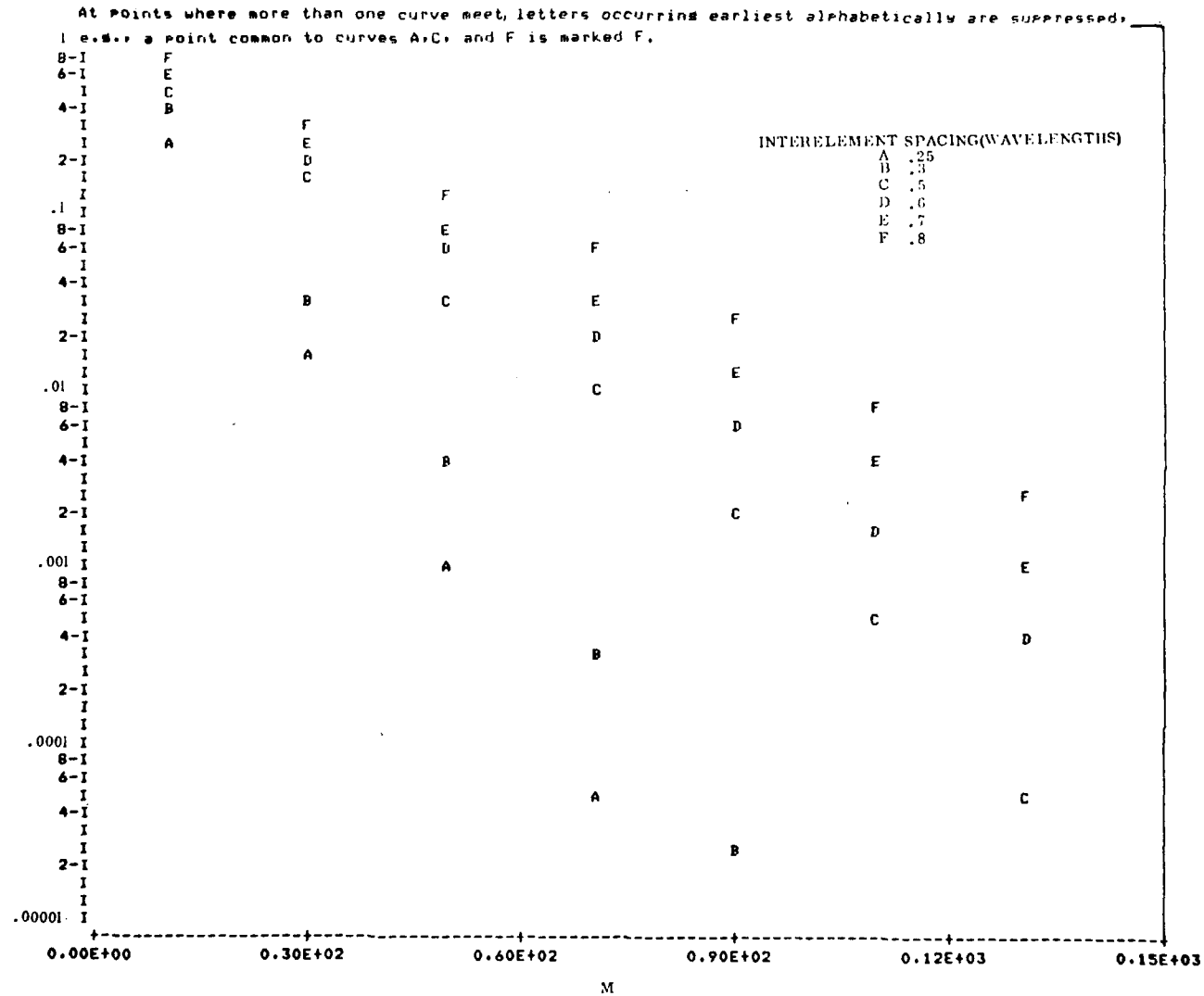

Figure 5-28. Convergence of Diagonal Element of $[Z^{gs}]$ for Wire Radius = 0.005λ

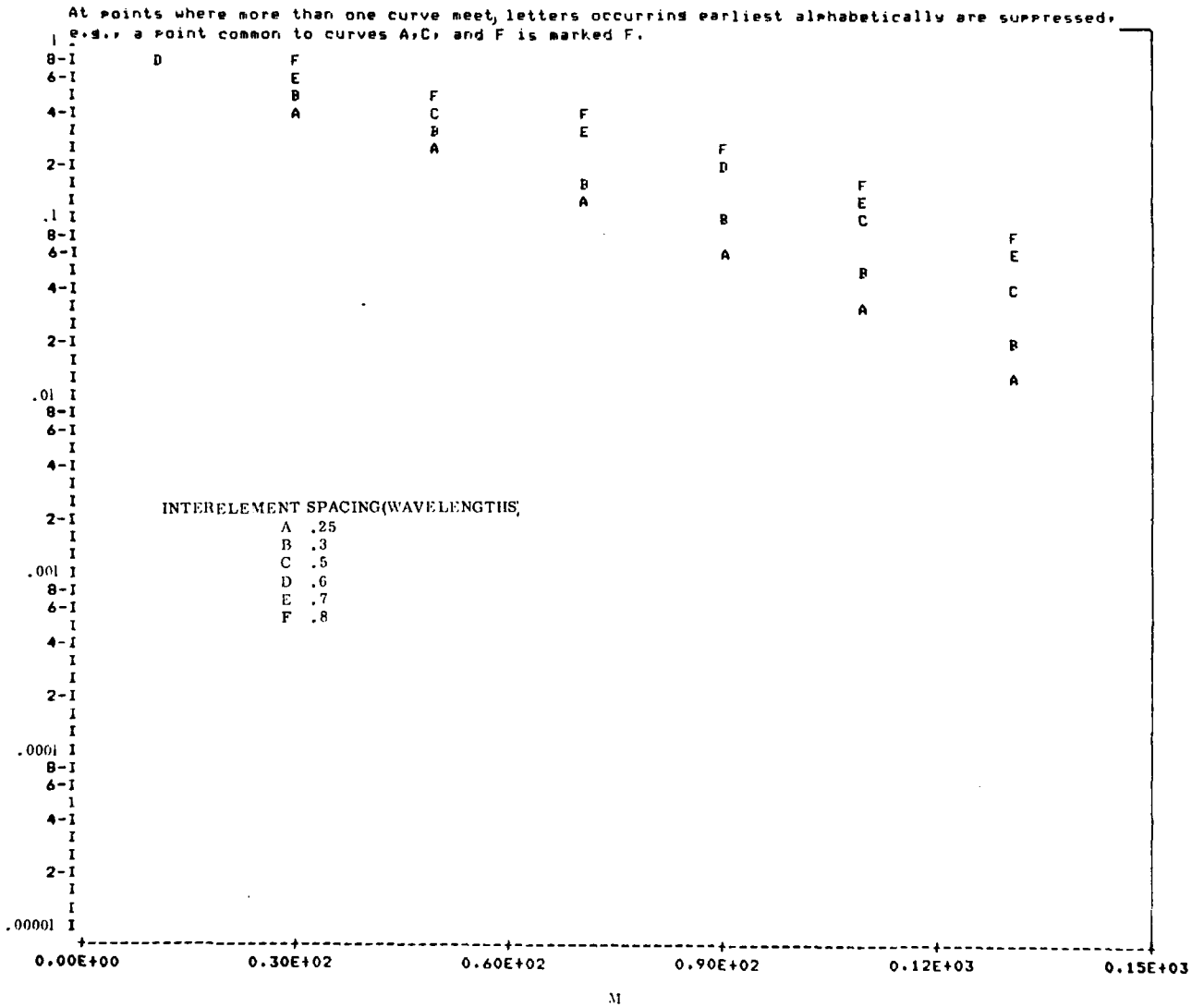

Figure 5-29. Convergence of Diagonal Element of $[Z^{gs}]$ for Wire Radius = 0.001λ

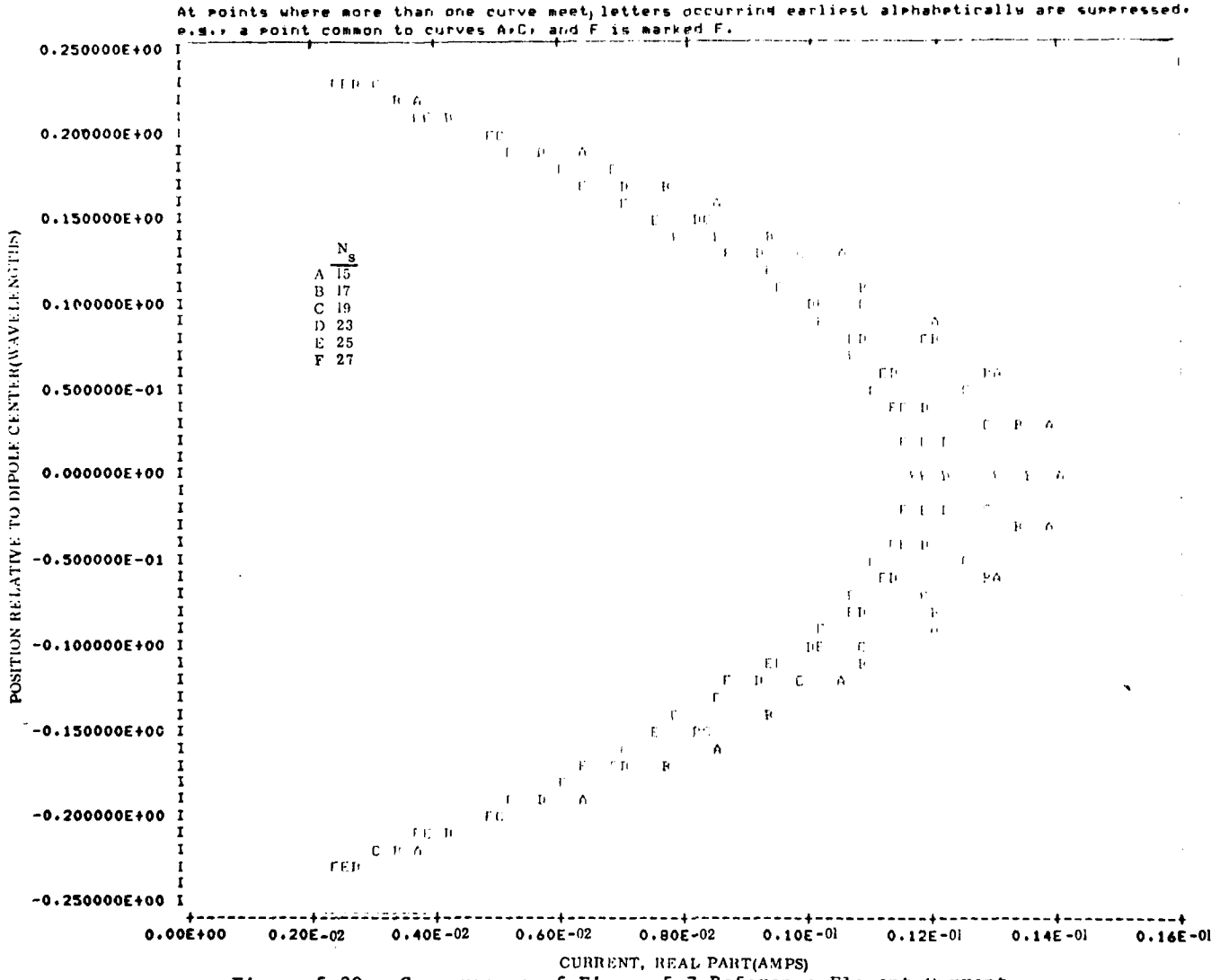

Figure 5-30. Convergence of Figure 5-7 Reference Element Current (Real Part) with Respect to Number of Segments

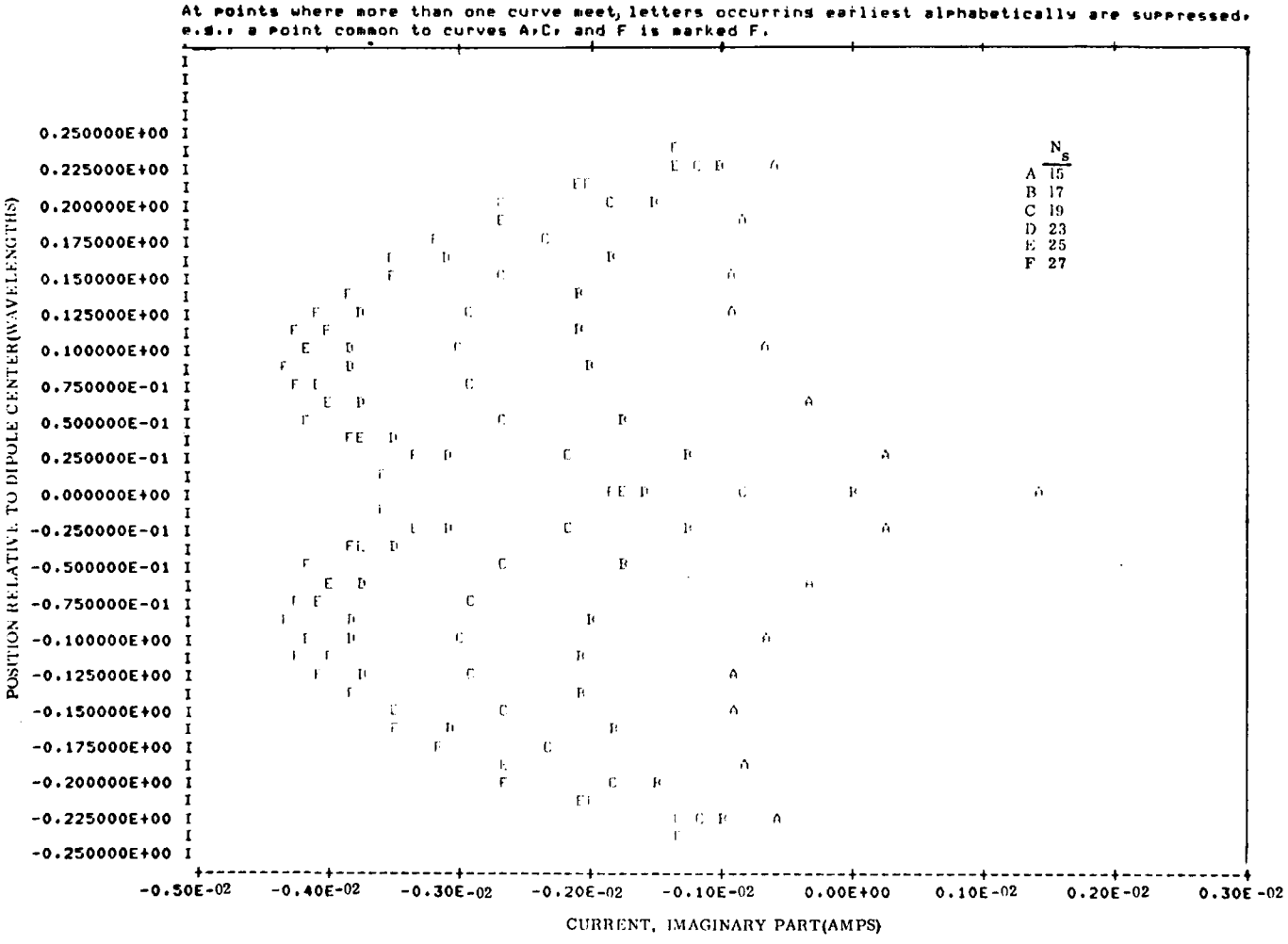

Figure 5-31. Convergence of Figure 5-7 Reference Element Current (Imaginary Part) with Respect to Number of Segments

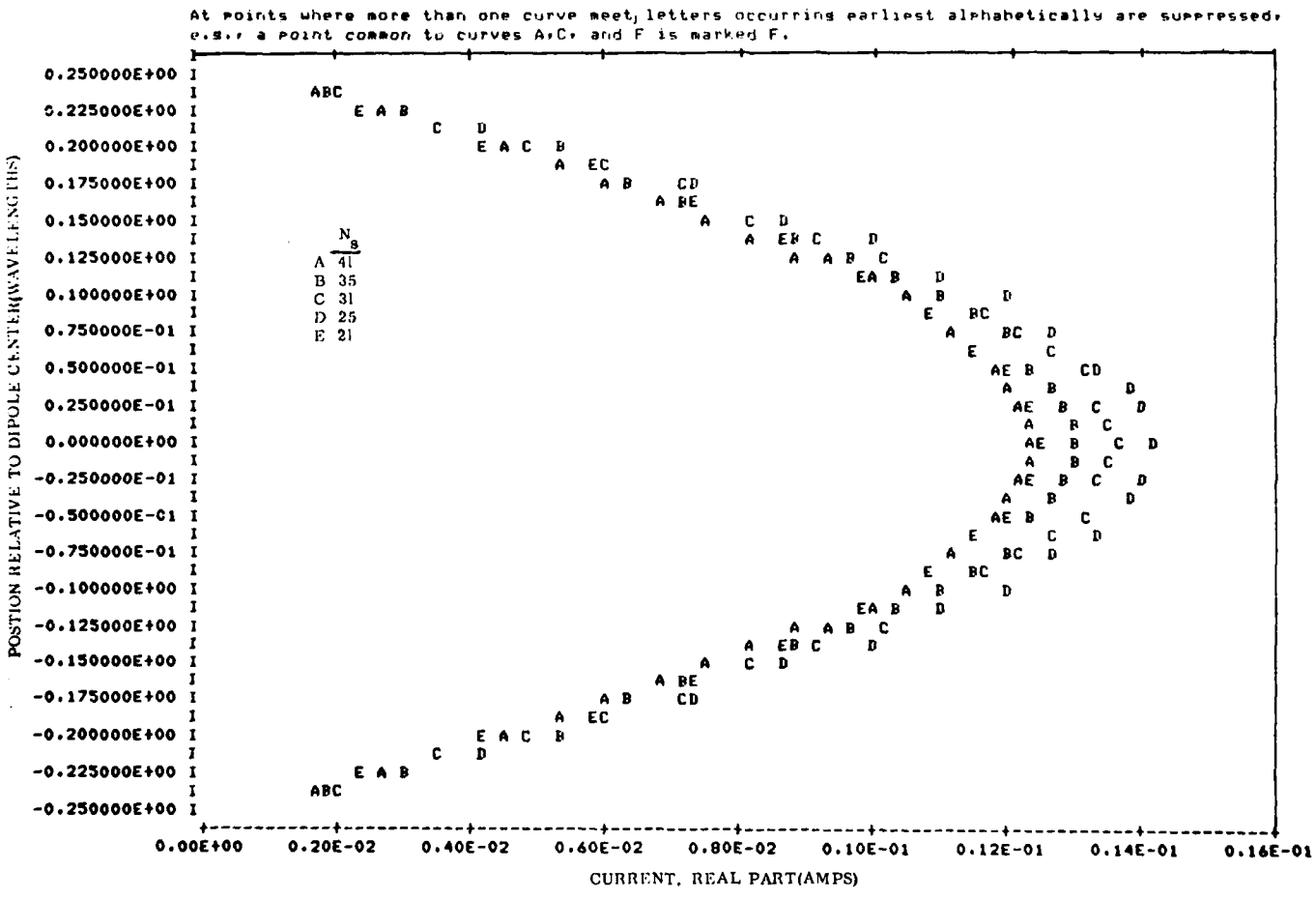

Figure 5-32. Figure 5-30 Problem with Wire Radius Cut in Half

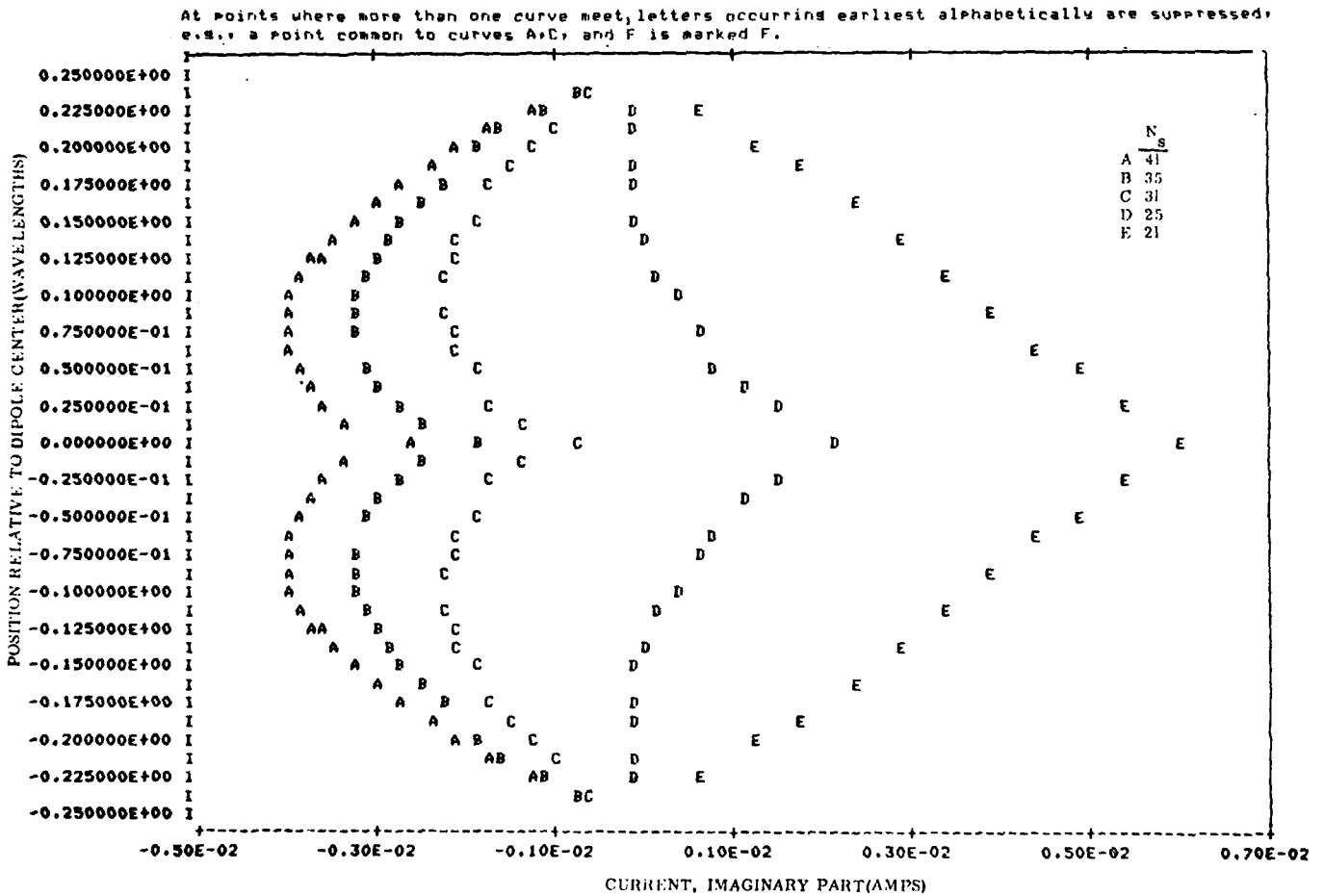

Figure 5-33. Figure 5-31 Problem with Wire Radius Cut in Half

SECTION 6

REFERENCES

1. B. A. Munk and G. A. Burrell, "Plane-Wave Expansion for Arrays of Arbitraily Oriented Piecewise Linear Elements and its Application to Determining the Impedance of a Single Linear Antenna in a Lossy Half-Space," IEEE Trans. on Antennas and Propagation, Vol. AP-27, No. 3, pp.331-343, May 1979.

2. R. F. Harrington, Field Computation by Moment Methods, Macmillian, 1968.

3. R. F. Harrington, Time Harmonic Electromagnetic Fields, McGraw-Hill, 1961, pp 60-61.

4. R. Robertson, System Data File (SDF) for the Intrasystem Analysis Program (IAP) Description, RADC-TR-79-213, Vol. I and Vol. II, December 1979.

5. Users Manual for the System File Handler , Atlantic Research Corporation, RADC Contract F30602-77-C-0106, February 1980.

6. T. W. Kornbau, Application of the Plane Wave Expansion Method to Periodic Arrays Having a Skewed Grid Geometry, AFAL-TR-77-112, October 1977.

7. P. C. Clemmow, The Plane Wave Spectrum Representation of Electromagnetic Fields, Pergamon Press Ltd., 1966.

8. H. H. Chao and B. J. Strait, Computer Programs for Radiation and Scattering by Arbitrary Configurations of Bent Wires, Syracuse University Scientific Report No. 7, AFCRL-70-0374, September 1970.

9. J. H. Richmond, Computer Program for Thin-Wire Structures in a Homogeneous Conducting Medium, The Ohio State ElectroScience Laboratory. See also NAPS document 02223.

10. D. E. Warren, Near Electric and Magnetic Fields of Wire Antennas, (Computer Program Description) Vol. AP-22, No. 2, pp. 364, March 1974

11. L. Stark, "Radiation Impedance of a Dipole in an Infinite Planar Phased Array," Radio Science, Vol. 1 (New Series), No. 3, pp. 361-377, March 1966.

12. A. L. VanKoughnett and J. L. Yen, "Properties of a Cylindrical Antenna in an Infinite Planar or Collinear Array," IEEE Trans. on Antennas and Propagation, Vol. AP-15, No. 6, pp 750-757, November 1967.

13. V. W. H. Chang, "Infinite Phased Dipole Array," Proc. IEEE, Vol. 56, No. 11, pp 1892-1900, November 1968.

14. P. S. Carter, Jr., "Mutual Impedance Effects in Large Beam Scanning Arrays," IRE Trans. on Antennas and Propagation, Vol. AP-8, No. 3, pp 276-285, May 1980.

15. E. L. Caffey, III and K. R. Carver, Antenna Evaluation Study for the Shuttle Multispectral Radar, Physical Science Laboratory, Las Cruces, New Mexico; Interim Report, July 1973; Final Report - Phase I, December 1973; Final Report - Phase II, May 1977; Final Report - Phase III, December 1978.

16. H. Bateman, Table of Integral Transforms, Vol. I, McGraw-Hill, 1954.

17. A. Papoulis, The Fourier Integral and its Applications, McGraw-Hill, pp 47-49, 1962.

18. R. J. Balestri, T. R. Ferguson, and E. R. Anderson, General Electromagnetic Model for the Analysis of Complex Systems, Vol. 2 - Engineering Manual, RADC-TR-77-137, April 1977. (See Vol. 1 - User's Manual for code description.)

19. AMP (Antenna Modeling Program) Engineering Manual, M. B. Associates, ONR Contract, IS-R-72/10, July 1972. (See associated User's Manual and Systems Manual for AMP code description.)

20. Private Communication, L. W. Pearson, University of Kentucky and D. R. Wilton, University of Mississippi, June 1980.

APPENDIX A

FIELD FROM AN INFINITE ARRAY OF INFINITESIMAL CURRENT DIPOLES

This appendix contains the derivation of the equations necessary to determine the radiation from an infinite, rectilinear array of infinitesimal current elements. All elements are identical in orientation, progressively phased, and of constant current amplitude (Figure A-1). The derivation is based on the work of Munk, Burrell, and Kornban.[1,6]

The vector potential for an infinite array can be written as a sum over the vector potentials of the individual elements

$$d\vec{A} = \sum_{p=-\infty}^{\infty} \sum_{q=-\infty}^{\infty} d\vec{A}_{pq} \tag{A-1}$$

where the ordered integer pair (p,q) uniquely locates an element in the array. The individual element vector potentials have the form

$$d\vec{A}_{pq} = \hat{\ell} \frac{\mu d\ell}{4\pi} I_{pq} \frac{e^{-\gamma R_{pq}}}{R_{pq}} \tag{A-2}$$

where $\hat{\ell}$ is the element orientation, μ is the permeability of free space, $d\ell$ is the infinitesimal dipole length, I_{pq} is the current on the pq^{th} element, R_{pq} is the distance from the pq^{th} element to the field point. The propagation constant, γ, is assumed complex to add generality to the argument.

The distance R_{pq} is given by

$$R_{pq} = \| \vec{r} - \vec{r}'_{pq} \| \tag{A-3}$$

where $\vec{r}$ points to the field point and $\vec{r}'_{pq}$ points to the pq^{th} current element. These vectors have the following rectangular coordinate representations:

$$\vec{r} = x\hat{x} + y\hat{y} + z\hat{z} \tag{A-4}$$

$$\vec{r}'_{pq} = x_{pq}\hat{x} + y_{pq}\hat{y} \tag{A-5}$$

where the array is assumed, for simplicity, to lie in the xy plane (Figure A-1). For the case of a rectilinear lattice on the array, the coordinates of the pq^{th} element satisfy

$$x_{pq} = pd_x \tag{A-6}$$

$$y_{pq} = qd_y + p\Delta y \tag{A-7}$$

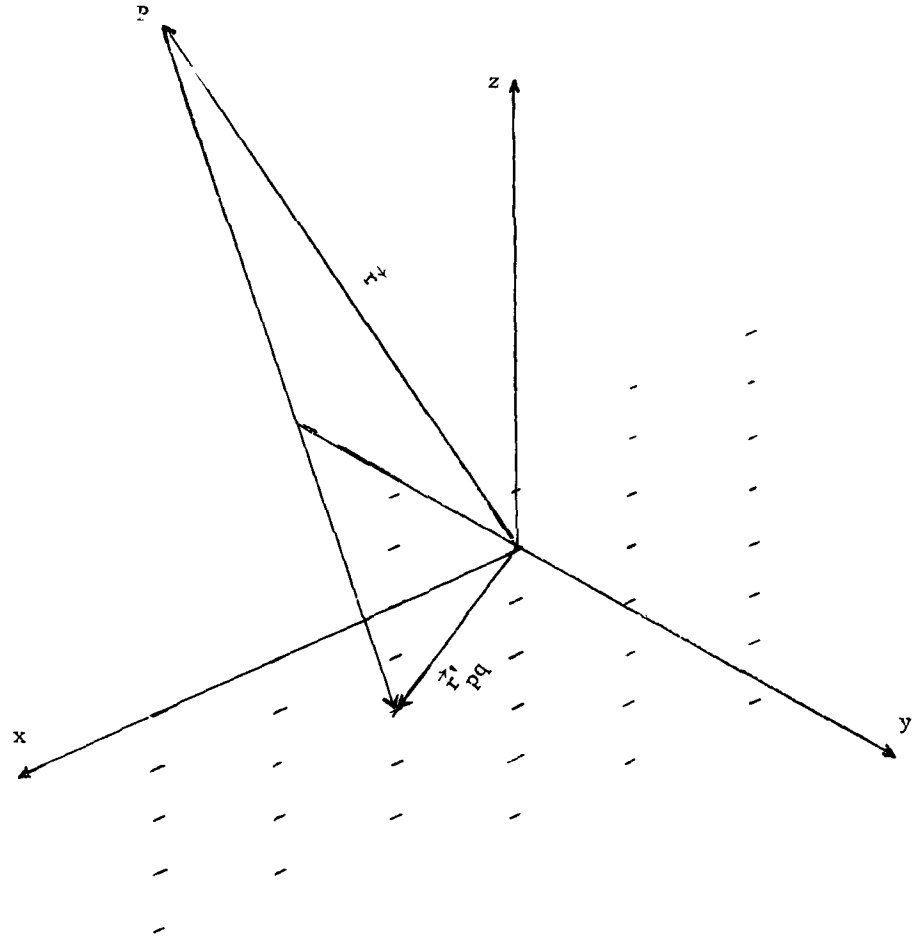

Figure A-1. Portion of Infinite Array of Infinitesimal Dipole Elements

where d_x and d_y are interelement separations and Δy is the array skew paremeter. (See Figure 3-7 for an illustration of these parameters.) The skew parameter will be zero for rectangular lattices. The distance R_{pq} now can be written as

$$R_{pq}^2 = (pd_x - x)^2 + (qd_y + p\Delta y - y)^2 + z^2 \tag{A-8}$$

Due to the constant amplitude and progressive phasing of the element currents, the current I_{pq} of the pq^{th} element can be written in terms of a reference current I_{00} as

$$I_{pq} = I_{00}\, e^{-jk\vec{r}'_{pq}\cdot\hat{s}} \tag{A-9}$$

where k is the wave number (k = imaginary part of γ) and s is the phase unit vector.

$$\hat{s} = s_x\hat{x} + s_y\hat{y} + s_z\hat{z} \tag{A-10}$$

The current I_{pq} in (A-9) now assumes the form

$$I_{pq} = I_{00}\, e^{-jkpd_x s_x - jk(qd_y + p\Delta y)s_y} \tag{A-11}$$

The array vector potential can be written as

$$d\vec{A} = \hat{\ell}\,\frac{\mu I_{00} d\ell}{4\pi}\sum_{p=-\infty}^{\infty} e^{-jkpd_x s_x - jkp\Delta y s_y}\, d\vec{A}_p \tag{A-12}$$

$$d\vec{A}_p = \sum_{q=-\infty}^{\infty} e^{-jkqd_y s_y}\,\frac{e^{-\gamma R_{pq}}}{R_{pq}} \tag{A-13}$$

and represents the vector potential for a row of elements. The distance R_{pq} is written for convenience as

$$R_{pq} = \left[a^2 + [qdy - (y - p\,y)^2]^{1/2}\right] \tag{A-14}$$

where

$$a^2 = z^2 + (pd_x - x)^2 \tag{A-15}$$

The equation for the array vector potential, (A-13), can be transformed to a more convenient form using Fourier transform methods. The required Fourier transform pair is

$$F(w) = \frac{e^{-\gamma[a^2 + (w-w_1)^2]^{\frac{1}{2}}}}{[a^2 + (w-w_1)^2]^{\frac{1}{2}}} \tag{A-16}$$

$$f(t) = \frac{e^{jw_1 t}}{2j} H_0^{(2)}\left(a\sqrt{-\gamma^2 - t^2}\right) \qquad \text{where } w_i \text{ is a constant} \tag{A-17}$$

The function $H_0^{(2)}(x)$ is the 0^{th} order Hankel function of the second kind and f(t) and f(w) are related by the usual Fourier transform equations.

$$F(w) = \int_{-\infty}^{\infty} e^{-jwt} f(t)dt \tag{A-18}$$

$$f(t) = \frac{1}{2\pi}\int_{-\infty}^{\infty} e^{jwt} F(w)dw \tag{A-19}$$

Using (A-16) through (A-19), the array row vector potential becomes

$$d\vec{A}_p = \sum_{q=-\infty}^{\infty} e^{-jkqd_y s_y} F(qd_y) \tag{A-20}$$

or, more conveniently,

$$d\vec{A}_p = \sum_{q=-\infty}^{\infty} e^{jqw_0 t} F(qw_0) \tag{A-21}$$

where

$$w_0 = d_y$$

$$t = -ks_y$$

The infinite series in (A-21) now can be transformed to a faster converging series using the Poisson sum rule (shifted version)[17] which states

$$\sum_{q=-\infty}^{\infty} e^{jqw_0 t} F(qw_0) = T \sum_{n=-\infty}^{\infty} f(t + nT) \tag{A-22}$$

for any Fourier transform pair F(w) and f(t). The parameter T is given by

$$T = \frac{2\pi}{w_0} = \frac{2\pi}{d_y} \tag{A-23}$$

Using (A-22), the array row vector potential in (A-21) is

$$d\vec{A}_p = T \sum_{n=-\infty}^{\infty} f(t + nT) \tag{A-24}$$

The function f(t + nT) is given by

$$f(t) = \frac{e^{jw_1(t + nT)}}{2j} H_0^{(2)}(a\sqrt{-\gamma^2 - (t + nT)^2}) \tag{A-25}$$

where the constant w_1 is picked to be

$$w_1 = y - p\Delta y \tag{A-26}$$

The array vector potential then satisifies

$$d\vec{A} = \hat{\ell} \frac{\mu I_{00} d\ell}{4jd_y} \sum_{p=-\infty}^{\infty} e^{-jkpd_x s_x} d\vec{A}_p \tag{A-26}$$

The row vector potential is

$$d\vec{A}_p = \sum_{n=-\infty}^{\infty} e^{jy[ks_y + \frac{2\pi n}{d_y}] - jp\Delta y \frac{2\pi n}{d_y}} H_0^{(2)}(akr') \tag{A-27}$$

where

$$r' = [\frac{\gamma}{jk}]^2 - ([-s_y + \frac{n\lambda}{d_y}]^2)^{\frac{1}{2}}$$

$$\gamma = \frac{2\pi}{k}$$

Interchange of summation operations and change of sign on the summation index in (A-26) and (A-27) yields

$$d\vec{A} = \hat{\ell} \frac{\mu I_{00} d\ell}{4jd_y} \sum_{n=-\infty}^{\infty} e^{-jyk[s_y + \frac{n\lambda}{d_y}]} d\vec{A}_n \tag{A-28}$$

where

$$d\vec{A}_n = \sum_{p=-\infty}^{\infty} e^{-jkpd_x\left[s_x - \frac{n\Delta y\lambda}{d_x d_y}\right]} H_0^{(2)}(akr') \qquad \text{(A-29)}$$

where

$$r' = \left[\left[\frac{\gamma}{jk}\right]^2 - \left[s_y + \frac{n}{d_y}\right]^2 \right]^{\frac{1}{2}}$$

It now is necessary to transform (A-29) using the Poisson sum rule. To begin the process, the Hankel function, $H_0^{(2)}(x)$, is written in terms of a modified Bessel function of the second kind, $K_0(y)$.

$$K_0(U) = \frac{\pi}{2j} H_o^{(2)}(-jU) \qquad \text{(A-30)}$$

where U is a variable. Using (A-30), the Hankel function in (A-29) becomes

$$H_0^{(2)}(akr') = \frac{2j}{\pi} K_0\left[U\sqrt{z^2 + (pd_x - x)^2}\right] \qquad \text{(A-31)}$$

where the variable U is chosen to be

$$U = \sqrt{\gamma^2 + k^2\left[s_y + \frac{n\lambda}{d_y}\right]^2}$$

The row vector potential in (A-29) then becomes

$$d\vec{A}_n = \sum_{p=-\infty}^{\infty} e^{-jkpd_x\left[s_x - \frac{n\Delta y\lambda}{d_x d_y}\right]} \frac{2j}{\pi} K_0\left[U\sqrt{z^2 + (pd_x - x)^2}\right] \qquad \text{(A-32)}$$

To transform (A-32) using the Poisson sum rule, the following Fourier transform pair is required.

$$g(t) = \frac{2j}{\pi} K_0\left[A\left[B^2 + (t-\zeta)^2\right]^{\frac{1}{2}}\right] \qquad \text{(A-33)}$$

$$G(w) = \frac{2j\, e^{-B(A^2+w^2)^{\frac{1}{2}} - jw\zeta}}{(A^2+w^2)^{\frac{1}{2}}} \qquad \text{(A-34)}$$

where A, B, and ζ are constants. The row vector potential in (A-32) takes the form

$$d\vec{A}_n = \sum_{p=-\infty}^{\infty} e^{-jp\tau_0\Omega}\, g(p\tau_0) \tag{A-35}$$

where

$$t = p\tau_0$$

$$\tau_0 = d_x$$

$$\Omega = k\left(s_x - \frac{n\Delta y\lambda}{d_x d_y}\right)$$

and the constants A, B, and ζ are chosen to be

$$A = U = \sqrt{\gamma^2 + k^2\left[s_y + \frac{n\lambda}{d_y}\right]^2}$$

$$B = z$$

$$\zeta = x$$

The Poisson sum rule for this transformation takes the form

$$\sum_{p=-\infty}^{\infty} e^{-jp\tau_0\Omega}\, g(p\tau_0) = \frac{1}{\tau_0} \sum_{m=-\infty}^{\infty} G(mW + \Omega) \tag{A-36}$$

where

$$W = \frac{2\pi}{\tau_0}$$

Upon transforming (A-35) using (A-36) the row vector potential becomes

$$d\vec{A}_n = \frac{2j}{\gamma d_x} \sum_{m=-\infty}^{\infty} e^{-jkx\left[s_x + \frac{m\lambda}{d_x} - \frac{n\Delta y\lambda}{d_x d_y}\right]} \frac{e^{-\gamma_z g_z}}{g_z} \tag{A-37}$$

where

$$g_z = \left[1 - \left[\frac{jk}{\gamma}\right]^2\left[s_y + \frac{n\lambda}{d_y}\right]^2 - \left[\frac{jk}{\gamma}\right]^2\left[s_x + \frac{m\lambda}{d_x} - \frac{n\Delta y\lambda}{d_x d_y}\right]^2\right]^{\frac{1}{2}}$$

The total array vector potential then becomes

$$d\vec{A} = \hat{\ell}\,\frac{\mu I_{00} d\ell}{2\gamma d_x d_y}\sum_{n=-\infty}^{\infty}\sum_{m=-\infty}^{\infty}\frac{e^{-\gamma\vec{r}\cdot\hat{g}_{\pm}}}{g_z} \tag{A-38}$$

for $\vec{r}\cdot\hat{z} \gtrless 0$ where

$$\hat{g}_{\pm} = \frac{jk}{\gamma}\left[s_x + m\,\frac{\lambda}{d_x} - \frac{n\Delta y\lambda}{d_x d_y}\right]\hat{x} + \frac{jk}{\gamma}\left[s_y + \frac{n\lambda}{d_y}\right]\hat{y} \pm g_z\hat{z}$$

The array vector potential in (A-38) thus is seen to be representable as a doubly infinite sum of attenuated plane waves. The fields are obtainable from the vector potential in (A-38) by use of the relations

$$d\vec{H} = \frac{1}{\mu}\,\nabla \times d\vec{A}$$

$$d\vec{E} = \frac{1}{jwe}\,\nabla \times d\vec{H}$$

The final results are expressed in terms of the $\vec{E}$ field.

$$d\vec{E} = \frac{nI_{00} d\ell}{2d_x d_y}\sum_{n=-\infty}^{\infty}\sum_{m=-\infty}^{\infty} e^{-jk\vec{r}\cdot\hat{g}_{\pm}}\vec{h}_{\pm} \tag{A-39}$$

for $\vec{r}\cdot\hat{z} \gtrless 0$ where

$$\vec{h}_{\pm} = \frac{1}{g_z}\,(\hat{\ell} \times \hat{g}_{\pm}) \times \hat{g}_{\pm}$$

APPENDIX B

LENS CELL SIZE

The size of a cell is limited mainly by module-to-module phase settings that differ significantly from those of linearly progressive phasing. The first approximation analysis, applied separately to each cell, assumes linear progressive phasing between modules in a cell (Sections 3.2.1 and 3.2.6). A nonlinear progressive phasing across a flat lens is necessary if a target return is to be focused on the radar receiver; however, this deviation from linear will be minimal across a sufficiently small cell. A typical SBR lens cell size is determined here. A circular wavefront segment is indicated in Figure B-1.

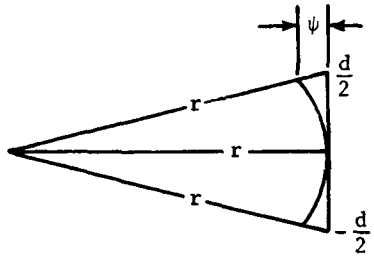

Figure B-1. Linear Modeling of a Circular Arc

The maximum deviation from linear is

$$\psi = \left[r^2 + \left[\frac{d}{2} \right]^2 \right]^{\frac{1}{2}} - r \qquad \text{(B-1)}$$

From (B-1), the segment length for a specified error, ψ, is

$$d = 2\,[(r+\psi)^2 - r^2]^{\frac{1}{2}} \qquad \text{(B-2)}$$

This length represents the height of a cell of containing modules, with linear progressive phasing that approximates the actual phasing to within an accuracy of ψ wavelengths.

The cell height required to maintain a specified maximum phase error will vary depending upon the distance of the cell from the lens center. The relationship of cell size relative to distance from the lens center is show in Figure B-2.

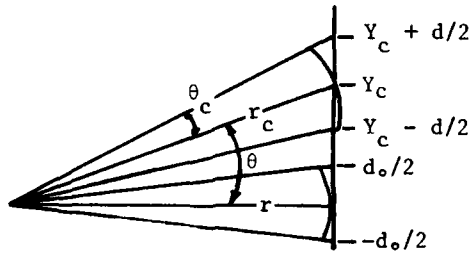

Figure B-2. Cell Height Relative to Distance from Lens Center

The radius of curvature of the wavefront at the lens increases as the distance from the lens center increases. The cell size, therefore, also increases for the same accuracy; for example, for a $\psi = 0.1\lambda$ deviation, and feed to lens separation of $r = 444\lambda$, the length, d, at the center of the lens is $d = 18.8\lambda$. If the lens radius is approximately 146λ, then the wavefront curvature radius at the edge of the lens is $r = 468\lambda$ and $d = 20\lambda$. In general, the cell height, d, is calculated as follows with reference to Figure B-2.

$$\theta_c = \tan^{-1} \frac{d_o}{2r_c} \tag{B-3}$$

$$\theta = \tan^{-1} \frac{Yc}{r_c} \tag{B-4}$$

where

d_o = cell height at lens center

r_c = radius from receiver to cell center

Y_c = distance from lens center to cell center

Now

$$Y_c + d/2 = r_c \tan (\theta + \theta_c) \tag{B-5}$$

$$Y_c - d/2 = r_c \tan (\theta - \theta_c) \tag{B-6}$$

Therefore,

$$d = r_c \left[\tan (\theta + \theta_c) - \tan (\theta - \theta_c)\right] \tag{B-7}$$

For the above example, the cell height at the edge of the lens ($\theta_c = 1.29°$, $\theta = 18°$) is $d = 22.2\lambda$, while at the lens center $d_o = 18.8\lambda$.

A simple approximation to the number of cells needed to model a lens to within an error of ψ is obtained by setting all cell heights $d = d_o$. The number of cells needed to model the lens then is calculated by dividing the lens into concentric rings and subdividing the rings into cells. The width of a cell is set equal to the height of the cell. The number of cells per ring increases for rings farther from the lens center. In the above example, since the lens radius is 148λ, the number of rings needed to cover the lens is eight. The number of cells per ring is shown below (0 ring is the inside ring).

Ring Number	Number of cells
0	4
1	10
2	16
3	22
4	29
5	35
6	41
7	47

The total number of cells needed to cover the lens is 204. A lens portion, subdivided into cells, is shown in Figure 4-3.

MISSION
of
Rome Air Development Center

RADC plans and executes research, development, test and selected acquisition programs in support of Command, Control Communications and Intelligence (C^3I) activities. Technical and engineering support within areas of technical competence is provided to ESD Program Offices (POs) and other ESD elements. The principal technical mission areas are communications, electromagnetic guidance and control, surveillance of ground and aerospace objects, intelligence data collection and handling, information system technology, ionospheric propagation, solid state sciences, microwave physics and electronic reliability, maintainability and compatibility.